Brain delivery of BDNF and a monoclonal antibody for the treatment of neurodegenerative animal models

By:

Brian Matthew Kopec

Submitted to the graduate degree program in Pharmaceutical Chemistry and the Graduate Faculty of the University of Kansas in partial fulfillment of the requirements for the degree of Doctor of Philosophy.

Chair: Dr. Teruna Siahaan

Dr. Michael Wang

Dr. Brandon DeKosky

Dr. Michael Hageman

Dr. Liqin Zhao

Date Defended: Decmber 6th 2019

The dissertation committee for Brian Matthew Kopec

certifies that this is the approved version of the following dissertation:

Brain delivery of BDNF and a monoclonal antibody for the treatment of neurodegenerative animal models

_____

Chairperson: Dr. Teruna Siahaan

Date Approved: December 18, 2019

Brain delivery of BDNF and a monoclonal antibody for the treatment of neurodegenerative animal models

Brian Matthew Kopec

The University of Kansas, 2019

There are a large number of protein-based therapeutics (biologics) that are FDA approved and available on the market for a number of diseases, and the number of biologics being approved every year has tripled in the past two decades. Biologics are highly attractive as therapeutic options due to their safety and efficacy; however, of all the marketed biologics, only several proteins are FDA approved for treatment of CNS. This is due to efficacy limitation of most proteins in the CNS. One of the reasons is due to the presence of the blood–brain barrier (BBB), which selectively limits protein drugs from entering the brain. Although the BBB is critical for things such as maintaining proper concentration of ions and preventing infection as well as harmful toxins from entering the brain, its selectivity makes it difficult to deliver diagnostic and therapeutic agents into the brain. Only a small fraction (i.e., 2%) of marketed small drugs has appreciable penetration into the CNS. Thus, there is a large unmet need to improve drug delivery to the brain for treatment of brain diseases such as multiple sclerosis (MS), Alzheimer's disease (AD), Parkinson's, and brain tumors. Currently, drugs that are not able to cross the BBB are sometimes administered via direct cranial injection or cerebral spinal fluid infusion; however, these are relatively invasive methods and they increase the risk for CNS infections. The goals of this project were specifically to investigate (i) if BBB modulation via the cadherin cyclic peptide, ADTC5, could be used to deliver brain-derived neurotrophic factor (BDNF) across the BBB to treat an experimental autoimmune encephalomyelitis (EAE), a mouse model of MS; (ii) if ADTC5 could also be used to deliver BDNF to treat an aggressive mouse model for Alzheimer's disease (i.e., APP/PS1 mice); and (iii)

how ADTC5 can improve brain delivery a monoclonal antibody (mAbs) for evaluating its clearance from the brain in healthy mice. First, we observed that ADTC5 was able to significantly enhance the deposition of BDNF to have efficacies in the EAE and Alzheimer's disease animal models. Compared to when BDNF was delivered alone or placebo, BDNF + ADTC5 improved clinical body scores and cognitive performance in EAE mice and APP/PS1, respectively. Additionally, both EAE and APP/PS1 mice that were treated with BDNF + ADTC5 showed increase levels of NG2 microglia, and EGR and ARC mRNA transcripts compared to BDNF alone or vehicle. In the EAE model, the NG2 glia was associated with increased levels of myelin. Second, we monitored monoclonal antibody (mAb) brain deposition and clearance after its brain delivery with ADTC5 peptide. In addition, the effect of ADTC5 in mAb depositions in other organs was also determined. We observed a rapid clearance of mAb from the brain after enhanced delivery by ADTC5 with two different phases. The estimated $t_{1/2alpha}$ and $t_{1/2beta}$ of IgG mAb were 0.34 ± 0.22 h and 65.50 ± 12.09 h, respectively. This clearance was heavily facilitated by the liver and ADTC5 did not affect antibody deposition into liver, spleen, kidney, lung, or heart. Overall, this project demonstrates a proof-of-concept that brain diseases can be effectively treated via brain delivery of therapeutic proteins using BBB modulation by cadherin peptides (e.g., ADTC5).

This thesis is dedicated to:

My Parents: Keith Kopec & Nancy Lorenzini

My Siblings: Emily & John Kopec

My girlfriend: Pooja Agrawal

Acknowledgements

I would like to first thank my parents, Keith Kopec and Nancy Lorenzini, for providing me with the support I needed throughout my Ph.D. They have always been there to support me in achieving my life goals. I next, I like to thank my siblings, Emily and John, for providing their encouragement throughout my Ph.D., providing me with additionally motivation that has aided in the completion of my degree. I would also like to thank my girlfriend, Pooja Agrawal, for everything she has done for me in the past few years. Without these people in my life, it is hard to imagine I would have been able to be awarded a doctorate degree.

Next, I would like to thank my advisor, Dr. Teruna Siahaan, for his guidance, which has been invaluable throughout my Ph.D. His positive feedback, open discussions, and excited attitude towards science have inspired me to do the best job I can both in and out of the lab. I am very proud to have been mentored by him, and to take what he has taught me into the next steps of my life. I would also like to thank Dr. Eduardo Rosa-Molinar for his guidance in tissue processing and microscopy. Dr. Rosa-Molinar taught me excellent techniques needed to perform high quality research. Additionally, I would like to thank my dissertation committee members, Drs. Brandon DeKosky, Michael Wang, Michael Hageman, and Liqin Zhao for reading my dissertation and asking insightful questions that further strengthen my understanding of my work.

I am also very thankful for the assistance of my lab members throughout my Ph.D. work, Dr. Kavisha Ulapane, Dr. Mario E.G. Moral, Dr. Paul Kiptoo, Xin Zhang, Jinyan He, Rucha Mahadik, Kelly Schwinghamer, Isaac Nevarez, Subra Patra, and Darci Ezell. Being in the lab with these fellow colleagues was fun and made experiments go by quickly. I would like to particularly thank Kavisha Ulapane for her work with me in studying protein deposition into the brain; she was a true

privilege to work with. I would like to thank my funding sources throughout my PhD: The KU Department of Pharmaceutical Chemistry, NIH Biotechnology Training Grant (T32-GM-08359), and KU Alzheimer's Disease Center Pilot Grant (P30-AG035982). Lastly, I would like to thank my cats, Tesla and Atlas. After coming home after a long day in the lab, it was always great to have little friends to relax with.

Table of Contents

Chapter 1: Methods of Delivering Molecules Through the Blood-Brain Barrier for Brain Diagnostics and Therapeutics

1.1. Introduction:

Every year, hundreds of thousands of people are diagnosed with brain disorders such as Alzheimer's, Parkinson's, multiple sclerosis (MS), and brain tumors. However, because the brain is protected by the blood-brain barrier (BBB), there are few efficacious drugs available for treating these conditions. Although many agents have been developed for early diagnosis of brain diseases, these, too, cannot readily be delivered to the brain due to the presence of the BBB. The BBB plays a critical role in protecting the brain from various harmful substances (*e.g.*, toxins) that may be present in the blood stream. The BBB is very selective, allowing only needed nutrients to cross while excluding many other molecules, including those that could be helpful, from the brain.

Many modern biological drugs and diagnostic agents such as peptides, proteins (including antibodies), and oligonucleotides can be used to treat brain diseases; unfortunately, the majority of these molecules cannot cross the BBB. Large molecule biologics (*e.g.,* antibodies, enzymes, cytokines, hormones) can be delivered to the brain only via intra-cerebral ventricular infusion (ICV) [1]. ICV is accomplished by drilling into the skull and surgically installing a port to deliver drugs directly to the brain; therefore, it is not a stress-free procedure for patients. In addition, this method involves a great deal of risk, as the brain becomes directly exposed to potential infection by pathogens. Thus, there is an urgent need to investigate and develop non-invasive and patient-friendly alternative methods to deliver diagnostic and therapeutic agents to the brain. This chapter is focused on progress and new methods in delivering molecules for diagnosing and treating brain diseases.

1.2. Anatomy of the Blood-Brain Barrier (BBB):

The BBB is composed of tightly packed vascular endothelial cells that are anchored to a basement membrane and surrounded by astrocytes (**Figure 1.1A**) [2]. These endothelial cells are connected at the intercellular junctions by "zipper" or "Velcro" proteins, which are divided into tight junctions, *adherens* junctions, and desmosomes regions (**Figure 1.1B**). These proteins form homophilic and/or heterophilic protein-protein interactions at these three regions to glue the endothelial cells forming the BBB microvessels. In this case, the surface proteins from one cell membrane of endothelial cells form a bridge with their respective counterparts on the surface of the opposing cell membrane [3-5]. The vascular endothelial cells are also decorated with various efflux pump molecules (*i.e.*, P-glycoprotein, multi-drug-resistant protein) and proteolytic and/or metabolizing enzymes that act as gate keepers to prevent or degrade molecules from crossing the BBB.

At the top of the intercellular junction membranes on the blood side of the BBB reside tight junctions or *occludens* junctions. They are connected by homophilic interactions of occludins, claudins, and junctional adhesion (JAM) proteins (**Figure 1.1B**). These tight interactions prevent the permeation of molecules with hydrodynamic radius larger than 11 Å through the intercellular junctions or paracellular pathways [6]. The *adherens* junction below the tight junction is linked by protein-protein interactions of cadherins, nectins, and platelet endothelial cell adhesion molecules (PECAM). These interactions are the primary adhesion force between two opposing cell membranes of the BBB. Thus, the tight junctions are the secondary seal of the intercellular junctions [2]. Finally, *desmosomes* are established below the *adherens junctions* and they produce homophilic desmocollin or desmoglein interactions as well as heterophilic desmocollin-

desmoglein interactions. The desmocollins and desmogleins are in the cadherin family of proteins. It should be noted that there is crosstalk among all the intercellular junction proteins through their interactions with the cytoskeleton proteins.

1.3. In Vitro Models to Study Brain Delivery of Therapeutic and Diagnostic Agents:

1.3.1. In Vitro Models of the Blood−Brain Barrier:

Because *in vivo* delivery of molecules into the brain is challenging, much effort has been invested in developing *in vitro* models for the BBB to rapidly identify molecules that can cross the BBB. Transport mechanisms of molecules across the BBB can be characterized into several categories. First, molecules can passively diffuse through the cell membranes of the endothelial cells, which is called the transcellular pathway (**Figure 1.1A**). It is well accepted that lipid-soluble nonpolar molecules can enter the brain via passive diffusion across the BBB. Unfortunately, some hydrophobic molecules that can partition to the cell membranes cannot cross the BBB because they are expelled by the efflux pumps (*e.g.*, P-glycoproteins or Pgp) from the membranes back into the blood stream (**Figure 1.1A**). Second, molecules such as nutrients (*i.e.*, folates, amino acid) and molecular carriers (*i.e.*, transferrin) can permeate the BBB via receptor-mediated transport mechanism. This transport system involves a vesicular endocytosis process. Receptor-mediated systems have so far been accepted as one of the most promising approaches for noninvasive delivery of molecules across the BBB. Vesicular endocytosis without receptor involvement can also occur and this is called fluid-phase pinocytosis. Third, very small hydrophilic molecules and ions can penetrate the BBB via the intercellular junction in a process called paracellular pathway transport (**Figure 1.1**).

Various *in vitro* BBB models have been developed and widely used to rapidly evaluate the transport properties of molecules across the BBB during the discovery process. Compared to *in vivo* models, the *in vitro* BBB models are less expensive and more conducive to high throughput with reproducible results. Thus, the *in vitro* models are very useful for screening potential candidates in the initial discovery phase of therapeutic or diagnostic agents for the central nervous systems (CNS). However, the *in vitro* models have their own disadvantages. For example, some of the models have leaky tight junctions; therefore, they are not good models to study penetration of molecules through the paracellular pathway. It is recommended that *in vitro* studies should be coupled with *in vivo* studies using the top candidate molecules after *in vitro* screening. It should be noted that, with appropriate choice and use of an *in vitro* model, the results from the *in vitro* model can be well correlated with the *in vivo* data [7,8].

A common *in vitro* model of the BBB consists of a cell monolayer isolated from primary brain endothelial microvessels or immortalized brain endothelial microvessels with many adaptations. Some *in vitro* models are composed of co-cultured cells with varying culture conditions to closely mimic the *in vivo* BBB. To generate the model, cerebral vascular endothelial cells from murine, rat, porcine, bovine, monkey, or human brains are isolated and cultured on the surface of a microporous membrane filter. The culture is fed with the appropriate nutrients to maintain the cell viability. The BBB co-coculture models were also developed using a combination of brain endothelial cells with pericytes, astrocytes, and neurons to mimic the anatomic and physiology complexity of the *in vivo* BBB. Normally, the BBB co-culture model has tight intercellular junctions with high *trans*-endothelial electrical resistance (TEER) values [9,10].

The *in vitro* BBB cell monolayer contains components similar to those of the *in vivo* microvessel with tight intercellular junctions, functional transporters, surface and intracellular

metabolic enzymes, and efflux pumps. The limited porosity of the tight junctions in allowing movement of ions is reflected in the TEER value of the cell monolayer [11]. The TEER value determines the electrical resistance between the apical (AP) and basolateral (BL) sides of the monolayer. A high TEER value indicates very restricted movement of ions across the transcellular and paracellular pathways of the cell monolayer. The intercellular junction proteins act as gatekeepers of the paracellular pathways. Therefore, modulation of the interactions among the intercellular junction proteins of the BBB can result in leakiness of the tight junctions, which is reflected in lowering of the TEER value due to the higher movement of the ions between the AP and BL sides.

To mimic the BBB vasculature in a three-dimensional (3D) mode, the dynamic *in vitro* BBB (DIV-BBB) model has been developed to complement the monolayer BBB models. In this model, the endothelial cells are cultured in hollow fibers that resemble the blood vessels [12]. The DIV-BBB model can be used to simulate *in vivo* blood flow with tunable shear stress. This is a good model to evaluate *trans*-endothelial trafficking of immune cells across the BBB and to study cerebrovascular physiology in various disease states [12]. Unfortunately, the DIV-BBB model is less suitable for evaluating transport of molecules in a high throughput manner because it is a difficult system to setup and establish. This model is also difficult to replicate because its generation requires special expertise.

Newer microfluidic models called “BBB on a chip” have been developed to model the dynamic flow of the BBB using a smaller number of cells and lower amounts of samples. These models consist of human brain endothelial cells (hCMEC/D3) that are cultured on a porous membrane placed at the interface between two microchannels, allowing the cell culture medium to flow through two electrodes. The electrodes are used to continuously measure TEER values of the cell

monolayers. The hCMEC/D3 cell monolayers in the microfluidic device have a TEER value comparable to that of the well-established standard Transwell® [13]. This model can be used to simulate disruption of the BBB in neuroinflammatory diseases such as Alzheimer's and Parkinson's diseases. This study showed that the integrity of this BBB model was influenced by shear stress and inflammatory cytokines TNF-α as in neurodegenerative diseases.

1.3.2. In Silico Models of the Blood−Brain Barrier:

As an alternative to laboratory experimental methods, computational simulation or *in silico* methods have been developed as tools to predict favorable properties of molecules for crossing the BBB [14]. These computational methods can be used during the early stages of drug design to include desirable properties in the molecule for penetrating the BBB. Compared to *in vitro* and *in vivo* experiments, computational methods are fast and low cost methods for screening molecules that can cross the BBB [14]. The algorithm for a certain method was developed using LogBB and LogPS parameters from *in vitro* and *in vivo* experiments of several known compounds [14]. LogBB is the concentration of drug in the brain divided by the concentration in the blood while logPS is the product of permeability and surface area. The unknown values for novel compounds are then derived from regression models [15]. Molecular dynamics simulations were used to calculate the one-dimensional diffusion coefficient for each molecule. A combination of diffusion coefficient and free energy landscape were used to determine the effective permeability (P_{eff}) of a compound. The P_{eff} was compared to LogBB and LogPS values to predict the ability of a molecule to cross the BBB [15]. This method has been shown to predict the BBB permeabilities of small molecules, and the predictions corelate with the experimental data [15].

1.4. Methods to Improve Brain Delivery of Drugs and Diagnostic Agents:

1.4.1. Transcellular Pathways:

The traditional method to deliver drugs and diagnostic agents to the brain is via the transcellular pathway by which the molecule permeates from the blood stream into the brain via the transcellular pathway of the BBB. Unfortunately, this pathway is only viable for small molecules with appropriate physicochemical properties that follow Lipinski's Rules of Five [16-18]. In this case, a drug molecule should have a molecular weight of less than 500 Da with cLogP of less than five. The molecule should have fewer than five hydrogen-bonding donors and no more than ten hydrogen-bonding acceptors. Therefore, during the discovery process, medicinal chemists utilize these rules to guide them in designing drug candidates that can penetrate the BBB. Alternatively, medicinal chemists have cleverly created prodrugs that shield the hydrogen-bonding moieties in the molecule to improve their BBB permeation [19,20]. Although a molecule can satisfy the Lipinski rules, its penetration through the BBB can also be inhibited by the efflux pumps and/or degradation by metabolizing enzymes [21].

Due to their physicochemical properties or violation of the Lipinski's rules, biologics such as peptides, proteins, and oligonucleotides cannot passively diffuse through the cell membranes of the BBB (*i.e.*, paracellular pathway). Therefore, it is very challenging to deliver these types of molecules to the brain. There is a very limited number of peptides and proteins that can cross the BBB. These molecules can do this because they have transport receptors that carry them across the BBB. Therefore, many efforts are underway to find alternative routes and methods to deliver peptides, proteins, and oligonucleotides into the brain.

1.4.1.1. Prodrug Formation for Passive Diffusion through Cell Membranes of the BBB:

Prodrugs have been developed to temporarily alter the physicochemical properties of hydrophilic and charged molecules (*i.e.*, drugs or diagnostic agents) to improve their BBB permeation. The prodrugs are formed by adding promoieties to the functional group(s) (*i.e.*, alcohol, acid, amine) of the drug to change physicochemical properties of the prodrug to make it more hydrophobic than the parent drug (**Figure 1.2**). Alternatively, prodrug formation can also be used to improve the solubility of hydrophobic and insoluble drugs in water [22,23]. Low water solubility prevents prevent drug administration in sufficient doses for oral and BBB bioavailability; thus, charged promoieties (*e.g.*, phosphate ester) have been attached to the drug to produce salts of the prodrug to increase water solubility and dose.

For charged drugs, the formation of uncharged prodrugs enhances their partition into cell membranes for passive diffusion across the BBB. Drugs with an acid functional group (pKa = 4.0) or a basic functional group (pKa = 8) functional group have a charge at physiological conditions, pH = 7.4; thus, they have low membrane permeation (**Figure 1.2**). In contrast, the formation of an ester prodrug for a drug containing a carboxylic acid removes the charge group; thus, the prodrug is expected to have a better BBB permeation than the parent acid drug. After crossing the BBB, the ester prodrug can be converted to the parent drug in the brain tissue by esterase enzyme(s) (**Figure 1.2**). This conversion traps the charged drug molecules in the brain tissues. There are several factors that prevent prodrug molecules from crossing the BBB. First, the prodrug could be recognized by the efflux pumps; thus, although it could partition effectively into the cell membranes, the efflux pumps would expel the prodrug from the cell membranes. Second, it cannot cross the BBB because of its premature conversion to the parent drug by an enzyme (*i.e.*, esterases) in the systemic circulation or inside the endothelial cells. Third, the prodrug could be converted

by metabolizing enzymes (*e.g.*, CYP_{450}) to a more hydrophilic molecule to prevent its exit from the endothelial cells.

Due to backbone amide bonds, peptides have a very high number of hydrogen-bonding donors and acceptors as well as a high molecular weight; these are the reasons that most peptides cannot readily cross the BBB [24,25]. One way to improve the partitioning of peptides or peptidomimetics into cell membranes is by forming cyclic peptide prodrugs (**Figure 1.3**) [24,25]. Formation of a cyclic peptide prodrug increases the number of intramolecular hydrogen bonds and lowers the hydrogen-bonding potential to surrounding water molecules. In addition, cyclic peptide prodrugs have rigid backbone structures with stable and compact conformations for better partitioning into cell membranes of the BBB. Cyclic prodrugs of RGD-peptidomimetics (*e.g.*, Aggrastat) were designed using "trimethyl lock" phenylpropionic acid and acyl(oxy)alkoxy promoiety (**Figure 1.3**) [26-28]. RGD-peptidomimetics and Aggrastat cannot be delivered orally because they cannot penetrate the biological barriers due to their charges. The formation of a cyclic prodrug (**1**) enhanced its cell membrane penetration 4.4 times compared to the parent RGD-peptidomimetic (**2**) in an *in vitro* cell culture model of the intestinal mucosa (*i.e.*, Caco-2 cell monolayer) [26]. Similar results were found in the formation of cyclic prodrugs of the opioid peptides using trimethyl lock" phenylpropionic acid and acyl(oxy)alkoxy promoieties [29-31]. The advantage of cyclic peptide prodrugs is that they can be converted to the parent linear peptides by esterase after crossing the biological barriers *in vitro* and *in vivo* (**Figure 1.3**). The ester bond is clipped by esterase to form an intermediate followed by fast chemical reaction to release the parent compound (**Figure 1.3**). The disadvantage is that the cyclic peptide prodrug can be prematurely converted to the parent peptide before or during transport across BBB. The metabolism of cyclic peptide prodrugs by CYP_{450} while crossing the BBB can also be a hurdle for the development of these

compounds.

1.4.1.2. Drug Conjugates for Receptor-mediated Transport through the BBB:

Native transport receptors on the BBB have been exploited to improve drug delivery to the brain. Transferrin, insulin, IGF-I, IGF-II, angiotensin II, and natriuretic peptide receptor-7 have been targeted by their respective ligands to deliver drugs to the brain as protein–drug conjugates (**Figure 1.2**). Monoclonal antibodies (mAbs) against transferrin receptors (TfRs) on the luminal side of the BBB have been used to carry drug payloads into the brain by forming antibody-drug conjugates (ADC) [32-36]. This method has been referred to as the "Trojan horse" method. The mAb targets an epitope on the receptor that is distinct from the binding site of its endogenous ligand without interfering with the receptor function to shuttle its native ligand into the BBB endothelial cells or across the BBB [37]. The ADC is internalized and transported from the luminal through the vascular endothelial cells to the abluminal side of the BBB to exert the drug activity in the brain.

Transferrin receptor (TfR) is an endogenous receptor that binds to holo-transferrin (hTf) carrying iron into the cells. Once the hTf-TfR complex enters the endosome intracellular, it experiences a pH change from 7.4 to 4.5–6.5, which triggers a the release of hTf from TfR and the release of the iron from hTf [37]. Then, the TfR is recycled back onto the cell surface. Thus, this mechanism has been explored to deliver anti-TfR mAbs such as OX26 and 8D3 mAbs that carry drugs or proteins across the BBB into the brain [37]. The I.V. administration of OX26 mAb resulted in its detection in the brain vasculature at 0.44% of the administered dose after injection. OX26 mAb was co-localized with Factor-VIII mAb that marked the branched capillaries of the rat brain [38-40]. OX26 mAb was deposited at the parenchyma region that was associated with

neurons and closed to the ventricular system. It was proposed that TfR was responsible for the transcytosis of OX26 mAb into the brain; the explanation given was that plasma clearance of OX26 mAb was faster than the IgG control [41]. Using immunohistochemistry and capillary depletion methods, it was found that 90–95% of OX26 was in capillaries in the brain parenchyma, suggesting that the majority of the mAb was trapped inside the endothelial cells without crossing the BBB. Because the mAb was detected in cerebrospinal fluid (CSF), it was also suggested that the mAb entered the brain via cerebroventricular organs or the blood-CSF barrier.

Administration of 8D3 anti-TfR mAb via I.V. injection indicated a brain deposition of the mAb at the 1-h time-point after injection; unfortunately, the extent of brain deposition was difficult to determine because capillary depletion experiments were not carried out [37,42,43]. Pegylated immunoliposomes (PILs) conjugated to 8D3 mAb and loaded with beta-galactosidase were found in various brain regions (septo-striatal, rostal, and claudal) of adult male Balb/c mice at 1–3 days after I.V. administration [44]. In another study, 1% of the I.V. administered dose per gram of biotinylated radiolabeled ^{125}I-amyloid-beta 1–40 (Bio-^{125}I-A$\beta_{1\text{-}40}$) bound to streptavidin-8D3 (SA-8D3) mAb was deposited in the brain of *App*^{Swe}*/Psen1* double-transgenic Alzheimer's Disease (AD) mice at the 1-h time point [45]. The peptide was found sequestered around the amyloid beta (Aβ plaques in the brain, suggesting the possibility of using this complex as a brain diagnostic tool for AD [45]. The low efficiency of the 8D3 mAb transport across the BBB into the parenchyma can be attributed to trapping of the mAb inside the BBB endothelial cells and the mAb localization in the brain parenchyma is still controversial [46]. Studies suggest that 8D3 mAb bound to vasculature endothelial cells. Confocal microscopy studies indicated that 8D3 mAb co-localized with collagen IV as a basal laminal marker, suggesting that the mAb traversed from the luminal (blood) to the abluminal side of the brain endothelial cells without releasing the mAb from the TfR

at the abluminal side. The inability to release the mAb was due to its high affinity to TfR [46].

One of the potential solutions to solve the problem of mAb release from TfR at the abluminal side is to design low affinity mAbs [46]. Alternatively, mAbs with pH-sensitive binding properties have been designed to improve their transcytosis. mAbs with lower binding to TfR at pH 5.5 than at pH 7.4 have higher transcytosis into the brain than mAbs that have higher binding at both pH 5.5. and 7.4 [47]. The majority of mAb molecules with high affinity to TfR were found in the brain capillaries even 24 h after administration; in contrast, the low affinity mAbs were detected at the brain parenchymal and co-localized with a neuronal marker [46]. The high affinity mAb-TfR complex degraded mainly in lysosomes compared to the low affinity complex; this is presumably due to the long residence time of the high affinity complex in the lysosomes [48]. This finding was congruent with *in vivo* observation where the high affinity mAb-TfR complex caused a low unbound fraction TfR on the cell surface. This low unbound fraction was due to the degradation of mAb-TfR complex in lysosomes. This was also one reason why the high affinity mAb had low brain exposure.

To attenuate mAb affinity for TfR, a monovalent TfR mAb was developed for improving brain exposure and suppressing degradation in the lysosomes [49]. In this case, the Fc region of mAb31 that recognizes amyloid-beta plaques was linked to one or two Fab fragment(s) of TfR mAb to produce sFab-mAb31 and dFab-mAb31 [49]. The majority of the monovalent sFab-mAb31 was transcytosed to the brain more efficiently than was divalent dFab-mAb31. sFab-mAb31 was distributed throughout the parenchyma and around Aβ plaques in the brains of PS2APP mice. The lysosome degradation of dFab-mAb31 was fast, suggesting one reason for its low transcytosis. dFab-mAb31 had no significant decoration of the plaques compared to control, which confirmed its slow transcytosis properties. In summary, the results suggest that mAb with a weak binding to

the carrier receptor is necessary for mAb release in the brain.

Although extensive research efforts have been carried out to exploit the use of TfR to transcytose Tf mAb with conjugated drugs into the brain, moving this technology into the clinic has been challenging [37]. One of the reasons is the low efficiency of drug transport from blood to the brain. The degradation of mAb in endosomes as well as its trapping in the endothelial cells contribute to its low brain deposition. It is challenging to find an appropriate balance between binding affinity and release property of the mAb from TfR at the abluminal side of the BBB. The presence of TfRs in various tissues or organs could potentially elicit off-target side effects. Although this method has not yet reach clinical applications, it has contributed insights into mechanisms of actions and stimulated interest in evaluating various transport receptors as carrier molecules on the BBB.

Insulin transporters other than TfR on the BBB have been exploited to deliver drugs, including proteins, into the brain by their conjugation to insulin [50,33]. Because insulin has a short half-life ($t_{1/2}$= 10 min) in the systemic circulation, a high dose of the conjugate has to be administered to reach the needed dose in the brain [50,33]. One disadvantage of this method is that the insulin conjugate can cause hypoglycemia in the subject after systemic delivery [50]. Alternatively, a mAb targeted to an insulin receptor has been studied for delivering brain-derived neurotrophic factor (BDNF) to the brain. BDNF has been shown to induce neuroregeneration in animal models of brain diseases (*i.e.*, MS, Alzheimer's disease) when administered via ICV. In another study, the heavy chain C-terminus of the Tf mAb (HIRMab) was fused to BDNF to produce HIRMab-BDNF. The fusion produced binding affinities similar to Tf mAb to TfR and BDNF to TrkB receptors with affinity similar to that of BDNF. The results suggest that fusion of the two proteins did not influence the binding affinity of each protein to its respective target receptor [33]. Three hours

after I.V. administration of ^{3}H-HIRMab-BDNF in rhesus monkeys, a significantly higher brain deposition of ^{3}H-HIRMab-BDNF (24 ng/g brain) than ^{3}H-IgG2a was observed in brain homogenates. It was found that the amount of fusion protein in the brain was tenfold higher than that of endogenous BDNF control, indicating that the mAb enhanced BDNF delivery into the brain [33].

1.4.1.3. Liposome-mediated Brain Delivery:

The abilities of different ligands to deliver liposomes into the brain were investigated by targeting their respective receptors on the BBB. Ligands such as proteins (*i.e.*, transferrin, RI7217 mAb, CRM19) or peptides (*i.e.*, ICOG133, angiopep-2) were used to decorate the surface of liposomes [51-53]. The receptors for these ligands are found on the endothelial cells of the BBB. Both transferrin and RI7217 mAb bind to TfR on the BBB. It is well known that TfR transports iron on transferrin (Tf) into the brain. RI7217 mAb has been shown previously to transport loperamide across the BBB [54]. CRM-197 is a ligand for diphtheria toxin receptor (DTR) and heparin-binding epidermal growth factor (HB-EGF) expressed on the BBB surface, and CRM-197 is a non-toxic mutant of diphtheria toxin (DT) that contains a single point G52D mutation. COG133 peptide is derived from apolipoprotein E (apoE) and COG133 peptide binds to low-density lipoprotein receptor (LDLR). LDLR is responsible for transporting cholesterol and lipids into CNS [55]. Angiopep-2 peptide binds to low-density lipoprotein receptor-related protein 1 (LRP1). The liposomes were decorated with targeting ligands via a maleimide PE linker embedded in the liposomes. The liposomes were composed of EPC, cholesterol, EPG, and MPB-PE with a molar ratio of 6.5:2.6:0.8:0.1 [56].

Mouse brain endothelial cells (bEnd.3) and human (hCMEC/D3) brain endothelial cell

monolayers were used to evaluate the receptor-mediated endocytosis of ^{3}H-labeled liposomes decorated with different ligands by incubating them at 4 ^{o}C or 37 ^{o}C for 1 h. The results showed that only liposomes decorated with CRM-197 have significant binding compared to control liposomes in both endothelial cells. In contrast, liposomes decorated with RI7217 mAb binds only to human (hCMEC/D3) brain endothelial cells; these liposomes were engulfed by hCMEC/D3 cells significantly better than liver and kidney cells, indicating the selectivity of the hCMEC/D3 cells. COG133-labeled liposomes did not bind and cross the BBB in the *in vitro* and *in vivo* models, suggesting that COG133 peptide does not have the necessary sequence or properties for binding and uptake by the LDLR. Although angiopep-2-paclitaxel conjugate has been shown to cross the BBB, there was no uptake of angiopep-2 liposomes by the endothelial cells; this could be due to the density and/or accessibility of peptides on the surface of liposomes for recognition by LRP1 on the endothelial cells. It has been shown previously that ligand density has an important role in the targeting efficacy of nanoparticles or liposomes [57], and different ligands can have different optimal ligand densities to elicit the same binding outcomes [58].

Because RI7217 liposomes were engulfed by hCMEC/D3 cells, further studies were carried out *in vivo*. RI7217 liposomes labeled with non-exchangeable [^{3}H]cholesteryl hexadecyl ether (5 Ci/mol total lipid) were administered via I.V. in mice and, after 12 h of circulation time, the mice were sacrificed to collect the blood, brain, and other major organs [51]. The liposomes were cleared from the blood in a 12-h time period. More RI7217 liposomes were found in the brain fractions compared to untargeted liposomes after capillary depletion. There was no significant difference in the uptake of RI7217 over untargeted liposomes in any other organs, suggesting selectivity of RI7217 for the brain [51]. The RI7217 liposomes were found in significant amounts in parenchyma, cerebrum, and cerebellum. The amounts of RI7217 liposomes in the brain

parenchyma fraction were 4.3 and 2.6 times higher than the untargeted liposomes at 6- and 12-hour time points after administration, respectively. The amount of RI7217 liposomes was 10-times higher than that of untargeted liposomes in the brain capillary fraction, suggesting that RI7217 liposomes bound to TfR on the BBB. Finally, a fraction of the RI7217 liposomes crossed the BBB endothelial cells into the brain. In conclusion, the amount of liposomes that reached the brain were about 0.18% after 12 h, which was considered a low amount of delivered liposomes [51]. It has been suggested that this delivery method be used only for very potent drugs such as opioids, which need a very low dose in the brain.

1.4.1.4. Brain Delivery of Nanoparticles:

Nanoparticles have been exploited for delivering molecules to the brain, and the types of nanoparticles such as shapes, sizes, and physical properties of the particles may play a significant factor in their uptake into the brain. The presence of targeting ligands can help direct the nanoparticles to the BBB and possibly into the brain. Ligands that can enhance the uptake of liposomes into the brain can also be used to deliver different types of nanoparticles (*e.g.*, polymeric, albumin, etc.).

Magnetic nanocrystals of Fe_3O_4 have been used as a magnetic resonance contrast agent for early detection of brain diseases. Nanoparticle surfaces have been decorated with lactoferrin (Lf) to make Lf-Fe_3O_4 nanoparticles. Lf is involved in host defense mechanisms against severe inflammation or infection and normally accumulates in the brains of neurodegenerative disease patients [59,60]. Lactoferrin receptors (LfR) are expressed on the BBB endothelial cells for transcytosis of Lf into the brain [59]. The uptake of Lf by LfR is more efficient than those of transferrin or OX-26 antibody by TfR; thus, Lf is potentially a better ligand to deliver nanoparticles

across the BBB [61]. Lf was conjugated to the nanoparticles via the one of the carboxylic acid terminals of the polyethylene glycol (HOOC-PEG-COOH) that coating the surface of iron nanoparticles. The role of PEG molecules is to improve water solubility and biocompatibility of the particles as well as to reduce protein adsorption, reticuloendothelial system (RES) uptake, and immunogenicity stimulation [60]. At all particle concentrations, PEG-coated Fe_3O_4 nanoparticles without Lf (untargeted nanoparticles) disrupt the tight junctions of the primary porcine brain capillary endothelial cell (PBCEC) monolayers as indicated by decreasing TEER values of cell monolayers. In contrast, incubation of Lf-Fe_3O_4 nanoparticles maintained the monolayer integrity at concentrations of 0.04 and 0.1 mg Fe/mL. Lf-Fe_3O_4 nanoparticles disrupt the BBB tight junction integrity at a high particle concentration (0.3 Fe mg/mL). The results suggest that Lf-conjugation suppresses the BBB tight junction disruption by untargeted nanoparticles.

The BBB transport properties of Lf-Fe_3O_4 (Lf-labeled) nanoparticles were evaluated *in vitro* and *in vivo*. *In vitro* incubation of Lf-Fe_3O_4 nanoparticles (0.04 and 0.1 Fe mg/mL) for 18 h on the apical (AP) side of PBCEC cell monolayers resulted in observation of the transported nanoparticle at the basolateral (BL) side as determined using atomic absorption spectrometer (AAS). About 22% of the nanoparticles crossed the BBB monolayers. The nanoparticle transport was inhibited by excess Lf alone (16x) from 22% to 1% transport, suggesting that the particle was transported via LfR-mediated transcytosis. The Lf-Fe_3O_4 nanoparticles were evaluated *in vivo* using SD rats, and the brain distribution of the nanoparticles was detected using a 7.0 T animal magnetic resonance imaging (MRI) instrument. Coronal and axial T2 relaxation data were collected at pre- and 24-h post-tail vein injections to detect nanoparticle deposition in the brain. Axial T2 contrast images showed that both Lf-labeled and unlabeled particles reached the brain, but the Lf-labeled nanoparticles showed greater contrast than the unlabeled particles in the thalamus, brain stem, and

frontal cortex. These results suggest that the labeled nanoparticles traverse the BBB and access the brain via LfR-mediated uptake. There was a higher localization of Lf-labeled nanoparticles in the brain microvessels compared to unlabeled nanoparticles. Because the unlabeled nanoparticles were also found in the brain, their transport across the BBB could be due to the disruption of the BBB intercellular junctions [60].

1.4.1.5. Exosome-mediated Brain Delivery:

Exosomes are 40–100 nm nanosized bubble-like particles found in body fluid that are secreted by various types of cells [62]. They are formed via invagination of multi-vesicular body followed by fusion of cell plasma membranes, but do not contain lysosomes or mitochondria. The surfaces of exosomes are decorated with endogenous proteins from the producing cells, and these exosomes can be exploited to target certain cells or tissues. The most exciting characteristic of exosomes is that they can travel from one cell to another to release their contents (*e.g.*, proteins, RNA) in the intracellular space of destination cells. There are several other unique exosome properties that are beneficial for drug delivery vehicles. First, small-to-large molecules can be loaded into exosomes for delivery. Second, surface proteins on exosomes can be used to direct them to intended target cells for uptake. Third, exosomes have high plasma stability with a long half-life in the systemic circulation and various tissues [62].

Rhodamine-loaded exosomes have been delivered to the brains of zebrafish and fluorescence dye was detected in the brain tissue, excluding the vasculature network [63]. The doxorubicin-loaded exosomes have also been shown to target DiD-labeled U-87 MG cancer cells in zebrafish brain. In addition, five days after treatment with doxorubicin-loaded exosomes, the tumor size in the brains of zebrafish was reduced. In another example, siRNA-loaded RVG exosomes were

delivered to wild-type mouse brain and BACE1 enzyme expression that is important in Alzheimer's disease was suppressed [64]. This delivery of this RVG exosomes was relatively selective to target siRNA into the brains and avoided uptake by tissues outside of the brain [62].

In summary, although the exosome delivery system seems better than other synthetic drug carriers, this technology still has many challenges to overcome. The first is to identify the proper donor cells to generate the desired and appropriate exosomes. Second, it is difficult to find the appropriate method to efficiently load the drug into exosomes. Third, the pharmacokinetic properties of exosomes have been challenging to determine. Fourth, it is still difficult to provide consistent targeting molecules on the surface of exosomes. Finally, the ability to scale up exosome production and to load them for clinical use are still barriers that need to overcome.

1.4.1.6. Viral Vectors Brain Delivery:

Delivering genes across the BBB faces the same challenges as delivering conventional therapeutics. Due to the chemical and enzymatic instability of genes, a high dose of genes is required for their successful therapeutic use; unfortunately, this high dose in the systemic circulation could increase side effects such as hepatoxicity [65]. Viral vectors have been somewhat successful in delivering genes to various tissues other than the brain; however, this success has been tainted by viral infections in treated patients due to impurity of the viral vectors. The viral vectors exploit their viral infection mechanisms to enter into the brain by crossing the BBB. To enter the brain, viral vectors utilize surface proteins to bind target receptors on the endothelial cells for crossing the BBB. The vectors also use their own surface proteins to bind receptors on the target cells to deliver genes into the cells. Inside the cell, the viral vectors follow the intracellular trafficking process and escape the endosome to enter the nuclear of cells. Finally, the capsid is

unpacked and the genome is inserted in the cell nuclear to initiate transcription and translation processes.

Non-pathogenic recombinant adeno-associated viruses (rAAVs) with certain capsid serotypes have been shown to cross the BBB and deliver genetic material to neurons and astrocytes in the brain. Thus, AAVs have been developed to carry 4.7 kb single-stranded DNA for gene expression in target-host cells. To design viral vectors that can cross the BBB for delivering the genes to the desired location or cells in the brain, the 60 viral proteins (VP) with sequence diversity were used to assembled to make AAVs [66]. AAV1 and AAVrh.10 are viral vectors that share 85% sequence homology; they were discovered through DNA shuffling. AAV1 viral vector did not cross the BBB and can transduce the brain vasculature only; in contrast, AAVrh.10 vector has a different capsid domain to traverse through the BBB [65]. To evaluate whether viral vectors could cross the BBB, a GFP-expressing cassette was packaged into AAV1, AAVrh.10, and six other chimeric variants of viral vectors. Then, they were administered via I.V. injections at a dose of 5×10^{11} viral genomes (vg)/per mouse) into 6- to 8-week-old mice. Three weeks later, the brains were isolated and subjected to immunostaining. It was found that AAV1 vector was located only in the brain vasculature while AAVrh.10 showed robust GFP transduction in neurons, glia, and endothelial cells.

An AAV1RX vector was developed by grafting eight residues from AAVrh.10 onto AAV1 to make this viral vector able cross the BBB. This vector can deliver genes to selectively transduce neurons, indicating that the eight residues have a critical role in allowing the vectors to penetrate the BBB. Unfortunately, AAV1RX viral vectors can also transduce liver and cardiac tissues in a manner similar to that of AAV1, suggesting that other structural domains of the AAVrh.10 capsid play a role in a systemic transduction profile. From the results, it is uncertain whether this 8-residue

footprint is sufficient to selectively deliver genes to the brain and facilitate a transduction profile similar to that of AAVrh.10 vector.

AAV1R6 and AAV1R7 are two viral vectors that were designed from AAV1 with 97% identical amino acid sequence that have an important 22-amino acid residue derived from AAVrh and AAVrh.10. This amino acid residue is important for crossing the BBB. The design was based on the overall beta-barrel structure of core viral protein 3 (VP3) with VP7 antiparallel beta-strands connected by interlocking loop regions. The highly variable and surface-exposed loop regions on AAV capsids have been modified to control tissue tropism, transduction profile, and antigenicity [66,67]. Similar to the AAVrh.10 vector, AAV1R6 and AAV1R7 vectors have a robust transduction on cortical neurons and other brain regions; in contrast, they reduced transduction in glia and vasculature when compared to AAVrh.10. This result confirms that AAV1R6 and AAV1R7 vectors can cross the BBB. AAV1RX6 and AAV1RX7 have the potential for developing gene therapies against neurological disorders including spinal muscular atrophy. These vectors do not target peripheral organs (*i.e.*, liver and cardiac tissues); thus, they avoid potential hepatoxicity side effects. Therefore, future successful clinical applications of these vectors will rely on their efficacy in large animals such as non-human primates [65,67].

1.4.2. Brain Delivery of Molecules through Paracellular Pathways of the BBB:

One alternative method to deliver molecules through the BBB is via the paracellular pathways by increasing the opening or porosity of the tight intercellular junctions. One of the most successful methods in the clinic to deliver molecules through paracellular pathways is osmotic delivery, which has been used to deliver anticancer drugs to treat brain tumor patients [68-76]. The osmotic method involves injecting a hypertonic solution of mannitol into the carotid artery to shrink the

BBB endothelial cells and creates a disruption of the tight intercellular junctions. This disruption generates larger pores in the intercellular junction to increase the penetration of anticancer drugs into the brain [75,77,73]. It should be noted that the hypertonic mannitol works via increasing the osmotic pressure in the blood stream and does not disrupt the intercellular junction proteins in a selective manner.

Several methods have been developed to increase the porosity of the intercellular junctions by disrupting protein-protein interactions in the intercellular junctions. Peptides derived from the sequences of the extracellular domains of intercellular junction proteins have been developed to selectively inhibit protein-protein interactions in an equilibrium fashion to increase permeation of molecules through the BBB. Claudin and occludin peptides have been shown to modulate the intercellular junctions of the biological barriers *in vitro* and *in vivo* [78-80]. The C1C2 peptide (**Table 1.1**) derived from claudin-1 can deliver opioids and tetrodotoxin into rat brains [78]. The C1C2 peptide can open the BBB for extended period of time (*i.e.*, 3 days); however, this long period of opening of the BBB may not be desirable. Thus, further investigation is needed to find peptide derivatives that can modulate the tight junctions of the BBB for a shorter period of time.

Several peptides that are related to tight junction proteins were designed to increase the paracellular porosity of the biological barriers. OCC2 peptide (**Table 1.1**) derived from loop 2 of chick occludin was active in disrupting the tight junctions and decreasing the TEER values of A6 epithelial cell monolayers. OCC2 peptide also enhanced paracellular permeation of dextran-3000 and 40,000 across the A6 epithelial monolayers. However, OCC2 has not been evaluated to improve the delivery of molecules across the BBB in *in vitro* and *in vivo* models. A peptide called AT-1002 (**Table 1**) that was derived from zonula occludens toxin (ZOT) protein improved the paracellular delivery of low molecular weight heparin orally. AT-1002 disrupts the tight junctions

of Caco-2 and brain endothelial cell monolayers. C-CPE peptide from a microbial toxin fragment can modulate claudin-3 and -4 in tight junctions of Caco-2 but not in brain endothelial cell monolayers. PN-78 and PN-159 peptides (**Table 1.1**) were discovered from phage display studies, and both peptides significantly lowered the TEER values of Caco-2 and brain endothelial cell monolayers. PN-159 was very potent in enhancing the delivery of fluorescein and albumin through Caco-2 and brain endothelial cell monolayers.

Peptides (*i.e.*, HAV and ADT peptides) that are derived from the extracellular 1 (EC1) domain of E-cadherin have been shown to modulate *in vitro* biological barriers (*i.e.*, Caco-2 and MDCK cell monolayers) [81-83]. HAV and ADT peptides can modulate the BBB intercellular junctions and enhance brain delivery of molecules in mice and rats [84-89]. The proposed mechanism of action of HAV and ADT peptides is via their binding to the EC1 domain of cadherins. Heteronuclear multiple quantum coherence (HMQC) NMR spectroscopy experiments show that HAV and ADT peptides bind to different binding sites on the EC1 domain of E-cadherin [90]. HAV6 and ADTC5 peptides enhanced the brain delivery of ^{14}C-mannitol as a paracellular marker [86,87]. In addition, HAV6 peptide enhances the brain delivery of efflux pump substrates such as ^{3}H-daunomycin into rat brains using *in-situ* rat brain experiments [84] and IRdye R800 into the mouse brain after I.V. administration [87]. These results suggest that cadherin peptides can be used as an alternative way to deliver efflux pump substrates to the brain.

To further evaluate the BBB modulatory activity of cadherin peptides, an MRI contrast agent, Gd-DTPA, was delivered via I.V. administration together with HAV6 or ADTC5 peptide in mice; the brain depositions of Gd-DTPA were detected using MRI in living animals [86,87]. The results showed that the deposition of Gd-DTPA was observed in the brains within 3.0 min after administration, and both peptides significantly enhanced brain delivery of Gd-DTPA compared to

a control vehicle in mice. The duration of tight junction modulation was evaluated using MRI; in this case, the HAV6 peptide was administered alone, and Gd-DTPA was administered via i.v. route after 1 h [87]. The result showed that there was no significant enhancement of Gd-DTPA compared to control, suggesting that the duration of opening of the BBB by HAV6 peptide was less than 1 h. A similar study showed that ADTC5 peptide could open the BBB between 2 to 4 h, which is longer than when using HAV6 peptide [86].

ADTC5 peptide enhances the brain delivery of 8-mer cIBR and 12-mer cLABL peptides in rats and mice, respectively [89]. The deposition of intact cIBR peptide can be detected in rat brain by LC-MS/MS. HAV6 and ADTC5 peptides have been shown to significantly enhance the delivery 65 kDa albumin conjugated with Gd-DTPA (*i.e.*, galbumin) compared to control peptide or PBS as detected by MRI. The deposition of the protein could be detected in the brain 3.0 min after administration [89]. For a large protein such as galbumin, HAV6 could be used only when both HAV6 and galbumin were delivered simultaneously; however, a 10-minute delay of galbumin administration after delivery of HAV6 did not enhance galbumin brain delivery. In contrast, ADTC5 was able to enhance the delivery of galbumin into the brain after a 10-minute delay; however, a 40-minute delay of galbumin after ADTC5 injection did not show any enhancement of brain delivery. The results suggest that the opening of the BBB by cadherin peptides is short for large molecules compared to the opening for small molecules. It is proposed that cadherin peptides generate large, medium, and small pores in the intercellular junctions of the BBB and the large pores rapidly collapse to medium and small pores followed by the collapse of medium pores to small pores in a time-dependent manner.

In summary, many potential disruptors of the intercellular junctions of the BBB have the potential to enhance the delivery of diagnostic and therapeutic molecules into the brain. The

applicability and safety of these modulators to deliver therapeutic and diagnostic agents to the brain still needs further investigation. The next step is to use these modulators to deliver functional molecules to the brains of animal models of brain diseases.

1.5. Current Methods to Diagnose Brain Disease:

Many imaging methods (*e.g.*, MRI, X-ray, CATscan) have been used to diagnose brain diseases (*i.e.*, Alzheimer's, Parkinson's, multiple sclerosis, stroke, and brain tumors). Some of these methods utilize molecular imaging techniques by delivering highly sensitive probes into the brain in a non-invasive manner. These probe molecules can be powerful detection tools for detecting changes in the brains during the progression of brain diseases; these changes include the brain cellular activities and morphologies as well as the protein compositions to diagnose brain diseases in clinical and preclinical settings. Early detection of brain diseases is important for halting their progress; therefore, the use of specific and sensitive molecular imaging techniques is necessary. In both preclinical and clinical studies, several molecular imaging techniques such as magnetic resonance imaging (MRI), positron emission tomography (PET), single photon emission computed tomography (SPECT), and optical imaging techniques including near-infrared (NIR) fluorescence imaging have been greatly advanced for diagnosing brain diseases *ex vivo* and *in vivo* [91].

Neuroinflammation can be a common sign of brain diseases such as stroke, multiple sclerosis, Alzheimer's, malignant cancer, and Parkinson's. The neuroinflammation process activates inflammatory immune cells that infiltrate the brain along with the upregulation of inflammatory cytokines. Therefore, changes in the balance between the activation of inflammatory and regulatory immune cells in the brain can be the target of diagnostic agents for brain disorders.

Many current diagnostic molecules for brain diseases are limited to small hydrophobic molecules that can cross the BBB. These small molecules typically have a molecular weight less than 500 Da and have high binding capacity to the target tissue(s) in the brain. In contrast, many peptides, nucleotides, and proteins (*e.g.*, enzymes and antibodies) are molecules that have high selectivity to bind cellular components of the brain (*e.g.*, proteins and sugars) for detecting changes in the brain. Unfortunately, these types of molecules cannot be delivered to the brain because they cannot cross the BBB. Thus, if these types of molecules could be delivered to the brain, they could be utilized to improve the diagnostics and treatments of brain diseases. Several methods used in attempts to deliver them to the brain have been described above.

The infiltration of leukocytes into the brain during inflammation occurs via extravasation through the intercellular junctions of the BBB [92]. This process involves various cell adhesion molecules on the leukocytes as well as the on the endothelial cells of the BBB [93]. The process of extravasation of immune cells is initiated by rolling of these cells of the surface of endothelium mediated by L- and E-selectins. When the immune cells stop rolling, they firmly adhere to the endothelial cells, which are mediated by ICAM-1 and VCAM-1 immunoglobulins on the endothelial cells that bind to LFA-1 ($\alpha_L\beta_2$) and VLA-4 ($\alpha_4\beta_1$) integrins, respectively, on the surface of leukocytes [93,92]. Natalizumab, a monoclonal antibody that binds to α_4-subunit of VLA-4 integrin, is being used to treat MS because it can prevent adhesion of immune cells to the BBB. Therefore, it prevents brain infiltration of immune cells to suppress disease exacerbation in MS patients. This indicates upregulation of cell adhesion molecules (*e.g.*, ICAM-1) on the endothelial cells of the BBB, and the increased expression of cell adhesion molecules on the BBB endothelial cells of MS patients can be explored as diagnostic markers of MS [94].

1.5.1. Magnetic Resonance Imaging (MRI):

MRI has been used extensively to diagnose brain diseases. The experimental autoimmune encephalomyelitis (EAE) disease in mice has been used as an animal model for multiple sclerosis (MS). In animal models and patients with MS, MRI detects T1 black holes in the brain and spinal cord [95,96]. In EAE animals, T1- and T2-weighted images using high-resolution spin-echo sequences are being used to determine the lesion loads. With the help of MRI contrast agents (*e.g.*, Gd-DTPA, Gd-DOTA), Type A or B lesions can be detected where the hypo-intensity in both T1- and T2-weighted MRI is usually related to Type A lesions. In contrast, Type B lesions usually are correlated with the observation of hyper-intensity in T2-weighted MRI with reduced signal of T1-weighted MRI [97]. A high infiltration of inflammatory cells and myelin loss are indications of Type A lesions; moderate inflammatory cell infiltration and myelin loss correspond to type B lesions [97].

The brain deposition of an MRI contrast agent, Gd-DTPA, has been used to assess the development of MS in patients as well as in EAE animal models. Prior to the infiltration of immune cells, the BBB breakdown is manifested in the leakiness of the paracellular pathways, allowing higher Gd-DTPA permeation through the BBB. In addition, ultra-small particles of iron oxide (USPIO) have been used to track brain infiltration of macrophages and monocytes as a diagnostic for the development of MS disease. In this case, USPIO 7228 (600 μmol iron oxide/kg) was administered via I.V. injection into EAE mice. Because macrophages and monocytes can engulf the particles in the blood stream, the level of immune cell infiltration of the brain can be quantified by determining the accumulation of iron oxide particles in the brain tissue using MRI [98]. T2 maps of MRI using a spin-echo sequence acquired 24 h after injection were used to determine the amount of iron oxide particles in the brain. One of the limitations of using USPIO particles is that

it is difficult to differentiate the brain infiltration between pro-inflammatory and anti-inflammatory cells [99].

Iron oxide particles have different sizes that can be divided into ultra-small superparamagnetic iron oxide (USPIO, 10–50 nm), superparamagnetic iron oxide (SPIO, 50–100 nm), and micrometer-sized iron oxide (MPIO, >1 μm). These particles are usually coated with a polymer shell containing citrate or dextran, which can be detected as a negative contrast on T2-weighted MRI images due to their large negative magnetic properties [91]. The USPIO image in MRI has also been used to detect lesions that have low T2 signal in EAE. As mentioned previously, the presence of USPIO in the brain due to phagocytosis by immune cells was confirmed using *ex vivo* brain histological studies. The MRI signal enhancement from USPIO is normally compared to Gd-DOTA enhancement because Gd-DOTA brain deposition is due to paracellular BBB breakdown. The USPIO lesion volume at the peak of disease in EAE can be correlated with stages of inflammation, phagocyte infiltration, demyelination, and axonal damage in the central nervous systems [100]. Iron oxide particles have also been used to track C6 cells in the *in vivo* rat glioma model because C6 cells have been shown to phagocytose nanoparticles with a diameter of 20 nm [101]. This method was later used in humans suffering from glial tumors, and the tumors were found to have high iron oxide signal compared to the Gd-DTPA signal [101].

The upregulation of VCAM-1 expression on the BBB endothelial cell during neuroinflammation can be determined using MPIO decorated with anti-VCAM-1 mAb (VCAM-1-MPIO) [102]. In this case, the animals were treated with IL-1β cytokine intracerebral injection for inducing neuroinflammation. The accumulation of VCAM-1-MPIO was detected by T2-signal of MRI caused by particles bound to the BBB endothelium. This particle accumulation was inhibited when anti-VCAM-1 was delivered prior to the delivery of VCAM-1-MPIO, indicating

that the particles bind specifically to VCAM-1 on the surface of endothelium [102]. In EAE mice, VCAM-1-MPIO particles were detected in all visible lesions that were detected using Gd-DTPA. However, VCAM-1-MPIO can also detect additional lesions that correspond to leukocyte infiltration across the BBB [103].

Similar to VCAM-1, ICAM-1 is also upregulated during neuroinflammation and this upregulation can be detected using Gd-loaded liposomes decorated with anti-ICAM-1 mAb [94]. The upregulation of ICAM-1 in EAE was detected using MRI [94]. In the *in vivo* stroke animal model, MPIO decorated with anti-ICAM-1 (ICAM-1-MPIO) showed increased T2 signal in brain areas one hour after induction of transient middle cerebral artery occlusion (MCAO) [104]. Similarly, the same ICAM-1-MPIO detected the upregulation of ICAM-1 in the brain after radiation injury [105].

Neuroinflammation in the brain induces oxidative stress that is mediated by activation of myeloperoxidase (MPO) that is secreted by macrophages and monocytes [106]. MPO activation converts H_2O_2 into HOCl in the inflamed tissues, which can be used as biomarker for imaging of brain tissue at a molecular level. Because oligomerization of Gd-DOTA was previously shown to enhance MRI signal in tissues, Gd-bis-5-HT-DTPA (**Figure 1.4**) was designed to oligomerize and react with surrounding proteins in the brain tissue during activation of MPO in neuroinflammation process [106]. The activation of MPO in EAE mice was used for early detection of the disease. In this case, oxidation of 5-HT moiety on the probe induces probe reaction and oligomerization to surrounding proteins, which causes an increase in T1 relaxation time observed by MRI. This model can detect smaller active brain lesions better than Gd-DTPA alone in EAE mice [107]. Further, the enhanced MRI images were located at MPO-expressing cells and demyelinated areas in EAE mice. This method has the potential for early detection in patients with a presymptomatic stage of

MS.

The oxidative stress process generates free radicals, which can be detected or trapped by 5,5-dimethyl-1-pyrroline N-oxide (DMPO, **Figure 1.4**). An antibody to DMPO was conjugated to bovine serum albumin (BSA)-linked to Gd-DTPA-biotin to make a DMPO-mAb-BSA-Gd-DTPA-biotin conjugate or anti-DMPO probe. After DMPO is delivered, it will react with membrane-bound radicals (MBR) to produce DMPO-MBR in various tissues [108]. The DMOP-MBR can then be detected and localized by an anti-DMPO probe in a certain tissue as a measure of free radicals in the tissue. The localization and concentration of the anti-DMPO probe can be determined by MRI via detection of Gd-DTPA [108]. The localization of anti-DMPO using MRI can also be confirmed by delivering streptavidin-Cy3, which strongly binds to the biotin segment linked to DMPO probe. This method has been successful in detecting free radical formation in the lung, kidney, and liver of the streptozotocin-induced diabetic mouse model. Due to the large size of the DMPO probe, this method can only be used in tissues or organs outside of the brain. The use of this method to detect free radicals in the brain is only possible when restriction of large molecules through the BBB can be overcome.

1.5.2. PET and SPEC Imaging:

During tumor angiogenesis, $\alpha_v\beta_3$ integrins are upregulated on the vasculature endothelial cells. Cyclic arginine-glycine-aspartic acid (RGD) peptides have been developed to selectively bind $\alpha_v\beta_3$ integrins; they have been investigated using diagnostic tools for tumor angiogenesis. Cyclic RGD peptides were conjugated with ^{18}F-galacto for detection of $\alpha_v\beta_3$ upregulation using PET and SPECT, respectively, during angiogenesis in tumor growth in humans [109]. In human studies, ^{18}F-galacto-RGD as a detector of angiogenesis was compared to ^{18}F-fluorodeoxyglucose (^{18}F-

FDG, **Figure 1.4**) as a substrate to measure metabolism in primary and metastatic tumors. The images generated in tumors by both probes were observed by PET [109]. The results showed that detection with ^{18}F-FDG was more sensitive than with ^{18}F-galacto-RGD, suggesting that glucose metabolism was more pronounced than the increase in expression of $\alpha_v\beta_3$ integrins in the vascular endothelium during angiogenesis. Similarly, a ^{99m}Tc-labeled RGD peptide called ^{99m}Tc-NC100692 has been used to detect upregulation of $\alpha_v\beta_3$ integrins in the vascular endothelium during angiogenesis. Although this radiotracer can detect breast cancer, the high uptake and clearance by the liver makes the use of this molecule inefficient for liver cancer diagnostic purposes. In addition to issues regarding the high clearance of the ^{99m}Tc-labeled RGD peptide, its use has not been explored for brain diseases due to its inability to cross the BBB. To improve the binding efficiency of RGD-derived radiotracers, multimeric cyclic RGD-peptides were developed. However, most studies of these multimeric RGD-peptides have only been carried out *in vitro* although, in general, the multimeric cyclic RGD radiotracers are more efficient than the monomeric cyclic RGD radiotracers [110].

A translocator protein (TSPO) is upregulated in micro- and macroglia cells during neuroinflammation; thus, the upregulation of this protein has been used as a diagnostic target of neurological diseases in rodents and humans [111]. The increase in expression of TSPO can be detected using ^{11}C-PK11195 (**Figure 1.4**) as a ligand of TSPO, and the increased uptake of ^{11}C-PK11195 by glial cells in a stroke rat model compared to normal rats has been observed using PET. Similarly, the increase in deposition of ^{11}C-PK11195 at the entorhinal, temporoparietal, and cingulate cortices of the brains of the transgenic Alzheimer's disease mouse model were observed due to the upregulation of TSPO. In addition, ^{11}C-PK11195 can detect microglia activation in traumatic brain injury (TBI), stroke, and MS patients [112]. Brain lesions were detected using

localization of ^{11}C-PK11195 in the brains of MS patients, and the detected lesions were similar to those identified using MRI. One of the disadvantages of *in vivo* detection of ^{11}C-PK11195 is that the observed signal-to-noise ratio is poor due to high levels of non-specific binding of the ligand to non-targeted cells or tissues. In addition, ^{11}C-PK11195 has a short *in vivo* half-life (*i.e.*, 20 min). As an alternative, a higher selectivity ligand, 1C-DAA1106 (**Figure 1.4**), has been developed and evaluated in rodent models of Parkinson's disease and TBI to overcome the poor signal-to-noise ratio of ^{11}C-PK11195 [113].

Leukocyte trafficking into the brain can also be followed using SPECT. In this case, the leukocytes are labeled with ^{99m}technetium (^{99m}Tc) or indium-111 (^{111}I). However, ^{111}I was found to be more toxic than ^{99m}Tc and can damage the leukocytes and their DNA [114]. The location of injected ^{99m}Tc-labeled leukocytes can be detected in the region of stroke damage in the brain using SPECT [115]. Similarly, PET/CT imaging with ^{18}F-FDG has also been used to monitor the location of injected cells to detect neuroinflammation; unfortunately, the success in using ^{18}F-FDG has been modest due to the short half-life of the radiolabel. Furthermore, ^{18}F-FDG can be released from the target cell to cause images to have high background noise.

Axon demyelination is a hallmark of MS, and early detection of demyelination *in vivo* is useful for MS patients to determine the course of treatment. Congo red has been shown to bind myelin, and ^{11}C-labeled Congo red has been used for detecting demyelination using PET imaging [116]. The advantage of Congo red is that it can readily cross the BBB due to its favorable physicochemical to diffuse through the cellular membranes of the vascular endothelial cells of the BBB. This method is promising because it has been shown to detect the demyelination in the brains of baboons. However, due to the hydrophobic nature of Congo red, it has low water solubility; thus, ^{11}C-CIC (**Figure 1.4**) was also developed to improve its solubility while it still can penetrate

the BBB to selectively bind to myelin rat brains to detect demyelination in EAE mice [117,118].

The ability to detect neuronal cell death can be very useful for early diagnosis of MS, Alzheimer's, and Parkinson's diseases because cell death is irreversible during the progression of these diseases. ^{11}C-flumazenil (**Figure 1.4**) has been evaluated to detect neuronal lost in the brain of Alzheimer's disease patients because ^{11}C-flumazenil binds to $GABA_A$ receptors that are downregulated during neuronal damage in the brain [119]. Thus, the downregulation of $GABA_A$ receptors can be detected by method ^{11}C-flumazenil using PET. In early Alzheimer's disease in patients, there is a decrease in ^{11}C-flumazenil signals in several different parts of the brain including several cortical regions and posterior prediluvian regions. This method has also been used to determine neuronal damage in early stages of stroke [120].

Neuronal cell death is correlated with the apoptotic process that expresses cell surface phosphatidylserine. Thus, ^{99m}TC labeled annexin-V can be used to image the presence of phosphatidylserine on the surfaces of dead neuronal cells [121]. SPECT imaging has been used to detect ^{99m}TC-labeled during fulminant hepatic cell apoptosis in a mouse model. In addition, ^{99m}Tc-annexin-V can detect neuronal damage in ischemic stroke patients. In Alzheimer's disease patients, the uptake of ^{99m}Tc-annexin-V in the cortex was increased; although the BBB normally does not allow such a large protein to penetrate, it is plausible that the brain uptake of annexin is due to the leakiness of the BBB [122-124]. Clinically, ^{99m}Tc-labeled annexin-V has been used to detect cell death after organ rejection during transplantation [125].

1.5.3. Near IR Fluorescence:

Near IR fluorescence (NIRF) dyes have been used to detect molecules in the brain that cross the BBB as well as in detecting tumor angiogenesis and localization of tumors for surgery. NIRF

imaging can be done *in vivo* in a non-invasive manner because of low scattering, tissue absorption, and autofluorescence of tissues at 700–900 nm. Brain depositions of NIRF dyes and their conjugation to molecules (*i.e.*, peptides, proteins, PEG) can be detected after their delivery using BBB modulator peptides to improve their penetration through the BBB [87,89]. The quantity of the delivered molecules in the brains can be conveniently determined by integrating the fluorescence intensity from the NIRF image.

The NIRF tumor image from IR780 dye (**Figure 1.4**) has been used to determine the location and size of glioma tumors in the brain. IR780 has low toxicity and high tumor targeting properties; however, it has low solubility that limits its preclinical and clinal applications [126]. To overcome the solubility problem, IR780 dye was formulated in liposome (IR780-liposomes, size 95 nm) and phospholipid micelle (IR780-micelles, size 26 nm) nanoparticles. It was found that the IR780-micelles were more stable than IR780-liposomes. Using confocal microscopy, *in vitro* incubation of IR780-micelles in a glioma cell culture resulted in uptake and detection of micelles in the intracellular space of U87MG glioma cells [126]. IR780-micelles were also intravenously delivered via tail vein into mice with glioma brain tumors in which U87MG glioma cells were ectopically and orthotopically xenografted into the brains [126]. IR780-micelles were accumulated in orthotopic xenograft tumors and could be detected using NIRF imaging 4 days after delivery. It was proposed that solid tumor accumulation of micelles was due to enhanced permeability and retention (EPR) effect of the micelle nanoparticles in the vasculatures. As a negative control, there was no observable NIRF image of micelles found in healthy mice. The tumor-specific targeting of IR780-micelles has been confirmed by *ex vivo* NIRF imaging of the brain [126].

NIR dyes have also been used to detect brain tumor xenografts using photoacoustic (PA)

imaging method with the goal of localizing tumors for surgery [127]. The PA image is produced by reconstructing collected acoustic waves from the NIR dye-conjugated nanoparticles that are excited by a laser beam penetrating deep into the tissue [127]. In general, PA detection of brain tumors using NIR-I wavelengths (650–980 nm) has a weak light signal due to the signal dampening by the skull. To overcome this problem, NIR-II-conjugate nanoparticles using P1 chromophore (**Figure 1.4**) were designed with an excitation of 1064 nm to avoid tissue suppression for better signal-to-noise ratio than with NIR-I. In this study, orthotopic xenografts of brain tumors were generated with luciferase-labelled U87 cells, and the presence, location, and size of the tumor was determined using MRI. Then, NIR-II nanoparticles were administered to the mice with brain tumor, followed by PA scanning. The results showed an increase in tumor detection with high background 1 h after administration; after 24 h, the image was observed exclusively from the tumor. There was 94-fold higher signal from the tumor than from the background before the administration of NIR-II-NP.

1.6. Conclusion:

The progress in diagnosing and treating brain diseases has been very slow because of the difficulty in delivering molecules non-invasively to the brain. Early diagnosis of brain diseases has been difficult, but it is important for halting the diseases in the early stage. Many advances have been made using small molecules to detect changes in the brain and to treat brain diseases. However, these advances are not occurring fast enough to overcome many problems in diagnosis and treatments of brain diseases. Many very selective and potent molecules such as peptides, proteins, carbohydrates, and oligonucleotides that can used for treatment of brain diseases have failed to advance in the clinic due to their inability to cross the BBB to exert their biological

activities in the brain. Thus, much effort should be devoted to improving the delivery of these molecules to the brain. Limited success has been achieved in delivering large molecules into the brain; however, the efficiencies of the methods used are lower than expected. The use of particles and exosomes for delivering diagnostics or therapeutics to the brain is still in the early stages and, due to the nature of the BBB, the use of particles for brain delivery could encounter an even higher barrier than that for delivering large molecules such as antibodies. Overall, there is a need to increase efforts in the brain delivery area to help in basic and applied sciences to solve brain disease problems as well as to study how the brain works at cellular levels.

1.7. Tables, Figures, and Figure Legends:

A

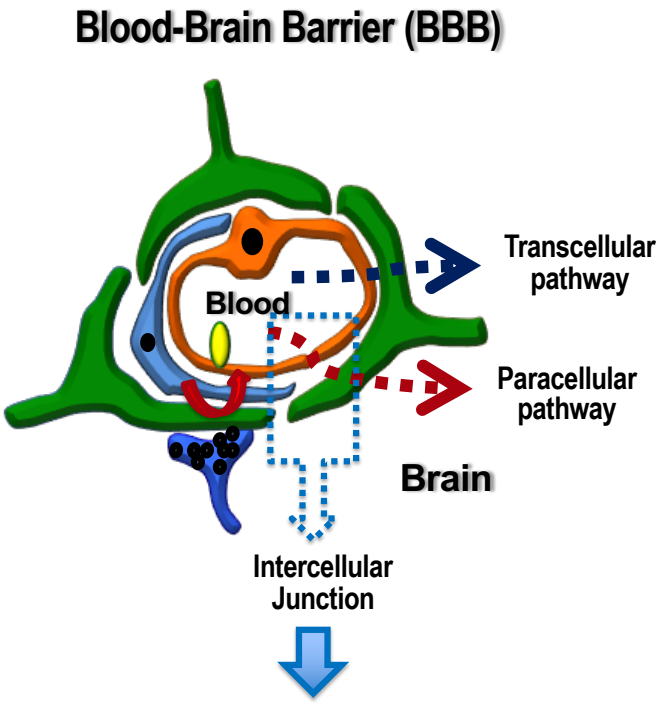
Blood-Brain Barrier (BBB)
Blood
Transcellular pathway
Paracellular pathway
Brain
Intercellular Junction

B

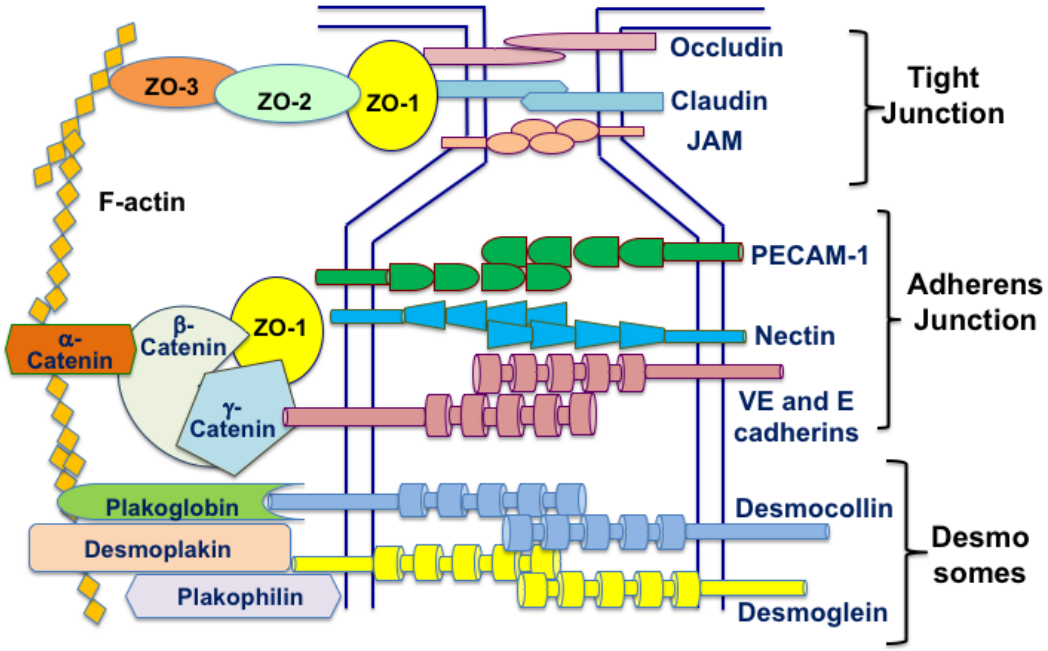
ZO-3
ZO-2
ZO-1
Occludin
Claudin
JAM
Tight Junction
F-actin
PECAM-1
α-Catenin
β-Catenin
ZO-1
Nectin
γ-Catenin
VE and E cadherins
Adherens Junction
Plakoglobin
Desmoplakin
Plakophilin
Desmocollin
Desmoglein
Desmo somes

Figure 1.1. (A) A cross-section diagram of the vascular endothelial cells of the BBB surrounded by pericytes, astrocytes, and neurons. Molecules that cross the BBB via transcellular- or paracellular-transport pathway are indicated by two different arrows. The presence of efflux pumps prevents some molecules to diffuse transcellularly across the membranes of the BBB. **(B)** A representation of the intercellular junction of microvessel endothelial cells of the BBB, which is composed of tight junction, *adherens* junction, and demosomes regions. The protein-protein interactions at the extracellular space act as "Velcro" to connect the membranes between opposing cells. The protein-protein interactions in the intercellular junctions are connected via cross-talk of the protein-protein interactions in the cytoplasmic domain.

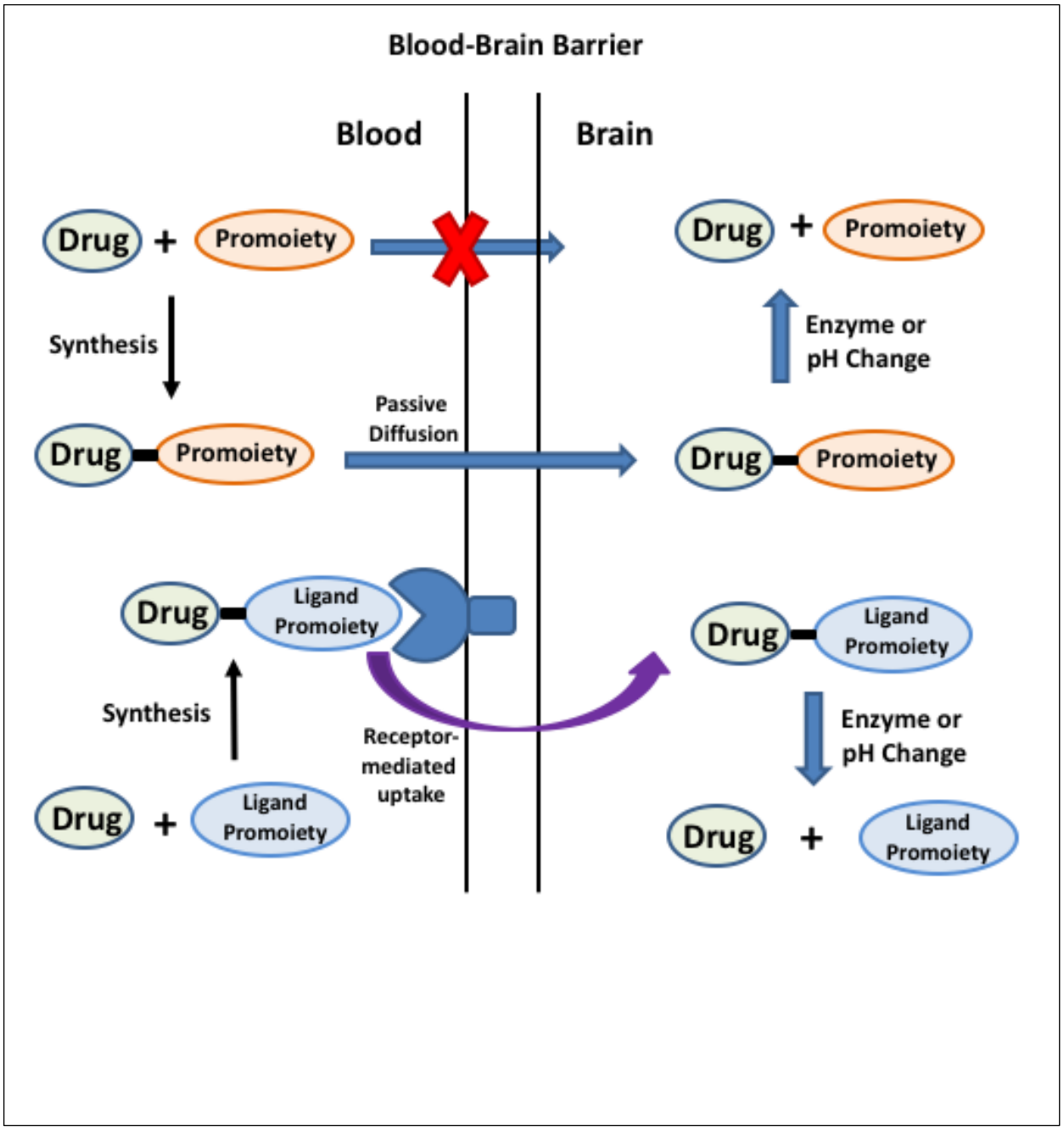

Figure 1.2. The formation of prodrug molecules has been done to improve the delivery of drug molecules across the BBB. The formation of a prodrug changes the physicochemical properties to allow efficient partition into cell membranes for passive diffusion across the BBB. Ligand-conjugated prodrugs were also used to target BBB transport receptors to shuttle the prodrug from

the blood to the brain. The prodrugs are converted to the parent drug by enzymes such as esterase or by chemical reaction upon pH change.

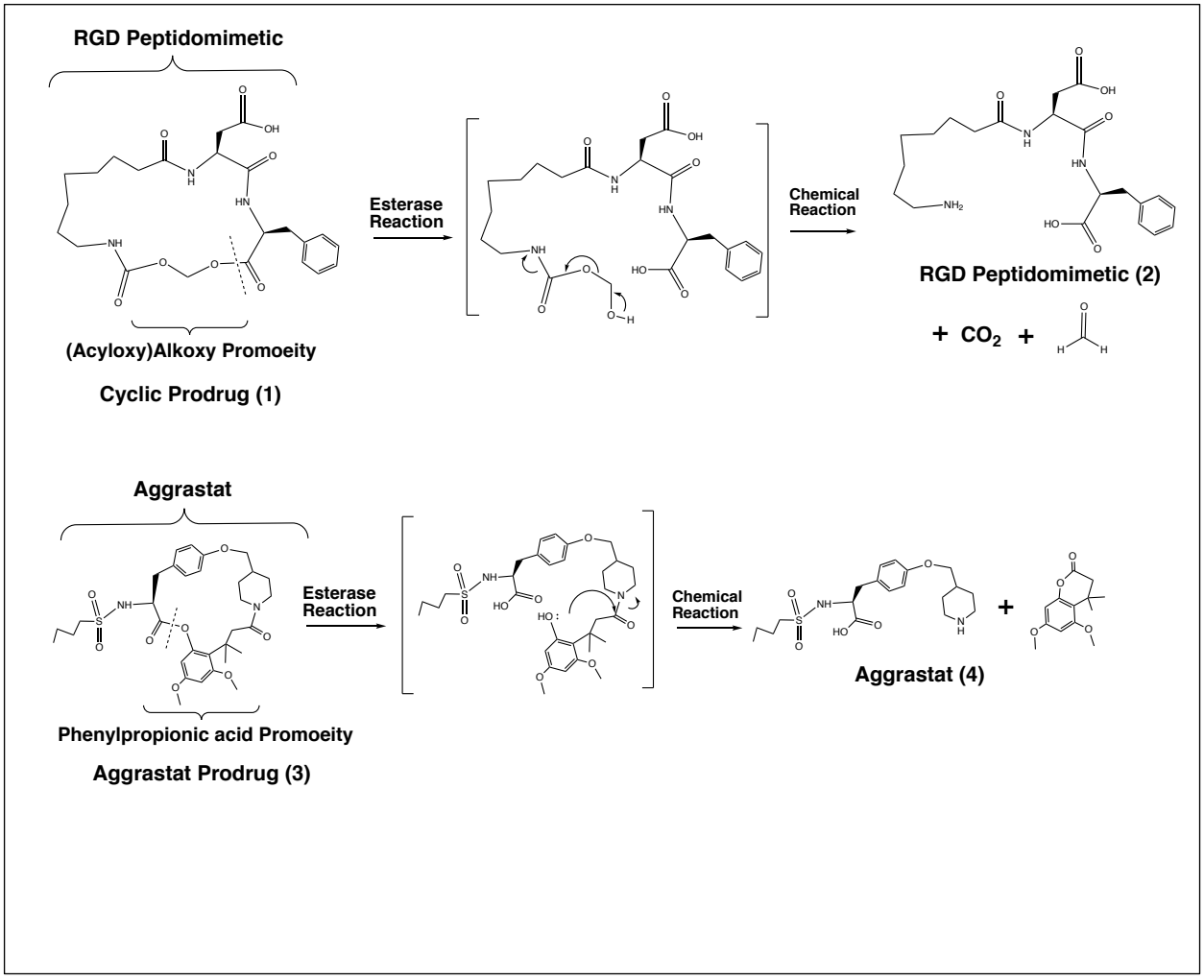

Figure 1.3. Cyclic prodrugs (**1** and **3**) from RGD-peptidomimetic (**2**) and Aggrastat (**4**) using (acyloxy)alkoxy and phenylpropionic acid promoieties, respectively. The cyclic prodrugs can be converted by clipping the ester bond by esterase to make the intermediate. The intermediates rapidly degraded chemically to release the parent drugs.

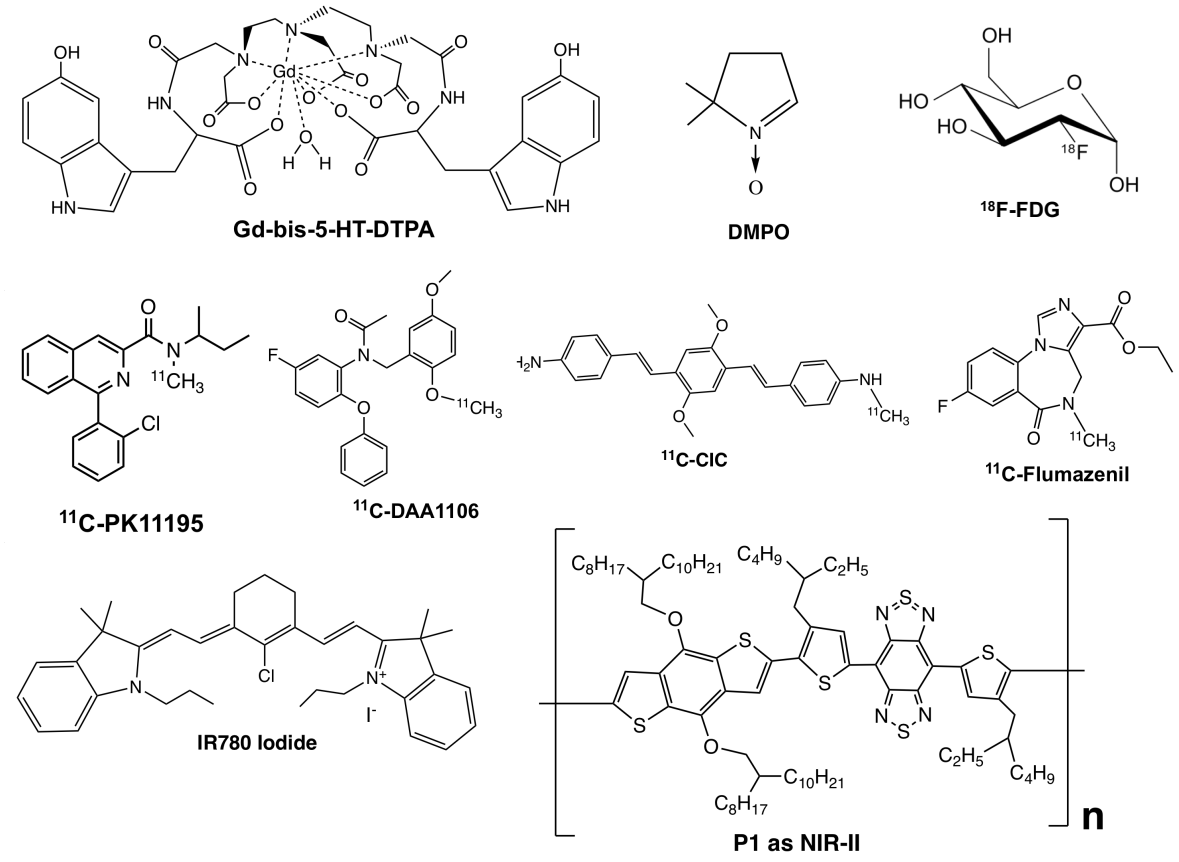

Figure 1.4. Structures of molecules used in brain analysis including: (a) Gd-bis-5-HT-DTPA, (b) DMPO, (c) ^{18}F-FDG, (d) ^{11}C-PK11195, (e) ^{11}C-DAA1106, (f) ^{11}C-CIC, (g) ^{11}C-Flumazenil, (h) IR780 Iodide, and (i) P1 as NIR-II dye.

Table 1.1. Peptide Names and Sequences

Peptide	Sequence
C1C2	SSVSQSTGQIQSKVFDSLLNLNSTLQATR-NH_2
OCC2	GVNPQAQMSSGYYYSPLLAMC(Acm)SQAYGSTYLNQYIYHYC(Acm)TVDPQE; Acm = Acetamido methyl
AT-1002	FCIGRL
PN-78	FDFWITP
PN-159	KLALKLALKALKLAALKLA-NH_2
HAV6	Ac-SHAVSS-NH_2
ADTC5	Cyclo1,7(CDTPPVC)
cIBR7	Cyclo1,8(CPRGGSVC)
cLABL	Cyclo1,12(PenITDGEATDSGC)

1.8. References:

1. Schabitz WR, Schwab S, Spranger M, Hacke W (1997) Intraventricular brain-derived neurotrophic factor reduces infarct size after focal cerebral ischemia in rats. J Cereb Blood Flow Metab 17 (5):500-506. doi:10.1097/00004647-199705000-00003
2. Laksitorini M, Prasasty VD, Kiptoo PK, Siahaan TJ (2014) Pathways and progress in improving drug delivery through the intestinal mucosa and blood-brain barriers. Therapeutic delivery 5 (10):1143-1163. doi:10.4155/tde.14.67
3. Lutz KL, Siahaan TJ (1997) Molecular structure of the apical junction complex and its contribution to the paracellular barrier. J Pharm Sci 86:977–984
4. Zheng K, Trivedi M, Siahaan TJ (2006) Structure and function of the intercellular junctions: barrier of paracellular drug delivery. Current pharmaceutical design 12:2813–2824
5. Kiptoo P, Laksitorini MD, Siahaan TJ (2013) Blood-Brain Peptides: Peptide Delivery. In: Kastin A (ed) Handbook of Biologically Active Peptides. Academic Press, Boston, pp 1702–1710
6. Adson A, Raub TJ, Burton PS, Barsuhn CL, Hilgers AR, Audus KL, Ho NFH (1994) Quantitative approaches to delineate paracellular diffusion in cultured epithelial cell monolayers. J Pharm Sci 83:1529–1536
7. Gumbleton M, Audus KL (2001) Progress and limitations in the use of in vitro cell cultures to serve as a permeability screen for the blood-brain barrier. Journal of pharmaceutical sciences 90:1681–1698
8. Kuntz M, Mysiorek C, Petrault O, Petrault M, Uzbekov R, Bordet R, Fenart L, Cecchelli R, Berezowski V (2014) Stroke-induced brain parenchymal injury drives blood-brain barrier

early leakage kinetics: a combined in vivo/in vitro study. J Cereb Blood Flow Metab 34 (1):95-107. doi:10.1038/jcbfm.2013.169

9. Lippmann ES, Al-Ahmad A, Azarin SM, Palecek SP, Shusta EV (2014) A retinoic acid-enhanced, multicellular human blood-brain barrier model derived from stem cell sources. Sci Rep 4:4160. doi:10.1038/srep04160
10. Wilhelm I, Krizbai IA (2014) In vitro models of the blood-brain barrier for the study of drug delivery to the brain. Molecular pharmaceutics 11 (7):1949-1963. doi:10.1021/mp500046f
11. Chen S, Einspanier R, Schoen J (2015) Transepithelial electrical resistance (TEER): a functional parameter to monitor the quality of oviduct epithelial cells cultured on filter supports. Histochem Cell Biol 144 (5):509-515. doi:10.1007/s00418-015-1351-1
12. Cucullo L, Marchi N, Hossain M, Janigro D (2011) A dynamic in vitro BBB model for the study of immune cell trafficking into the central nervous system. J Cereb Blood Flow Metab 31 (2):767-777. doi:10.1038/jcbfm.2010.162
13. Griep LM, Wolbers F, de Wagenaar B, ter Braak PM, Weksler BB, Romero IA, Couraud PO, Vermes I, van der Meer AD, van den Berg A (2013) BBB on chip: microfluidic platform to mechanically and biochemically modulate blood-brain barrier function. Biomed Microdevices 15 (1):145-150. doi:10.1007/s10544-012-9699-7
14. S Shityakov S, Salvador E, Förster C (2013) In silico, in vitro and in vivo methods to analyse drug permeation across the blood–brain barrier: A critical review. OA Anaesthetics 1:1-7
15. Carpenter TS, Kirshner DA, Lau EY, Wong SE, Nilmeier JP, Lightstone FC (2014) A method to predict blood-brain barrier permeability of drug-like compounds using molecular dynamics simulations. Biophys J 107 (3):630-641. doi:10.1016/j.bpj.2014.06.024

16. Lipinski CA, Lombardo F, Dominy BW, Feeney PJ (2001) Experimental and computational approaches to estimate solubility and permeability in drug discovery and development settings. Advanced drug delivery reviews 46 (1-3):3-26
17. Lipinski CA (2004) Lead- and drug-like compounds: the rule-of-five revolution. Drug Discov Today Technol 1 (4):337-341. doi:10.1016/j.ddtec.2004.11.007
18. Lipinski CA (2016) Rule of five in 2015 and beyond: Target and ligand structural limitations, ligand chemistry structure and drug discovery project decisions. Advanced drug delivery reviews 101:34-41. doi:10.1016/j.addr.2016.04.029
19. Lecomte JM, Costentin J, Vlaiculescu A, Chaillet P, Marcais-Collado H, Llorens-Cortes C, Leboyer M, Schwartz JC (1986) Pharmacological properties of acetorphan, a parenterally active "enkephalinase" inhibitor. The Journal of pharmacology and experimental therapeutics 237 (3):937-944
20. Oldendorf WH, Hyman S, Braun L, Oldendorf SZ (1972) Blood-brain barrier: penetration of morphine, codeine, heroin, and methadone after carotid injection. Science 178 (4064):984-986
21. Banks WA (2009) Characteristics of compounds that cross the blood-brain barrier. BMC Neurol 9 Suppl 1:S3. doi:10.1186/1471-2377-9-S1-S3
22. Stella VJ, Nti-Addae KW (2007) Prodrug strategies to overcome poor water solubility. Advanced drug delivery reviews 59 (7):677-694. doi:10.1016/j.addr.2007.05.013
23. Dhareshwar SS, Stella VJ (2010) A novel prodrug strategy for beta-dicarbonyl carbon acids: syntheses and evaluation of the physicochemical characteristics of C-phosphoryloxymethyl (POM) and phosphoryloxymethyloxymethyl (POMOM) prodrug derivatives. Journal of pharmaceutical sciences 99 (6):2711-2723. doi:10.1002/jps.22021

24. Borchardt RT, Jeffrey A, Siahaan TJ, Gangwar S, Pauletti GM (1997) Improvement of oral peptide bioavailability: Peptidomimetics and prodrug strategies. Advanced drug delivery reviews 27 (2-3):235-256. doi:S0169409X97000458 [pii]

25. Gangwar S, Pauletti GM, Siahaan TJ, Stella VJ, Borchardt RT (1999) Synthesis of an esterase-sensitive cyclic prodrug of a model hexapeptide having enhanced membrane permeability and enzymatic stability using an acyloxyalkoxy promoiety. Methods Mol Med 23:37-51. doi:10.1385/0-89603-517-4:37

26. He HT, Xu CR, Song X, Siahaan TJ (2003) Syntheses of cyclic prodrugs of RGD peptidomimetics with various macrocyclic ring sizes: evaluation of physicochemical, transport and antithrombic properties. J Pept Res 61 (6):331-342

27. Song X, He HT, Siahaan TJ (2002) Synthesis of cyclic prodrugs of Aggrastat and its analogue with a modified phenylpropionic acid linker. Org Lett 4 (4):549-552

28. Song X, Xu CR, He HT, Siahaan TJ (2002) Synthesis of a novel cyclic prodrug of RGD peptidomimetic to improve its cell membrane permeation. Bioorg Chem 30 (4):285-301

29. Wang W, Camenisch G, Sane DC, Zhang H, Hugger E, Wheeler GL, Borchardt RT, Wang B (2000) A coumarin-based prodrug strategy to improve the oral absorption of RGD peptidomimetics. Journal of controlled release : official journal of the Controlled Release Society 65 (1-2):245-251

30. Pauletti GM, Gangwar S, Okumu FW, Siahaan TJ, Stella VJ, Borchardt RT (1996) Esterase-sensitive cyclic prodrugs of peptides: Evaluation of an acyloxyalkoxy promoiety in a model hexapeptide. Pharm Res 13:1613–1621

31. Gudmundsson OS, Pauletti GM, Wang W, Shan D, Zhang H, Wang B, Borchardt RT (1999) Coumarinic acid-based cyclic prodrugs of opioid peptides that exhibit metabolic stability to peptidases and excellent cellular permeability. Pharm Res 16 (1):7-15

32. Boado RJ, Zhang Y, Wang Y, Pardridge WM (2009) Engineering and expression of a chimeric transferrin receptor monoclonal antibody for blood-brain barrier delivery in the mouse. Biotechnol Bioeng 102 (4):1251-1258. doi:10.1002/bit.22135

33. Boado RJ, Zhang Y, Zhang Y, Pardridge WM (2007) Genetic engineering, expression, and activity of a fusion protein of a human neurotrophin and a molecular Trojan horse for delivery across the human blood-brain barrier. Biotechnol Bioeng 97 (6):1376-1386. doi:10.1002/bit.21369

34. Boado RJ, Zhou QH, Lu JZ, Hui EK, Pardridge WM (2010) Pharmacokinetics and brain uptake of a genetically engineered bifunctional fusion antibody targeting the mouse transferrin receptor. Molecular pharmaceutics 7 (1):237-244. doi:10.1021/mp900235k

35. Pardridge WM (2002) Blood-brain barrier drug targeting enables neuroprotection in brain ischemia following delayed intravenous administration of neurotrophins. Adv Exp Med Biol 513:397-430

36. Zhang Y, Pardridge WM (2006) Blood-brain barrier targeting of BDNF improves motor function in rats with middle cerebral artery occlusion. Brain research 1111 (1):227-229. doi:10.1016/j.brainres.2006.07.005

37. Paterson J, Webster CI (2016) Exploiting transferrin receptor for delivering drugs across the blood-brain barrier. Drug Discov Today Technol 20:49-52. doi:10.1016/j.ddtec.2016.07.009

38. Friden PM, Walus LR, Musso GF, Taylor MA, Malfroy B, Starzyk RM (1991) Anti-transferrin receptor antibody and antibody-drug conjugates cross the blood-brain barrier.

Proceedings of the National Academy of Sciences of the United States of America 88 (11):4771-4775

39. Jefferies WA, Brandon MR, Hunt SV, Williams AF, Gatter KC, Mason DY (1984) Transferrin receptor on endothelium of brain capillaries. Nature 312 (5990):162-163

40. Pardridge WM, Buciak JL, Friden PM (1991) Selective transport of an anti-transferrin receptor antibody through the blood-brain barrier in vivo. The Journal of pharmacology and experimental therapeutics 259 (1):66-70

41. Moos T, Morgan EH (1998) Evidence for low molecular weight, non-transferrin-bound iron in rat brain and cerebrospinal fluid. J Neurosci Res 54 (4):486-494. doi:10.1002/(SICI)1097-4547(19981115)54:4<486::AID-JNR6>3.0.CO;2-I

42. Kharitonova T, Ahmed N, Thoren M, Wardlaw JM, von Kummer R, Glahn J, Wahlgren N (2009) Hyperdense middle cerebral artery sign on admission CT scan--prognostic significance for ischaemic stroke patients treated with intravenous thrombolysis in the safe implementation of thrombolysis in Stroke International Stroke Thrombolysis Register. Cerebrovasc Dis 27 (1):51-59. doi:000172634 [pii] 10.1159/000172634

43. Lee HJ, Engelhardt B, Lesley J, Bickel U, Pardridge WM (2000) Targeting rat anti-mouse transferrin receptor monoclonal antibodies through blood-brain barrier in mouse. The Journal of pharmacology and experimental therapeutics 292 (3):1048-1052

44. Shi N, Zhang Y, Zhu C, Boado RJ, Pardridge WM (2001) Brain-specific expression of an exogenous gene after i.v. administration. Proceedings of the National Academy of Sciences of the United States of America 98 (22):12754-12759. doi:10.1073/pnas.221450098

45. Lee HJ, Zhang Y, Zhu C, Duff K, Pardridge WM (2002) Imaging brain amyloid of Alzheimer disease in vivo in transgenic mice with an Abeta peptide radiopharmaceutical. J Cereb Blood Flow Metab 22 (2):223-231. doi:10.1097/00004647-200202000-00010

46. Yu YJ, Zhang Y, Kenrick M, Hoyte K, Luk W, Lu Y, Atwal J, Elliott JM, Prabhu S, Watts RJ, Dennis MS (2011) Boosting brain uptake of a therapeutic antibody by reducing its affinity for a transcytosis target. Sci Transl Med 3 (84):84ra44. doi:10.1126/scitranslmed.3002230

47. Sade H, Baumgartner C, Hugenmatter A, Moessner E, Freskgard PO, Niewoehner J (2014) A human blood-brain barrier transcytosis assay reveals antibody transcytosis influenced by pH-dependent receptor binding. PLoS One 9 (4):e96340. doi:10.1371/journal.pone.0096340

48. Bien-Ly N, Yu YJ, Bumbaca D, Elstrott J, Boswell CA, Zhang Y, Luk W, Lu Y, Dennis MS, Weimer RM, Chung I, Watts RJ (2014) Transferrin receptor (TfR) trafficking determines brain uptake of TfR antibody affinity variants. J Exp Med 211 (2):233-244. doi:10.1084/jem.20131660

49. Niewoehner J, Bohrmann B, Collin L, Urich E, Sade H, Maier P, Rueger P, Stracke JO, Lau W, Tissot AC, Loetscher H, Ghosh A, Freskgard PO (2014) Increased brain penetration and potency of a therapeutic antibody using a monovalent molecular shuttle. Neuron 81 (1):49-60. doi:10.1016/j.neuron.2013.10.061

50. Wang YY, Lui PC, Li JY (2009) Receptor-mediated therapeutic transport across the blood-brain barrier. Immunotherapy 1 (6):983-993. doi:10.2217/imt.09.75

51. van Rooy I, Mastrobattista E, Storm G, Hennink WE, Schiffelers RM (2011) Comparison of five different targeting ligands to enhance accumulation of liposomes into the brain. Journal

of controlled release : official journal of the Controlled Release Society 150 (1):30-36. doi:10.1016/j.jconrel.2010.11.014

52. Gaillard PJ, de Boer AG (2006) A novel opportunity for targeted drug delivery to the brain. Journal of controlled release : official journal of the Controlled Release Society 116 (2):e60-62. doi:10.1016/j.jconrel.2006.09.050

53. Gaillard PJ, Visser CC, de Boer AG (2005) Targeted delivery across the blood-brain barrier. Expert Opin Drug Deliv 2 (2):299-309. doi:10.1517/17425247.2.2.299

54. Ulbrich K, Hekmatara T, Herbert E, Kreuter J (2009) Transferrin- and transferrin-receptor-antibody-modified nanoparticles enable drug delivery across the blood-brain barrier (BBB). Eur J Pharm Biopharm 71 (2):251-256. doi:10.1016/j.ejpb.2008.08.021

55. Laskowitz DT, Thekdi AD, Thekdi SD, Han SK, Myers JK, Pizzo SV, Bennett ER (2001) Downregulation of microglial activation by apolipoprotein E and apoE-mimetic peptides. Exp Neurol 167 (1):74-85. doi:10.1006/exnr.2001.7541

56. van Rooy I, Cakir-Tascioglu S, Hennink WE, Storm G, Schiffelers RM, Mastrobattista E (2011) In vivo methods to study uptake of nanoparticles into the brain. Pharm Res 28 (3):456-471. doi:10.1007/s11095-010-0291-7

57. Fakhari A, Baoum A, Siahaan TJ, Le KB, Berkland C (2011) Controlling ligand surface density optimizes nanoparticle binding to ICAM-1. Journal of pharmaceutical sciences 100 (3):1045-1056. doi:10.1002/jps.22342

58. Koning GA, Schiffelers RM, Wauben MH, Kok RJ, Mastrobattista E, Molema G, ten Hagen TL, Storm G (2006) Targeting of angiogenic endothelial cells at sites of inflammation by dexamethasone phosphate-containing RGD peptide liposomes inhibits experimental arthritis. Arthritis Rheum 54 (4):1198-1208. doi:10.1002/art.21719

59. Gonzalez-Chavez SA, Arevalo-Gallegos S, Rascon-Cruz Q (2009) Lactoferrin: structure, function and applications. Int J Antimicrob Agents 33 (4):301 e301-308. doi:10.1016/j.ijantimicag.2008.07.020

60. Qiao R, Jia Q, Huwel S, Xia R, Liu T, Gao F, Galla HJ, Gao M (2012) Receptor-mediated delivery of magnetic nanoparticles across the blood-brain barrier. ACS nano 6 (4):3304-3310. doi:10.1021/nn300240p

61. Ji B, Maeda J, Higuchi M, Inoue K, Akita H, Harashima H, Suhara T (2006) Pharmacokinetics and brain uptake of lactoferrin in rats. Life Sci 78 (8):851-855. doi:10.1016/j.lfs.2005.05.085

62. Jain KK (2012) Nanobiotechnology-based strategies for crossing the blood-brain barrier. Nanomedicine (Lond) 7 (8):1225-1233. doi:10.2217/nnm.12.86

63. Yang T, Martin P, Fogarty B, Brown A, Schurman K, Phipps R, Yin VP, Lockman P, Bai S (2015) Exosome delivered anticancer drugs across the blood-brain barrier for brain cancer therapy in Danio rerio. Pharm Res 32 (6):2003-2014. doi:10.1007/s11095-014-1593-y

64. Alvarez-Erviti L, Seow Y, Yin H, Betts C, Lakhal S, Wood MJ (2011) Delivery of siRNA to the mouse brain by systemic injection of targeted exosomes. Nat Biotechnol 29 (4):341-345. doi:10.1038/nbt.1807

65. Albright BH, Storey CM, Murlidharan G, Rivera RMC, Berry GE, Madigan VJ, Asokan A (2018) Mapping the Structural Determinants Required for AAVrh.10 Transport across the Blood-Brain Barrier. Molecular Therapy 26:510–523. doi:doi.org/10.1016/j.ymthe.2017.10.017

66. Agbandje-McKenna M, Kleinschmidt J (2011) AAV capsid structure and cell interactions. Methods Mol Biol 807:47-92. doi:10.1007/978-1-61779-370-7_3

67. Madigan VJ, Asokan A (2016) Engineering AAV receptor footprints for gene therapy. Curr Opin Virol 18:89-96. doi:10.1016/j.coviro.2016.05.001

68. Neuwelt EA (1984) Therapeutic potential for blood-brain barrier modification in malignant brain tumor. Prog Exp Tumor Res 28:51-66

69. Neuwelt EA, Barnett PA, McCormick CI, Remsen LG, Kroll RA, Sexton G (1998) Differential permeability of a human brain tumor xenograft in the nude rat: impact of tumor size and method of administration on optimizing delivery of biologically diverse agents. Clinical cancer research : an official journal of the American Association for Cancer Research 4 (6):1549-1555

70. Neuwelt EA, Brummett RE, Doolittle ND, Muldoon LL, Kroll RA, Pagel MA, Dojan R, Church V, Remsen LG, Bubalo JS (1998) First evidence of otoprotection against carboplatin-induced hearing loss with a two-compartment system in patients with central nervous system malignancy using sodium thiosulfate. The Journal of pharmacology and experimental therapeutics 286 (1):77-84

71. Neuwelt EA, Brummett RE, Remsen LG, Kroll RA, Pagel MA, McCormick CI, Guitjens S, Muldoon LL (1996) In vitro and animal studies of sodium thiosulfate as a potential chemoprotectant against carboplatin-induced ototoxicity. Cancer research 56 (4):706-709

72. Neuwelt EA, Frenkel EP, D'Agostino AN, Carney DN, Minna JD, Barnett PA, McCormick CI (1985) Growth of human lung tumor in the brain of the nude rat as a model to evaluate antitumor agent delivery across the blood-brain barrier. Cancer research 45 (6):2827-2833

73. Neuwelt EA, Hill SA, Frenkel EP (1984) Osmotic blood-brain barrier modification and combination chemotherapy: concurrent tumor regression in areas of barrier opening and progression in brain regions distant to barrier opening. Neurosurgery 15 (3):362-366

74. Neuwelt EA, Pagel MA, Kraemer DF, Peterson DR, Muldoon LL (2004) Bone marrow chemoprotection without compromise of chemotherapy efficacy in a rat brain tumor model. The Journal of pharmacology and experimental therapeutics 309 (2):594-599. doi:10.1124/jpet.103.063347

75. Neuwelt EA, Specht HD, Barnett PA, Dahlborg SA, Miley A, Larson SM, Brown P, Eckerman KF, Hellstrom KE, Hellstrom I (1987) Increased delivery of tumor-specific monoclonal antibodies to brain after osmotic blood-brain barrier modification in patients with melanoma metastatic to the central nervous system. Neurosurgery 20 (6):885-895

76. Neuwelt EA, Specht HD, Hill SA (1986) Permeability of human brain tumor to 99mTc-gluco-heptonate and 99mTc-albumin. Implications for monoclonal antibody therapy. J Neurosurg 65 (2):194-198. doi:10.3171/jns.1986.65.2.0194

77. Muldoon LL, Neuwelt EA (2003) BR96-DOX immunoconjugate targeting of chemotherapy in brain tumor models. J Neurooncol 65 (1):49-62

78. Zwanziger D, Hackel D, Staat C, Bocker A, Brack A, Beyermann M, Rittner H, Blasig IE (2012) A peptidomimetic tight junction modulator to improve regional analgesia. Molecular Pharmaceutics 9 (6):1785-1794. doi:10.1021/mp3000937

79. Tavelin S, Hashimoto K, Malkinson J, Lazorova L, Toth I, Artursson P (2003) A new principle for tight junction modulation based on occludin peptides. Mol Pharmacol 64:1530–1540

80. Yuan X, Lin X, Manorek G, Howell SB (2011) Challenges associated with the targeted delivery of gelonin to claudin-expressing cancer cells with the use of activatable cell penetrating peptides to enhance potency. BMC Cancer 11:61. doi:10.1186/1471-2407-11-61

81. Makagiansar I, Avery M, Hu Y, Audus KL, Siahaan TJ (2001) Improving the selectivity of HAV-peptides in modulating E-cadherin-E-cadherin interactions in the intercellular junction of MDCK cell monolayers. Pharm Res 18:446–553

82. Sinaga E, Jois SD, Avery M, Makagiansar IT, Tambunan US, Audus KL, Siahaan TJ (2002) Increasing paracellular porosity by E-cadherin peptides: Discovery of bulge and groove regions in the EC1-domain of E-cadherin. Pharm Res 19:1170–1179

83. Calcagno AM, Fostel JM, Reyner EL, Sinaga E, Alston JT, Mattes WB, Siahaan TJ, Ware JA (2004) Effects of an E-cadherin-derived peptide on the gene expression of Caco-2 cells. Pharm Res 21:2095–2104

84. Kiptoo P, Sinaga E, Calcagno AM, Zhao H, Kobayashi N, Tambunan US, Siahaan TJ (2011) Enhancement of drug absorption through the blood-brain barrier and inhibition of intercellular tight junction resealing by E-cadherin peptides. Mol Pharm 8 (1):239-249. doi:10.1021/mp100293m

85. Alaofi A, On N, Kiptoo P, Williams TD, Miller DW, Siahaan TJ (2016) Comparison of Linear and Cyclic His-Ala-Val Peptides in Modulating the Blood-Brain Barrier Permeability: Impact on Delivery of Molecules to the Brain. Journal of pharmaceutical sciences 105 (2):797-807. doi:10.1016/S0022-3549(15)00188-4

86. Laksitorini MD, Kiptoo PK, On NH, Thliveris JA, Miller DW, Siahaan TJ (2015) Modulation of intercellular junctions by cyclic-ADT peptides as a method to reversibly increase blood-brain barrier permeability. Journal of pharmaceutical sciences 104 (3):1065-1075. doi:10.1002/jps.24309

87. On NH, Kiptoo P, Siahaan TJ, Miller DW (2014) Modulation of blood-brain barrier permeability in mice using synthetic E-cadherin peptide. Molecular pharmaceutics 11 (3):974-981. doi:10.1021/mp400624v

88. Tabanor K, Lee P, Kiptoo P, Choi IY, Sherry EB, Eagle CS, Williams TD, Siahaan TJ (2016) Brain Delivery of Drug and MRI Contrast Agent: Detection and Quantitative Determination of Brain Deposition of CPT-Glu Using LC-MS/MS and Gd-DTPA Using Magnetic Resonance Imaging. Molecular pharmaceutics 13 (2):379-390. doi:10.1021/acs.molpharmaceut.5b00607

89. Ulapane KR, On N, Kiptoo P, Williams TD, Miller DW, Siahaan TJ (2017) Improving brain delivery of biomolecules via BBB modulation in mouse and rat: Detection using MRI, NIRF, mass spectrometry. Nanotheranostics 1 (217–231)

90. Alaofi A, Farokhi E, Prasasty VD, Anbanandam A, Kuczera K, Siahaan TJ (2017) Probing the interaction between cHAVc3 peptide and the EC1 domain of E-cadherin using NMR and molecular dynamics simulations. J Biomol Struct Dyn 35 (1):92-104. doi:10.1080/07391102.2015.1133321

91. Pulli B, Chen JW (2014) Imaging Neuroinflammation - from Bench to Bedside. J Clin Cell Immunol 5. doi:10.4172/2155-9899.1000226

92. Steinman L (2005) Blocking adhesion molecules as therapy for multiple sclerosis: natalizumab. Nat Rev Drug Discov 4 (6):510-518. doi:10.1038/nrd1752

93. Yusuf-Makagiansar H, Anderson ME, Yakovleva TV, Murray JS, Siahaan TJ (2002) Inhibition of LFA-1/ICAM-1 and VLA-4/VCAM-1 as a therapeutic approach to inflammation and autoimmune diseases. Med Res Rev 22 (2):146-167

94. Sipkins DA, Gijbels K, Tropper FD, Bednarski M, Li KC, Steinman L (2000) ICAM-1 expression in autoimmune encephalitis visualized using magnetic resonance imaging. Journal of neuroimmunology 104 (1):1-9

95. Zivadinov R, Rudick RA, De Masi R, Nasuelli D, Ukmar M, Pozzi-Mucelli RS, Grop A, Cazzato G, Zorzon M (2001) Effects of IV methylprednisolone on brain atrophy in relapsing-remitting MS. Neurology 57 (7):1239-1247

96. Pirko I, Johnson A, Gamez J, Macura SI, Rodriguez M (2004) Disappearing "T1 black holes" in an animal model of multiple sclerosis. Front Biosci 9:1222-1227

97. Nessler S, Boretius S, Stadelmann C, Bittner A, Merkler D, Hartung HP, Michaelis T, Bruck W, Frahm J, Sommer N, Hemmer B (2007) Early MRI changes in a mouse model of multiple sclerosis are predictive of severe inflammatory tissue damage. Brain 130 (Pt 8):2186-2198. doi:10.1093/brain/awm105

98. Floris S, Blezer EL, Schreibelt G, Dopp E, van der Pol SM, Schadee-Eestermans IL, Nicolay K, Dijkstra CD, de Vries HE (2004) Blood-brain barrier permeability and monocyte infiltration in experimental allergic encephalomyelitis: a quantitative MRI study. Brain 127 (Pt 3):616-627. doi:10.1093/brain/awh068

99. Boven LA, Van Meurs M, Van Zwam M, Wierenga-Wolf A, Hintzen RQ, Boot RG, Aerts JM, Amor S, Nieuwenhuis EE, Laman JD (2006) Myelin-laden macrophages are anti-inflammatory, consistent with foam cells in multiple sclerosis. Brain 129 (Pt 2):517-526. doi:10.1093/brain/awh707

100. Brochet B, Deloire MS, Touil T, Anne O, Caille JM, Dousset V, Petry KG (2006) Early macrophage MRI of inflammatory lesions predicts lesion severity and disease development in relapsing EAE. NeuroImage 32 (1):266-274. doi:10.1016/j.neuroimage.2006.03.028

101. Stroh A, Zimmer C, Werner N, Gertz K, Weir K, Kronenberg G, Steinbrink J, Mueller S, Sieland K, Dirnagl U, Nickenig G, Endres M (2006) Tracking of systemically administered mononuclear cells in the ischemic brain by high-field magnetic resonance imaging. NeuroImage 33 (3):886-897. doi:10.1016/j.neuroimage.2006.07.009

102. McAteer MA, Sibson NR, von Zur Muhlen C, Schneider JE, Lowe AS, Warrick N, Channon KM, Anthony DC, Choudhury RP (2007) In vivo magnetic resonance imaging of acute brain inflammation using microparticles of iron oxide. Nat Med 13 (10):1253-1258. doi:10.1038/nm1631

103. Serres S, Mardiguian S, Campbell SJ, McAteer MA, Akhtar A, Krapitchev A, Choudhury RP, Anthony DC, Sibson NR (2011) VCAM-1-targeted magnetic resonance imaging reveals subclinical disease in a mouse model of multiple sclerosis. FASEB J 25 (12):4415-4422. doi:10.1096/fj.11-183772

104. Deddens LH, van Tilborg GA, van der Toorn A, van der Marel K, Paulis LE, van Bloois L, Storm G, Strijkers GJ, Mulder WJ, de Vries HE, Dijkhuizen RM (2013) MRI of ICAM-1 upregulation after stroke: the importance of choosing the appropriate target-specific particulate contrast agent. Mol Imaging Biol 15 (4):411-422. doi:10.1007/s11307-013-0617-z

105. Zhu Y, Ling Y, Zhong J, Liu X, Wei K, Huang S (2012) Magnetic resonance imaging of radiation-induced brain injury using targeted microparticles of iron oxide. Acta Radiol 53 (7):812-819. doi:10.1258/ar.2012.120040

106. Querol M, Chen JW, Bogdanov AA, Jr. (2006) A paramagnetic contrast agent with myeloperoxidase-sensing properties. Org Biomol Chem 4 (10):1887-1895. doi:10.1039/b601540a

107. Chen JW, Breckwoldt MO, Aikawa E, Chiang G, Weissleder R (2008) Myeloperoxidase-targeted imaging of active inflammatory lesions in murine experimental autoimmune encephalomyelitis. Brain 131 (Pt 4):1123-1133. doi:10.1093/brain/awn004

108. Towner RA, Smith N, Saunders D, Henderson M, Downum K, Lupu F, Silasi-Mansat R, Ramirez DC, Gomez-Mejiba SE, Bonini MG, Ehrenshaft M, Mason RP (2012) In vivo imaging of immuno-spin trapped radicals with molecular magnetic resonance imaging in a diabetic mouse model. Diabetes 61 (10):2405-2413. doi:10.2337/db11-1540

109. Beer AJ, Lorenzen S, Metz S, Herrmann K, Watzlowik P, Wester HJ, Peschel C, Lordick F, Schwaiger M (2008) Comparison of integrin alphaVbeta3 expression and glucose metabolism in primary and metastatic lesions in cancer patients: a PET study using 18F-galacto-RGD and 18F-FDG. J Nucl Med 49 (1):22-29. doi:10.2967/jnumed.107.045864

110. Zhou Y, Chakraborty S, Liu S (2011) Radiolabeled Cyclic RGD Peptides as Radiotracers for Imaging Tumors and Thrombosis by SPECT. Theranostics 1:58-82

111. Benavides J, Capdeville C, Dauphin F, Dubois A, Duverger D, Fage D, Gotti B, MacKenzie ET, Scatton B (1990) The quantification of brain lesions with an omega 3 site ligand: a critical analysis of animal models of cerebral ischaemia and neurodegeneration. Brain research 522 (2):275-289

112. Ramlackhansingh AF, Brooks DJ, Greenwood RJ, Bose SK, Turkheimer FE, Kinnunen KM, Gentleman S, Heckemann RA, Gunanayagam K, Gelosa G, Sharp DJ (2011) Inflammation after trauma: microglial activation and traumatic brain injury. Ann Neurol 70 (3):374-383. doi:10.1002/ana.22455

113. Venneti S, Lopresti BJ, Wang G, Slagel SL, Mason NS, Mathis CA, Fischer ML, Larsen NJ, Mortimer AD, Hastings TG, Smith AD, Zigmond MJ, Suhara T, Higuchi M, Wiley CA

(2007) A comparison of the high-affinity peripheral benzodiazepine receptor ligands DAA1106 and (R)-PK11195 in rat models of neuroinflammation: implications for PET imaging of microglial activation. J Neurochem 102 (6):2118-2131. doi:10.1111/j.1471-4159.2007.04690.x

114. Thakur ML, Gottschalk A, Zaret BL (1979) Imaging experimental myocardial infarction with indium-111-labeled autologous leukocytes: effects of infarct age and residual regional myocardial blood flow. Circulation 60 (2):297-305

115. Wang PY, Kao CH, Mui MY, Wang SJ (1993) Leukocyte infiltration in acute hemispheric ischemic stroke. Stroke 24 (2):236-240

116. Stankoff B, Freeman L, Aigrot MS, Chardain A, Dolle F, Williams A, Galanaud D, Armand L, Lehericy S, Lubetzki C, Zalc B, Bottlaender M (2011) Imaging central nervous system myelin by positron emission tomography in multiple sclerosis using [methyl-(1)(1)C]-2-(4'-methylaminophenyl)- 6-hydroxybenzothiazole. Ann Neurol 69 (4):673-680. doi:10.1002/ana.22320

117. de Paula Faria D, de Vries EF, Sijbesma JW, Dierckx RA, Buchpiguel CA, Copray S (2014) PET imaging of demyelination and remyelination in the cuprizone mouse model for multiple sclerosis: a comparison between [11C]CIC and [11C]MeDAS. NeuroImage 87:395-402. doi:10.1016/j.neuroimage.2013.10.057

118. de Paula Faria D, Copray S, Sijbesma JW, Willemsen AT, Buchpiguel CA, Dierckx RA, de Vries EF (2014) PET imaging of focal demyelination and remyelination in a rat model of multiple sclerosis: comparison of [11C]MeDAS, [11C]CIC and [11C]PIB. Eur J Nucl Med Mol Imaging 41 (5):995-1003. doi:10.1007/s00259-013-2682-6

119. Pascual B, Prieto E, Arbizu J, Marti-Climent JM, Penuelas I, Quincoces G, Zarauza R, Pappata S, Masdeu JC (2012) Decreased carbon-11-flumazenil binding in early Alzheimer's disease. Brain 135 (Pt 9):2817-2825. doi:10.1093/brain/aws210

120. Rojas S, Martin A, Pareto D, Herance JR, Abad S, Ruiz A, Flotats N, Gispert JD, Llop J, Gomez-Vallejo V, Planas AM (2011) Positron emission tomography with 11C-flumazenil in the rat shows preservation of binding sites during the acute phase after 2 h-transient focal ischemia. Neuroscience 182:208-216. doi:10.1016/j.neuroscience.2011.03.013

121. Koopman G, Reutelingsperger CP, Kuijten GA, Keehnen RM, Pals ST, van Oers MH (1994) Annexin V for flow cytometric detection of phosphatidylserine expression on B cells undergoing apoptosis. Blood 84 (5):1415-1420

122. Bahmani P, Schellenberger E, Klohs J, Steinbrink J, Cordell R, Zille M, Muller J, Harhausen D, Hofstra L, Reutelingsperger C, Farr TD, Dirnagl U, Wunder A (2011) Visualization of cell death in mice with focal cerebral ischemia using fluorescent annexin A5, propidium iodide, and TUNEL staining. J Cereb Blood Flow Metab 31 (5):1311-1320. doi:10.1038/jcbfm.2010.233

123. Yagle KJ, Eary JF, Tait JF, Grierson JR, Link JM, Lewellen B, Gibson DF, Krohn KA (2005) Evaluation of 18F-annexin V as a PET imaging agent in an animal model of apoptosis. J Nucl Med 46 (4):658-666

124. Lampl Y, Lorberboym M, Blankenberg FG, Sadeh M, Gilad R (2006) Annexin V SPECT imaging of phosphatidylserine expression in patients with dementia. Neurology 66 (8):1253-1254. doi:10.1212/01.wnl.0000208436.75615.8c

125. Narula J, Acio ER, Narula N, Samuels LE, Fyfe B, Wood D, Fitzpatrick JM, Raghunath PN, Tomaszewski JE, Kelly C, Steinmetz N, Green A, Tait JF, Leppo J, Blankenberg FG, Jain

D, Strauss HW (2001) Annexin-V imaging for noninvasive detection of cardiac allograft rejection. Nat Med 7 (12):1347-1352. doi:10.1038/nm1201-1347

126. Li S, Johnson J, Peck A, Xie Q (2017) Near infrared fluorescent imaging of brain tumor with IR780 dye incorporated phospholipid nanoparticles. J Transl Med 15 (1):18. doi:10.1186/s12967-016-1115-2

127. Guo B, Sheng Z, Kenry, Hu D, Lin X, Xu S, Liu C, Zheng H, Liu B (2017) Biocompatible conjugated polymer nanoparticles for highly efficient photoacoustic imaging of orthotopic brain tumors in the second near-infrared window. Materials Horizons 4:1151–1156. doi:10.1039/c7mh00672a

Chapter 2: Non-Invasive Brain Delivery and Efficacy of BDNF to Stimulate Neuroregeneration and Suppression of Disease Relapse in EAE Mice

1. Introduction:

Brain diseases are difficult to diagnose and treat; thus, thousands of individuals suffer from brain diseases annually, including Alzheimer's disease (AD), multiple sclerosis (MS), and brain tumors (*e.g.,* glioblastoma, medulloblastoma). One of the primary reasons for this difficulty is the blood-brain barrier (BBB) that prevents functional molecules (*e.g.,* drugs) and harmful toxins introduced into the bloodstream from entering the brain.[1] To cross the BBB, a molecule must possess the appropriate physicochemical properties. Furthermore, efflux pumps and enzymes expel and metabolize molecules, respectively, preventing certain molecular species from crossing the BBB. Because of the protective nature of the BBB, its selectivity imposes challenges for scientists to develop diagnostic and therapeutic agents for patients with brain diseases. This is especially apparent for modern biological drugs, such as monoclonal antibodies (mAbs), enzymes, and hormones. The physicochemical properties (*i.e.,* size, charges, high hydrogen-bonding potentials, and hydrophilicity) of biologics prevent them from partitioning into the cell membranes of the BBB vascular endothelial cells and crossing through the cells (*i.e.,* transcellularly).[1] Due to their size, these molecules also cannot penetrate between the endothelial cells of the BBB (*i.e.,* paracellularly) because the paracellular pathway's tight junctions restrict the permeation of molecules with hydrodynamic radius larger than 11 angstroms (Å).

Most available drugs for treatment of multiple sclerosis (MS) suppress only the immune response to halt the disease; for example, natalizumab (Tysabri®) is a monoclonal antibody (mAb) drug that prevents brain infiltration of activated immune cells that could damage the axon myelin sheath.[2] Another widely prescribed treatment, glatiramer acetate (Copaxone®), has a mechanism

of action that is not entirely understood, but it is believed to ameliorate the disease by modulating Th1 to Th2 cells responses.[3] Although these current drugs may halt MS disease progression, they do not reverse neuronal damage in the central nervous system (CNS). Although many researchers are currently investigating potential drugs for remyelination, no available drugs on the market can reverse damage of the myelin sheaths of neuronal axons. It has been shown previously that the extent of MS patient's disability can be correlated to the levels of the axonal damage in the CNS;[4] therefore, a means to reverse axon demyelination could greatly improve MS patients' quality of life.

One way to reverse MS is to deliver molecules that can repair demyelination and/or neuronal damage to the CNS. Monoclonal antibodies (mAb) such as anti-Nogo-A,[5] anti-LINGO-1,[6] sHIgM22,[7] and VX15/2503[8] have been developed for inducing remyelination. Unfortunately, clinical trials for several of these mAbs, including anti-Nogo-A and anti-LINGO-1, have been terminated—anti-LINGO-1 mAb for lack of significant therapeutic efficacy, and anti-Nogo-A for reasons that have not been released. Alternatively, brain delivery of brain-derived neurotrophic factor (BDNF), [9, 10] nerve growth factor (NGF),[11] and insulin-like growth factor 1 (IGF-1)[12] has a potential benefit in reversing neurodegenerative diseases. BDNF stimulates neuron growth and remyelination in cell-culture systems and *ex vivo* brain slices and *in vivo*.[9, 10] Direct delivery of BDNF via intracerebroventricular (ICV) injection to the lateral ventricle of brains of adult rats generates new neurons in the olfactory bulb, thalamus, hypothalamus, and parenchyma-striatum.[13] Remyelination in the brains of diseased animals allows the recovery of physical function, demonstrating a correlation between remyelination and recovery from disease symptoms in the EAE animal model.[14, 15] While intravenous (I.V.) administration of neuroregenerative proteins (*e.g.,* BDNF, NGF) would be more practical, many attempts to deliver these proteins directly

across the BBB via the systemic circulation have not proven successful in inducing neuro-regeneration/repair because they cannot cross the BBB.[16] Therefore, there is an urgent need to develop effective and non-invasive *trans*-BBB delivery methods for supplying remyelinating neurotrophic factors into the brain.

One alternative strategy to deliver drugs including proteins into the brain is via the paracellular pathway (*i.e.,* intercellular junctions) of the BBB. In this case, modulation of intercellular junctions of the BBB can increase the paracellular pathways of the BBB. The osmotic method of using a hypertonic mannitol solution has been successful in modulating intercellular junctions.[17] The hypertonic solution shrinks the BBB endothelial cells to increase the porosity of the paracellular pathway and allows anticancer drugs, including mAbs, to cross the BBB to treat brain tumors.[17] Alternatively, our group has investigated a new approach to modulating the BBB using cadherin peptides. In this case, cadherin peptides were designed inhibit cadherin–cadherin interactions in an equilibrium and dynamic fashion to increase the porosity of the paracellular pathway.[1, 18] In healthy animals, *in vivo,* cadherin peptides (*e.g.,* HAV6: Ac-SHAVSS-NH_2 and ADTC5: Cyclo(1,7)Ac-CDTPPVC-NH_2) have been shown to deliver small molecules, peptides, and proteins (*e.g.,* galbumin) to the brain by modulating the BBB for a very short period of time.[19-22] Recently, HAV6 and ADTC5 peptides have been shown to deliver various sizes of protein (i.e., 15 kDa lysozyme, 65 kDa albumin, 150 kDa IgG mAb) into the brain of healthy C57BL/6 mice when both BBB modulator and protein were delivered via I.V. administration.[23] Secondly, Novel cyclic HAV and ADT peptides have been designed to improve the BBB modulatory activity to deliver IgG mAb into the brain of C57BL/6 mice.[24] Thirdly, a combination of HAV6 and an anticancer drug, adenanthin, was effective in suppressing medulloblastoma brain tumor growth

and increasing survival rate of the mice.[25] Finally, HAV6 peptide improved oral absorption and brain delivery of eflornithine by improving its paracellular permeation.[26]

In this study, BDNF (13 kDa monomer) was delivered to the brains of relapsing-remitting experimental autoimmune encephalomyelitis (RR-EAE) mice using ADTC5 peptide via I.V. administrations to induce remyelination and neurorepair as a less invasive method compared to ICV.[13] Four different groups of EAE mice were treated eight times with BDNF+ADTC5, BDNF alone, ADTC5 alone or vehicle during the remission period of EAE. Therapeutic effects of delivering BDNF *in vivo* were evaluated by observing the amelioration of EAE relapse and comparing clinical body scores across treatment groups. Finally, the effects of BDNF in the brains of EAE mice were evaluated using several *ex vivo* analyses to indicate remyelination and the degree of NG2-glia activity as well as by probing mRNA transcript upregulation of proteins affected by BDNF.

2.2. Materials and Methods:

2.2.1 Animals:

The protocols to use live mice have been approved by the Institutional Animal Care and Use Committee (IACUC) at The University of Kansas. SJL/elite mice were purchased from Charles River Laboratories, Inc. (Wilmington, MA). All mice were housed under specific pathogen-free conditions at the animal facility at The University of Kansas approved by the university Animal Care Unit (ACU). The animals were maintained in the Animal Care Unit with free access to food, water, and rotating stimuli.

2.2.2. Cadherin Peptide Synthesis and Purification:

The syntheses of the ADTC5 and $PLP_{139-151}$ peptides were accomplished using a solid-phase peptide synthesizer (Gyros Protein Technologies, Tucson, AZ). After peptide cleavage from the resin using TFA, the crude peptides were precipitated overnight in cold diethyl ether. In most cases, the crude precipitate showed high concentrations of the desired peptide. The formation of a disulfide bond in the cyclic peptide (*i.e.,* ADTC5) was accomplished by vigorously stirring the precursor linear peptide in bicarbonate buffer solution under air oxidation at pH 9.0 in high dilution. The cyclization reaction produced primarily the desired monomer with minor oligomer side products; the monomer peptide was isolated from the mixture using a semi-preparative HPLC X-bridge C18 column (Waters, Milford, MA). After purification with semi-preparative HPLC, the isolated peptides had high purity (> 95%) as determined by analytical HPLC. The exact mass of each peptide was determined by mass spectrometry.

2.2.3. EAE Mouse Model:

EAE disease in animals (5−8-week-old SJL/elite female mice, Charles River) was stimulated by injecting 200 μg of $PLP_{139–151}$ peptide in a 0.2 mL emulsion containing equal volumes of PBS and complete Freund's adjuvant (CFA) with killed mycobacterium tuberculosis strain H37RA (Difco, Detroit, MI; final concentration 4 mg/mL) as described previously.[27, 28] Briefly, 50 μL of PLP/CFA emulsion was administered to four different regions above the shoulders and the flanks on Day 0 followed by intraperitoneal injection of 200 ng of pertussis toxin (List Biological Laboratories, Campbell, CA) on Days 0 and 2. Clinical scores that reflect the disease progression were determined using an 11-point scale with 0.5 increments ranging from 0 to 5; 0 being no apparent disease and 5 being moribund. On Day 21, mice were randomly separated into 3 treatment

groups: **(i)** BDNF (5.7 nmol/kg) + ADTC5 (10 µmol/kg; *n* = 7), **(ii)** BDNF alone (5.71 nmol/kg, *n* = 6), **(iii)** ADTC5 alone (10 µmol/kg; *n* = 5), and **(iv)** vehicle (*n* = 5). All mice received 8 intravenous injections every 4 days beginning on Day 21. The mice were euthanized via CO_2 inhalation on Day 55. Area under the curve (AUC) calculations were used to compare clinical scores across groups; AUC calculations were performed using the trapezoid rule from Days 21 to 55.

2.2.4. Euthanasia, Brain Perfusion, and Extraction:

All mice were euthanized via a CO_2 chamber. Immediately following euthanasia, mice underwent cervical dislocation and were transcardially perfused with PBS + 0.2% Tween-20 followed by perfusion-fixation with a 4% paraformaldehyde and 30% sucrose PBS solution. Following the fixation, the brains were extracted and post-fixed overnight in the perfusion-fixation solution.

2.2.5. Immunohistochemistry:

Fixed brain samples were submitted to IHC World (Ellicott City, MD) for paraffin embedding, tissue sectioning (5 µm), anti-NG2 (Abcam, Cambridge, UK) staining via DAB, and Luxol-fast blue staining. Staining protocols described on the IHC World website for Luxol-fast blue and immunohistochemistry enzyme HRP were performed. For both procedures, brains were cut into 5 µm sections and then deparaffinized and rehydrated using xylenes and an ethanol-water gradient. For Luxol staining, sections were incubated in Luxol-fast blue solution at 56 ºC overnight and subsequently rinsed with 95% ethyl alcohol followed by distilled water. For anti-NG2 mAb staining, sections underwent antigen retrieval, followed by rinsing with PBS-Tween 20 for 2 x 2

minutes. Sections were incubated with normal serum block followed by primary antibody incubation with anti-NG2 mAb at 4 ºC overnight and subsequently rinsed with PBS-Tween 20. Sections were then blocked using a peroxidase blocking solution for 10 min at room temperature (RT). Next, samples were incubated with a biotinylated secondary antibody at 1–10,000 dilution in PBS for 30 min at RT. Sections were then incubated in streptavidin-HRP in PBS for 30 min at RT followed by incubation in DAB solution for 1–3 min. Sections were dehydrated through 95% ethanol for 2 min, 100% ethanol for 2 x 3 min, and cleared with xylene. Sections were mounted using aqueous mounting media and coverslipped using 1.5 coverslips.

Luxol-fast blue and anti-NG2 mAb images were taken under identical conditions on a Zeiss Axioplan 2 microscope (Oberkochen, Germany) equipped with a mercury lamp excitation source, and 40X (Luxol) and 20X (anti-NG2) air objective lenses. Greyscale images for quantification were taken using a 1344 x 1024 Orca ER CCD camera (Hamamatsu Photonics, Japan), color images for qualitative purposes were taken using a 1.3 MP Spot Color camera (Spot Imaging, Sterling Heights, MI). To determine the degree of demyelination (*i.e.,* breakages in the myelin sheath), 5 greyscale images from each group were randomly selected and converted to binary, and regions of interest (ROI) were manually selected within the lateral corpus callosum using ImageJ (National Institute of Health, Bethesda, MD). A binary value of '1' (*i.e.,* white signal) implied a lack of myelin, whereas a binary value of '0' (*i.e.,* black signal) implied myelin. The mean value of each ROI from each image was recorded. To determine the degree of anti-NG2 staining, densitometry analysis was performed on DAB stained sections; greyscale images were taken under equal exposure times and 5 images per group were randomly selected and used for analysis. ROIs of identical size were selected within the medial corpus callosum. The integrated mean grey value

for each ROI from each image was recorded. Staining background was controlled for by subtracted an aggregate of mean grey values from 5 ROIs of negative controls from each group.

2.2.6. Fluorescent In Situ Hybridization:

Coronal brain sections (5 μm thickness) from mid- and hind-brain were sectioned and washed three times in PBS before mounting on gelatin-coated glass slides (Superfrost Plus, Thermo Fisher Scientific). Tissue was allowed to dry at RT and then stored at –20 ºC until use. Fluorescent *in situ* hybridization (FISH) was performed using RNAscope® Technology 2.0, Advanced Cell Diagnostics (ACD), Hayward, CA) Multiplex Reagent Kit V2.[29-31] In short, mounted tissue sections were deparaffinized using xylene and serially dehydrated in 50%, 70%, 95%, and 100% ethanol for 5 min each. In between all pretreatment steps, tissue sections were briefly washed with nanopure water. Pretreatment solution 1 (hydrogen peroxide reagent) was applied for 10 min at RT and then the tissue sections were boiled in pretreatment solution 2 (target retrieval reagent) for 15 min. Mounted slices were pretreated with solution 3 (protease reagent) for 30 min at 40 ºC in the HybEz™ hybridization system (ACD). Following tissue pretreatment, the following transcript probes were applied to all sections: Mm-EGR1-C1 (Cat. # 423371), Mm-NOS1-C2 (Cat. # 437651-C2), and Mm-ARC-C3 (Cat. # 316911-C3), which correspond to early growth response 1 (EGR1), nitric oxide synthase 1 (NOS1), and activity-related cytoskeleton-associated protein (ARC). Probes were hybridized to sections for 2 hours (h) at 40 ºC and then subsequently washed for 2 min at room temperature. Following hybridization, hybridize AMP 1 was applied to each slide, which was then incubated for 30 min at 40 ºC. The same process was repeated for hybridize AMP 2 and 3. For HRP-C1 signal development (EGR1), HRP-C1 was applied to each slide, which was incubated for 15 min at 40 ºC and then washed. For C1, TSA® Plus fluorescein (Perkin Elmer,

Akron, OH) was applied and incubated for 30 min at 40 ºC and then washed. Following the wash, HRP blocker was applied to each slide, which was incubated for 15 min at 40 ºC and then washed. This process was repeated for C2 (NOS1)**,** and C3 (EGR1) using TSA® Plus Cy3 and Cy5, respectively. The resulting transcript-fluorophore labeling is as follows: EGR1-fluorescein, NOS1-Cy3, EGR1-Cy5. All sections were counterstained by incubating DAPI for 30 seconds (sec) at RT following by rinsing. Slides were then covered using ProLong Gold Antifade Mountant and 1.5 coverslips. Slides were allowed to dry in the dark overnight at 4 ºC. All sections were imaged within 2 weeks.

Fluorescent images were taken using an Olympus Inverted Epifluorescence Microscope XI81 (Olympus Life Solutions, Waltham, MA) running SlideBook Version 5.5 (3i, Ringsby, CT) equipped with a digital CMOS camera (2000x2000), automatic XYZ stage position, ZDC autofocus, and a xenon lamp excitation source. Images were taken using a 20X objective and appropriate filter sets for each fluorophore (*i.e.,* DAPI, FITC, Cy3, C5). To determine the degree of mRNA transcript expression, 5 images of analogous regions of the cerebral cortex were randomly selected from mouse samples of each group, and the total number of cells expressing each mRNA transcript were counted using ImageJ. The number of cells expressing each mRNA transcript was normalized against the total number of cells (as determined by DAPI) to ensure that analyzed areas had equal cell density. For display purposes, images were pseudo colored using ImageJ; green was assigned to fluorescein (EGR1), magenta was assigned to Cy5 (ARC), and blue to DAPI. NOS images were not incorporated due to virtually no signal detection.

2.2.7. Western Blots:

Female SJL/elite mice, 5 weeks of age (Charles River) were initially intravenously injected via

lateral tail vein with 5.71 nmol/kg BDNF (Peprotech, Rocky Hill, NJ) with (n = 3) or without (n =3) 10 μmol/kg ADTC5. BDNF was allowed to circulate for 20–30 min prior to euthanasia via CO_2. Immediately following euthanasia, mice were transcardially perfused with protease inhibitor infused TRIS buffer (pH 7.4). The brains of the mice were extracted and placed in the perfusate buffer on ice. For Western blotting, 100–150 mg of brain tissue was sectioned from the most ventro-posterior portion of the brain and placed in 200–250 μL of solution mixture containing 66% tissue protein extraction reagent (TPER; Thermo Fisher, Waltham, WA) and 33% 50 μL of neural protein extraction reagent (NPER; Thermo Fisher) with protease and phosphatase inhibitors (Thermo Fisher). The tissue samples were lysed via sonication using a Sonic Disembrator 500 (Thermo Fisher) at an amplitude level of 15 Hz for a maximum of 10 sec. Following sonication, the samples were vortexed for one minute and then centrifuged at 4 ºC and 13,000 RPM for 30 min. The sonication, vortexing, and centrifugation were repeated 2 times. Following lysis and centrifugation, NuPAGE™ 4–12% Bis-Tris Protein Gels (1.5 mm, 10-well, Thermo Fisher) were loaded with 60 μg of protein and Licor (Lincoln, NE) loading buffer. A BDNF standard of less than 1.0 μg was also loaded for positive control. The gel was run at 100 V for 2 h. Following the gel, the protein bands were transferred to a nitrocellulose membrane (Licor) at 36 V overnight. Following the transfer, the membrane was stained with REVERT (Licor) for 3 min and then washed using the REVERT Wash Solution for 2 min followed immediately by scanning using a Licor Odyssey at 700 nm. Next, the membrane was washed using the REVERT Reversal Solution (Licor) and subsequently blocked for 2 h at 4 ºC using Licor TBS blocking reagent. The membrane was then incubated with the primary antibody, anti-BDNF (Abcam), at a 1:1,000 ratio in TBS + 0.1% Tween-20 for 36 h at 4 ºC. Following primary antibody, the membrane was rinsed and incubated with the IR800-conjugated secondary antibody (Licor) for 1.5 h at room temperature in

the dark. The membrane was then immediately scanned using a Licor Odyssey CLX at a wavelength of 800 nm. Following imaging of BDNF bands on the membrane, the membrane was stripped using stripping buffer to be reprobed for the phosphorylated-TrkB (pTrkB) receptor with anti-phospho-TrkB (EMD Millipore, Burlington, MA) at a 1:1,000 dilution in TBS + 0.1% Tween-20 for 24 h at 4 ºC. Following primary antibody incubation, the membrane was rinsed and incubated with the IR800-conjugated secondary antibody for 1.5 h at room temperature in the dark. The membrane was then immediately scanned using the same parameters as for the BDNF imaging. These bands were not densiometrically analyzed due to high background signal; however, they are shown for qualitative analysis.

To improve the level of detection of BDNF and pTrkB bands via Western blot, the above process was repeated with an increase in dosages of BDNF. The dosages of ADTC5 remained constant; mice received either 57.1 nmol/kg BDNF (10-fold increase) + 10 µmol/kg ADTC5 (n = 2), 28.6 nmol/kg BDNF (5-fold increase) + 10 µmol/kg ADTC5 (n = 1), or 28.6 nmol/kg BDNF alone (5-fold increase; n = 3). These images were not quantified due to the variation in dosing regiments; however, they are provided for qualitative analysis of BDNF brain depositions.

2.2.8. Statistics:

All statistics were performed using GraphPad Prism (San Diego, CA). Analysis of variance (ANOVA) and Student's T-test were performed when appropriate, both operating at 95% confidence intervals with a p-value of less than 0.05 used as the criterion for statistical significance unless otherwise stated.

2.3. Results:

2.3.1 Effect of BDNF Brain Delivery by ADTC5 on Suppression of EAE Relapse:

The ability of ADTC5 to deliver BDNF into the brains of mice after I.V. administrations was assessed by determining the effects of BDNF in suppressing disease relapse in the relapsing-remitting EAE animal model. The efficacy of BDNF (5.71 nmol/kg) + ADTC5 (10 μmol/kg; n = 7) was compared to that of BDNF alone (5.71 nmol/kg; n = 6), ADTC5 alone (10 μmol/kg; n = 5), and vehicle (n = 5). I.V. injections were performed every 4 days up to eight injections starting from day 21 during the time of disease remission and relapse. EAE clinical scores were monitored daily from the beginning to the end of the study. The EAE mice that received injections of BDNF + ADTC5 had clinical body scores significantly lower over time compared to the mice that received BDNF alone, ADTC5 alone or vehicle **(Figure 2.1A)**. The mice that received injections of BDNF + ADTC5 showed normal locomotion on all four limbs, with some residual tail paralysis. In contrast, mice that received BDNF alone, ADTC5 alone or vehicle showed partial or full hind leg paralysis and full tail paralysis.

The differences in clinical body scores were distinguished by generation of the areas under the curve (AUC) disease scores of all four groups from day 21 to day 55, after the peak of the disease. It was found that mice that received injections of BDNF + ADTC5 had significantly lower ACU disease scores compared to those that received BDNF alone, ADTC5 alone or vehicle ($F_{(3,19)}$ = 3.180; $p \leq 0.05$; **Figure 2.1B**). There was no significant difference in the clinical scores between treatments with BDNF alone, ADTC5 alone and PBS ($F_{(2,13)}$ = 0.128; p = 0.881). The results suggest that ADTC5 helps BDNF to penetrate the BBB to exert its biological activity in the brain while BDNF alone did not have efficacy due to its inability to penetrate the BBB. Further

evaluation of the therapeutic efficacy of systemically delivered BDNF using ADTC5 peptide was assessed using histological, immunohistochemical, and hybridization methods.

2.3.2. Effect of BDNF on Remyelination:

The ability of BDNF to induce remyelination has been previously demonstrated using BDNF knockout mice in which myelin loss was shown to be sensitive to a lack of BDNF expression.[32] Additionally, BDNF has been shown to improve remyelination and regeneration of nerve fibers after C7 ventral root avulsion and replantation.[33] Thus, we probed myelin levels in the brains of mice as an indication that BDNF is successfully entering the CNS and exerting an effect. Myelin levels in the brain were imaged using Luxol fast-blue chromogen staining. **Figure 2.2A** shows noticeably more dense myelin staining in the lateral corpus callosum in mice that received BDNF + ADTC5 (n = 5) compared to those that received BDNF alone (n = 5), or vehicle (n = 5). The mice that received BDNF alone or vehicle showed myelin discontinuity (white spaces) in the corpus callosum. Quantification via densitometry using binary images of myelin staining showed a statistically significant increase in myelin density in the lateral corpus for mice that received BDNF+ADTC5 compared to those that received BDNF alone or vehicle ($F_{(2,12)} = 21.72$; $p \leq .001$) **Figure 2.2B**). This result supports the idea that BDNF successfully entered the brain with the help of ADTC5 and induced remyelination in the corpus callosum.

2.3.3. Effect of BDNF on NG2-Glia:

The NG2 receptors have previously been shown to facilitate the maturation of oligodendrocyte precursor cells and have been demonstrated to be distinctly upregulated in $BDNF^{+/+}$ mice following the development of cuprizone-induced lesions.[32, 34] We further probed NG2 receptor

presence as an additional indicator that BDNF is indeed entering the CNS and exerting a therapeutic effect. NG2 receptor levels were quantified using anti-NG2 immunohistochemistry staining. A higher degree of NG2 staining in the medial corpus callosum of mice was found in animals that received BDNF + ADTC5 (n = 5) compared to those that received BDNF alone (n = 5) or vehicle (n = 5; **Figure 2.3A**). Quantification of the degree of NG2 staining was determined using mean grey values. Mice that received BDNF + ADTC5 showed a significantly increased level of anti-NG2 staining compared to those that received BDNF alone or vehicle ($F_{(2,12)} = 10.44$, $p \leq 0.01$; **Figure 2.3B**). These results are evidence that BDNF is inducing oligodendrocyte maturation and, in turn, remyelination.

2.3.4. Effects of BDNF on EGR1, ARC, and NOS1 mRNA Transcript Expression:

BDNF exposure is well known to affect downstream transcription factors including c-fos, cAMP response element binding protein (CREB), early growth response-1 (EGR-1), and EGR3.[35, 36] Furthermore, EGR1 has been demonstrated to target the activity-regulated ARC gene, and EGR1 is also upregulated by BDNF exposure.[37, 38] In addition, BDNF has not only been shown to upregulate specific downstream transcripts, but has also been shown to inhibit the expression of nitric oxide synthase 1 (NOS1).[39] Therefore, we probed three mRNA transcripts, EGR1, ARC, and NOS1 for evidence that BDNF is entering the brain and exhibiting effects. The mRNA expression levels of EGR1, ARC, and NOS1 mRNA were quantified using fluorescent *in situ* hybridization (FISH). **Figures 2.4A** and **2.4B** show brain sections from the mid and hind brain, respectively; mice that received BDNF + ADTC5 have noticeable upregulation of EGR1 and ARC mRNA transcripts compared to mice that received BDNF alone or vehicle. However, images for the NOS1 mRNA expressions are not shown due to low level of detectability. The mRNA expression levels

were quantified using cell counting that was normalized against the number of cell nuclei to ensure that analyzed areas were of equal cell density. Composite images of all fluorescent channels showed a pronounced increase in mRNA transcripts that can be seen for the mice that received BDNF + ADTC5 (n = 5) compared to the mice that received BDNF alone (n = 5) or vehicle (n = 5; **Figures 2.4A, B**). **Figure 2.4C** shows a significant increase in EGR1 ($F_{(2,12)} = 47.10$; $p \leq 0.001$) and ARC ($F_{(2,12)} = 33.43$; $p \leq 0.001$) expression levels for mice that received BDNF+ADTC5 compared to those of the mice that received BDNF alone or vehicle. In contrast, there was no significant difference in NOS ($F_{(2,12)} = 1.826$; $p = 0.203$) or DAPI ($F_{(2,12)} = 0.504$; $p = 0.617$) staining across the three groups (**Figure 2.4D**).

2.3.5. Detection of BDNF in the Brain using Western Blots:

The ability of ADTC5 to deliver BDNF into the brain was confirmed by Western blot analysis of the brain homogenates. To determine if BDNF entered the brain using the ADTC5 peptide, mice were initially given a 5.71 nmol/kg BDNF injection with (n = 3) or without (n = 3) 10 µmol/kg ADTC5 and were sacrificed after 20 minutes to allow for sufficient circulation and activation of the pTrkB pathway. **Figure 2.5A** shows a notable increase in detection of BDNF bands in the brains of mice that received injections of BDNF + ADTC5 compared to those that received BDNF alone, where delivered BDNF was undetected. Because of high background, pTrkB could not be detected with confidence using this Western blot.

Due to suboptimal detection of pTrkB using 5.71 nmol/kg BDNF injections, the above process was repeated with increases in dosage of BDNF to 57.1 nmol/kg but with the dosages of ADTC5 remaining constant. Mice received either 57.1 µmol/kg BDNF (10-fold increase) + 10 µmol/kg ADTC5 (n = 2), 28.6 nmol/kg BDNF (5-fold increase) + 10 µmol/kg ADTC5 (n = 1), or 28.6

nmol/kg BDNF alone (5-fold increase; n = 3). **Figure 2.5B** more clearly shows an increase in detection of BDNF and pTrkB bands for mice that were treated with BDNF + ADTC5 compared to mice that were treated with BDNF alone. Additionally, to ensure that total protein loaded into each well across all groups was consistent, a total protein stain was performed (**Figure 2.5C**); this serves as a more reliable and accurate loading control in comparison to detecting a ubiquitous protein such as actin. There was no significant difference in the total protein loading across each group ($t_{(4)}$ = 1.808; p = 0.145). Due to the variation of dosages of BDNF administered, the densiometric BDNF and pTrkB bands cannot be statistically compared with confidence; however, the relative intensities are shown in **Figure 2.5D**. The aggregate results of these two Western blots indicate that BDNF is successfully entering the CNS and inducing an immediate effect on upregulation of pTrkB.

2.4. Discussion

Here, we have demonstrated that multiple injections of BDNF using ADTC5 peptide during the remission period of the relapsing-remitting EAE mice suppressed the disease relapse compared to treatment with BDNF alone, ADTC5 alone or vehicle. The selection of BDNF in this study because it is an endogenous molecule; thus, its delivery may not cause an adverse side effects in EAE mice. There is a significant improvement of the disease clinical scores during remission when the EAE mice were treated with BDNF+ADTC5 compared to those treated with BDNF alone, ADTC5 alone, and vehicle (**Figures 2.1A-B**). A combination of BDNF + ADTC5 induced remyelination of the axons to reverse the neuronal damage caused by the immune cells (**Figures 2A-B**). As expected, administering BDNF alone, ADTC5 alone, or vehicle did not have any effect on suppressing the disease relapse. BDNF alone did not induce remyelination because BDNF alone

could not penetrate the BBB. In addition, ADTC5 alone has no inherent neuroregenerative properties. The suppression of disease symptoms in the treatment group with BDNF + ADTC5 indirectly suggests that ADTC5 helps to deliver BDNF into the brain (**Figure 2.1**).

Our previous study showed that the effect of ADTC5 alone on the integrity the BBB intercellular junctions *in vivo* was reversible in healthy mice. Using transmission electron microscopy (TEM), evaluation of the BBB endothelial microvessels 2-h after treatment with ADTC5 showed the morphology of the endothelial cells were similar to those of in vehicle-treated mice.[20] ADTC5-treated mice have no change in appearance of the brain capillaries and their tight junctions have normal ultrastructural characteristics. The vehicular activity in the vascular endothelial cells appears normal 2-h after ADTC5 treatment. In a parallel study, *in vivo* modulation of the BBB using a cadherin peptide, HAV6 peptide, in mice did not upregulate ionized calcium binding adaptor molecule 1 (Iba1), which is a marker for microglia activation and glial fibrillary acidic protein (GFAP), which is a marker of astrogliosis. This suggests that cadherin peptides may not induce neuroinflammation. This is different than the effects of osmotic BBB modulation which shows altered morphology and disruption of the tight junction ultrastructure as well as potential astrogliosis.[40-42] The opening of the intercellular junctions by ADTC5 has a limited time duration. In this case, the duration of BBB opening for small molecules like Gd-DTPA is between 2–4 h while for a large molecule like 65 kDa galbumin is between 10–40 min. A more important question is what is the effects of repeated treatment with ADTC5 on the BBB, animal behavior and toxicities to the brain and other organs in healthy and diseased animals. This study is currently planned to evaluate the potential side effects of cadherin peptides.

As direct evidence that ADTC5 can deliver BDNF into the brain, unlabeled BDNF was delivered with and without ADTC5. After delivery, Western blots showed that recombinant BDNF

was detected in brain homogenates from mice treated with BDNF + ADTC5 compared to no detection of recombinant BDNF for mice that received BDNF without ADTC5 (**Figures 2.5B-C**). Qualitatively, the increase in BDNF doses in BDNF + ADTC5-treated mice shows increases in the amounts of detected BDNF in the brain homogenates in Western blots. In addition, the increase in BDNF doses upregulates the pTrkB receptor expression (**Figures 2.5B-C**).[43, 44] This is a first proof-of-concept for preclinical demonstration that ADTC5 can deliver BDNF into the brain after I.V. administrations to suppress EAE disease relapse in the mouse model.

Demyelination is a hallmark trait of multiple sclerosis as well as in cuprizone and EAE mouse models. Reduced myelin levels in the corpus callosum in humans and both animal models are commonly observed.[45, 46] In our case, mice treated with BDNF + ADTC5 showed a significant increase in both myelin density as determined by Luxol fast blue (**Figures 2.2A-B**) and NG2 presence in the corpus callosum, as indicated by immunohistochemistry staining (**Figures 2.3A-B**) compared to mice that received BDNF alone or vehicle. These data are consistent with those from previous studies indicating that BDNF plays an integral role in remyelination and NG2 upregulation.[34, 47, 48]

Neurotrophins such as NGF, BDNF, neurotrophin-3,4/5 (NT3, NT4/5), and IGF1 have been known to regulate the viability, development, and function of neurons. However, BDNF has been by far the most studied to reveal its role in brain health.[49] A decrease in BDNF levels *in vivo* in $BDNF^{+/-}$ mice reduces the number of $NG2^{+}$ cells and myelin levels throughout the development, suggesting a correlation between NG2 cells and remyelination.[34, 47, 48] In the cuprizone animal model used for studying remyelination, the demyelination in the corpus callosum is correlated with the decrease in BDNF, suggesting a relationship between BDNF levels in the brain and demyelination. A cuprizone mouse model shows demyelination after 4- and 5-week treatments

with cuprizone. Administration of cuprizone to $BDNF^{+/+}$ mice exhibited a counter response by increasing remyelination of NG2 cells as indicated by upregulation of NG2 receptors. However, this increase in NG2 receptors in cuprizone-treated $BDNF^{+/+}$ mice was significantly lower than those in untreated of $BDNF^{+/+}$ mice. The results indicate that BDNF has an integral role in the proliferation of NG2 cells and the remyelination process.[32, 34]

To further evaluate the effects of BDNF brain delivery in EAE mice, upregulations of several BDNF-stimulated mRNAs were determined for those that delivered the information from the gene to protein expressions. BDNF is known to activate signaling pathways for rapidly modifying the function of local targets (*e.g.*, phosphorylating TrkB); it also has a long-term effect on gene transcription (*e.g.,* CREB, EGR1 upregulation, ARC synthesis).[35] In this study, BDNF has been shown to stimulate phosphorylation of TrkB in normal mice (**Figure 2.5C**). The brain slices from BDNF+ADTC5-treated EAE mice exhibited a significant increase in activity-regulated cytoskeletal-related (ARC) and early growth response-1 (EGR1) transcripts (**Figure 2.4**) compared to those of controls treated with BDNF alone or vehicle. Thus, this indicates that BDNF enters the brain with the help of ADTC5 to exude its biological activity to stimulate ARC and EGR1 mRNA upregulations.[36, 50, 51] BDNF has been demonstrated to upregulate ARC in cell cultures, and transcription of the ARC gene is essential for late-phase, long-term potentiation in the cortex.[36, 51] In addition, EGR1 and EGR3 have been shown to directly regulate ARC synthesis.[37] EGR1- or EGR3-deficient mice lack ARC protein in some neurons; however, when the mice are deficient in both EGR1 and EGR3, all the neurons lack ARC protein. In this study, upregulation of EGR1 and ARC mRNAs was presumably due to delivered BDNF in the brain (**Figures 2.4A-C**).

Nitric oxide synthase 1 (NOS1) mRNA was also probed; however, no significant change in the NOS1 mRNA was observed by comparing brain slices for all three groups, indicating no effect of BDNF on NOS1 mRNA. It has been shown that the increase in BDNF mRNA is dependent on the increase in NOS1 mRNA upon exercise because NOS1 mRNA stimulates BDNF increase in the hippocampus during exercise as well as in the mouse brain after stroke.[52] The lack of NOS1 notable expression may be because BDNF does not use the nitric oxide pathway as other neurotrophins (*e.g.,* NGF, IGF1) do.[53] Additionally, BDNF has been shown to block NOS expression in rats to achieve BDNF homeostasis levels in the brain.[39]

Many researchers have also investigated different ways for non-invasive brain delivery of BDNF. One of these is via transcytosis across the BBB using receptor-mediated transport; in this case, BDNF is conjugated to OX26 monoclonal antibody (mAb), which is a transferrin receptor (TfR) mAb.[54, 55] This method has been referred to as the "Trojan horse" method, and the conjugate has been shown to cross the BBB in an animal model. Unfortunately, this transcytosis process may not be very efficient for carrying sufficient amounts of BDNF into the brain. There are several potential reasons for the inefficiency of this transcytosis method. First, due to the tight binding of mAb to TfR, a higher percentage of the conjugate is degraded in lysosomes of the BBB microvessel endothelial cells; thus, a lower amount of the delivered conjugate undergoes transcytosis into the brain side of the microvessels. Second, when the conjugate is transported into the brain side of the vascular endothelium, the conjugate cannot be released from TfR into the brain due to the very high affinity of the mAb to the TfR. As a result, the conjugate cannot effectively diffuse into brain tissues where BDNF is needed. Finally, conjugation to the mAb moiety could lower the BDNF binding affinity to the BDNF receptor, resulting in lower *in vivo* efficacy. Another BDNF delivery method across the BBB utilizes ultrasound along with

microbubbles; however, this method has not been applied to deliver BDNF in animal models of disease.[56-58] Ultrasound methods have been regarded as safe and reversible based upon a short-term histological assessment; however, the risks associated with recurrent and frequent uses of ultrasound have not been fully determined.[59, 60]

Our previous studies have shown that ADTC5 enhanced brain delivery of 65 kDa galbumin into the brains of living mice as detected using magnetic resonance imaging (MRI) imaging.[22] Galbumin distributions were found throughout the posterior, mid-brain, and anterior regions of the brain with the highest deposition at the posterior followed by mid-brain and finally the lowest deposition in the anterior region. Recently, ADTC5 has been shown to deliver various size proteins into the brain of healthy mice, including IRdye800CW-labeled 15 kDa lysozyme, 60 kDa albumin, and 150 kDa IgG mAb.[23] As in galbumin, with NIR, the protein was distributed throughout different brain regions. The quantitative amounts of each protein in the brain homogenates (picomol/g brain) were determined using a newly developed near IR fluorescence (NIRF) imaging method.[23] With the same condition, the amount of albumin is higher than IgG mAb, suggesting the delivery of a larger size molecule such as IgG mAb was more difficulty than that of a smaller size albumin.[23] Using the same condition, the study found that ADTC5 did not enhance the delivery of 220 kDa fibronectin, suggesting a potential cut-off size that can be delivered is 220 kDa.[23]

Recently, we developed novel cyclic peptides with N- to C-terminal cyclization derived from the HAV6 and ADTC5 peptide to improve conformational rigidity, target selectivity for cadherin, and plasma stability.[24] It was shown cyclic peptides HAVN1 (Cyclo(1,6)SHAVSS) and HAVN2 (Cyclo(1,5)SHAVS) significantly enhanced the brain delivery of 150 kDa IgG mAb compared to control while linear HAV6 did not increase the brain delivery of IgG mAb.[24] Finally, a cyclic

ADTHAV (Cyclo(1,8)TPPVSHAV) with a sequence combination from ADTC5 and HAV6 has a better BBB modulatory activity than its linear counterpart.[24] The results suggest that N- to C-terminal cyclization could improve the selectivity and BBB modulatory activity of cadherin peptides.[24]

HAV6 has also been shown to deliver anticancer drug adenanthin into the brain of mice with medulloblastoma brain tumor.[25] Adenanthin is a substrate for the efflux pump, P-glycoprotein (Pgp); thus, adenanthin alone cannot effectively penetrate the BBB. In this study, multiple treatments with HAV6+adenanthin and adenanthin alone were compared to no-treatment in mice with medulloblastoma brain tumor (*i.e.*, D425-Med-Luc tumors). The group treated with HAV6+adenanthin shown significant suppression of brain tumors compared to adenanthin-treated and non-treated groups.[25] In addition, HAV6+adenanthin group had a median survival of 30 days post-tumor cell injection. In contrast, the median day of survival after tumor cell injection for Ade-alone was 20 days, which was similar to that of non-treated groups (19 days).[25] About 50% of HAV6+adenathin-treated group was able to complete a five cycle-treatment, which resulted in 45 days of survival post tumor cell injection. These mice showed a complete elimination of brain tumor as detected by bioluminescence imaging.[25] These results support the potential applicability of HAV6 peptide and other cadherin peptides (i.e., ADTC5, ADTHAV, HAVN1, HAVN2) for delivering therapeutic agents in models of brain diseases.

Throughout the course of our studies, we found that the *in vivo* I.V. administration small and large molecules in mice was a better and more sensitive method than the *in-situ* rat brain perfusion method. Previously, ADTC5 has been used to deliver ^{3}H-PEG-1500 and ^{14}C-PEG-40,000 into the brain using *in-situ* rat brain perfusion method.[20] However, the results gave a trend of enhanced brain delivery for both PEG molecules when co-delivered with ADTC5 but these enhancements

were not statistically significant when compared to control.[20] In that study, the delivered radioactive PEG molecules were diluted with the non-radioactive PEG; thus, the detected radioactivity was a fraction of delivered molecules in the brain. In contrast, the brain deposition of IRdye800CW-labeled 25 KDa PEG was significantly higher when administered with a cadherin peptide (HAV6) compared to without the peptide using *in vivo* I.V. administration with 15 min circulation time.[21] The differences in results in brain delivery of molecules (i.e., PEGs or proteins) in the *in-situ* rat brain and *in vivo* delivery method in mice could be attributed to the differences in experimental conditions in these two methods. In the *in-situ* rat brain perfusion method, the BBB exposure time to ADTC5 and PEG molecules was only 2 min with one pass perfusion through the BBB vasculature before detecting deposition of delivered molecules in the brain. In contrast, *in vivo* delivery via I.V. administration of IRdye800CW-labeled molecules with cadherin peptides (i.e., ADTC5 or HAV6) has 15 min circulation time; thus, the BBB exposure to the administered molecule was longer than those in the *in-situ* rat brain perfusion studies. We also found that the dose of delivered molecules and the labeled used to detect the molecule could help the quantitation of the delivered molecules in the brain.

A common concern of our method is extended duration of BBB modulation that allows unwanted molecules to cross the BBB into the brain. Using *in vivo* MRI studies to detect the delivery of 65 kDa albumin in living mice, we have demonstrated a significant brain deposition of galbumin after I.V. administration of the ADTC5 + galbumin mixture compared to administration of galbumin alone.[22] When the mice were pretreated with ADTC5 followed by administration of galbumin 10 min later, galbumin was still detected in the brain; however, galbumin was no longer detected in the brain when it was administered 40 min after ADTC5. These results indicate that the BBB porosity increase due to ADTC5 modulation returns to normal after 10 to 40 min. This is

a short duration of opening for modulation of the BBB compared to the "osmotic method's" use of a hypertonic mannitol solution that disrupts the BBB for several hours. Previously, we have demonstrated that the *ex vivo* intercellular pathology of the BBB of mice treated with ADTC5 after both two and four hours shows a BBB appearance similar to that of untreated, healthy mice, indicating that BBB modulated by ADTC5 is reversible to normal BBB conditions.[20] In the present study, multiple I.V. injections of ADTC5 in the presence of BDNF up to eight times did not show any toxicity to the mice. These findings in aggregate suggest that BBB modulation using ADTC5 is reversible, nontoxic, and does not induce long term effects on the BBB junctions.

It is proposed that modulation of the BBB by cadherin peptides (*i.e.,* ADTC5 and HAV6) to increase paracellular porosity is due to their binding to cadherins and inhibiting cadherin-cadherin interactions in a reversible and dynamic fashion. Cadherin-cadherin interactions are part of cell-cell adhesion and act as "Velcro" in the adherens junctions of the BBB, and ADTC5 and HAV6 peptides have been shown to enhance the penetration of molecules through the paracellular pathway.[1, 20] NMR binding studies between ADTC5 or HAV6 peptide to the EC1 domain of E-cadherin have indicated that each peptide binds to a different region of the EC1 domain. From these binding studies, ADTC5 is proposed to bind to the EC1-EC1 domain swapping region by blocking the EC1-EC1 *trans*-cadherin interactions to increase paracellular porosity. In contrast, HAV6 peptide is proposed to interact with the EC1 domain to block *cis* EC1-EC2 cadherin interactions. Although both peptides bind to different sites on the EC1 domain of E-cadherin, they are able to modulate cadherin interactions in the BBB.[19, 20] E-cadherin is primarily found in epithelial cells such as intestinal mucosa epithelium, and VE-cadherin (cadherin-5) is expressed in peripheral endothelium. However, it is still not clear whether the BBB has only VE-cadherin or a combination E- and VE-cadherins. In Western blots analysis, anti-E-cadherin antibody but not

anti-VE-cadherin (anti-cadherin-5) can detect cadherin in the homogenates of bovine brain microvessel endothelial cells (BBMEC).[61] It has been suggested that cadherin in the intercellular junction of the BBB has E-cadherin-like properties and that the VE-cadherin might be contributing to the BBB function.[62, 63] Thus, there is still a need to study the selectivity of cadherin peptides to cadherins in the BBB versus cadherins in other body parts (*e.g.,* intestinal mucosa, kidney and lung).

2.5. Conclusions

The present study has demonstrated that BDNF can be delivered to the brains of mice via systemic administration using ADTC5 as a BBB modulator. To the best of our knowledge, this is the first demonstration of non-invasive delivery of BDNF that suppresses disease relapse in EAE mice, an animal model for multiple sclerosis. Multiple I.V. administrations of BDNF + ADTC5 significantly improve the clinical body scores of EAE mice compared to mice that received BDNF alone, ADTC5 alone or vehicle. BDNF can permeate the BBB and exert an immediate effect to upregulate pTrkB receptors. Additionally, delivered BDNF was shown to induce remyelination and increase the presence of NG2 glia cells as well as stimulate downstream EGR1 and ARC mRNA transcripts. These results demonstrate that ADTC5 could be used to modulate the BBB to improve non-invasive brain delivery of BDNF or other proteins to treat brain diseases. Further studies are being conducted for brain delivery of various sized proteins in healthy and brain disease animal models.

2.6. Figures and Figure Legends:

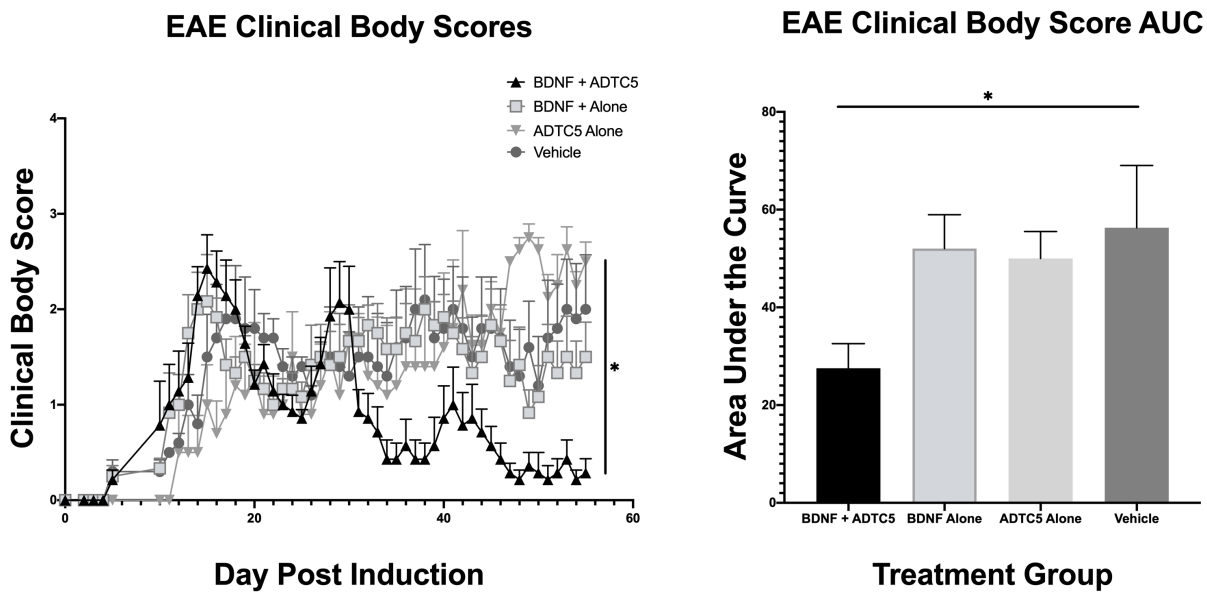

Figure 2.1. The effect of treatment of SJL/elite EAE mice, an animal model for MS, with BDNF (5.71 nmol/kg) + ADTC5 (10 µmol/kg; n = 7), BDNF alone (5.71 nmol/kg; n = 6), ADTC5 alone (10 µmol/kg; n = 5), or vehicle (n = 5) during remission on days 21, 25, 29, 33, 37, 4;1, 45, and 48. **(A)** Clinical disease score vs. time of mice treated 8 times with either BDNF + ADTC5, BDNF alone, ADTC5 alone or vehicle; arrows indicate treatment days. **(B)** Comparison of area under the curve (AUC) of the disease scores from days 21–55 from EAE mice treated with BDNF + ADTC5, BDNF alone, ADTC5 alone, or vehicle. *$p \leq 0.05$*; one-way ANOVA (95% confidence).*

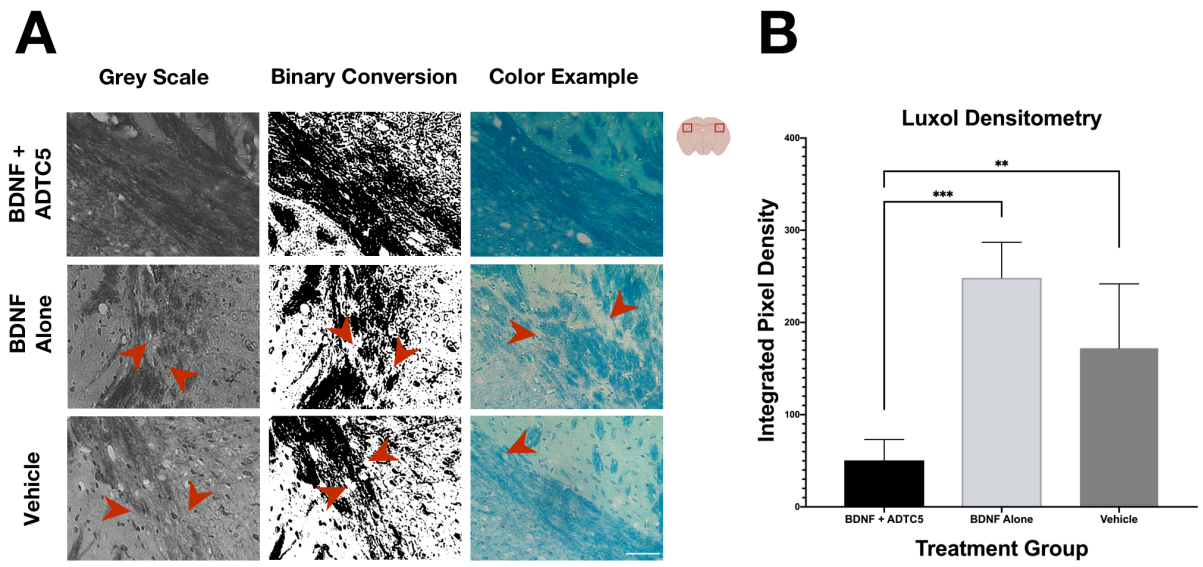

Figure 2.2. The effects of BDNF (5.71 nmol/kg) + ADTC5 (10 µmol/kg), BDNF alone (5.71 nmol/kg), or vehicle treatments on remyelination in the lateral corpus callosum and surrounding cortex of the brains of SJL/elite EAE mice as stained by Luxol fast blue. **(A)** Greyscale, the binary conversion, and color photomicrograph of myelin images taken under identical exposure of the lateral corpus callosum of EAE mice treated with BDNF + ADTC5, BDNF Alone, or vehicle; red arrows indicate breakages in the myelin **(B)** Quantitative myelin densiometric comparison in the brain of BDNF + ADTC5, BDNF Alone, and vehicle treated EAE mice; Scale bar = 50 µm; $^{**}p \leq 0.01$ $^{***}p \leq 0.001$; *one-way ANOVA (95% confidence; n = 5).*

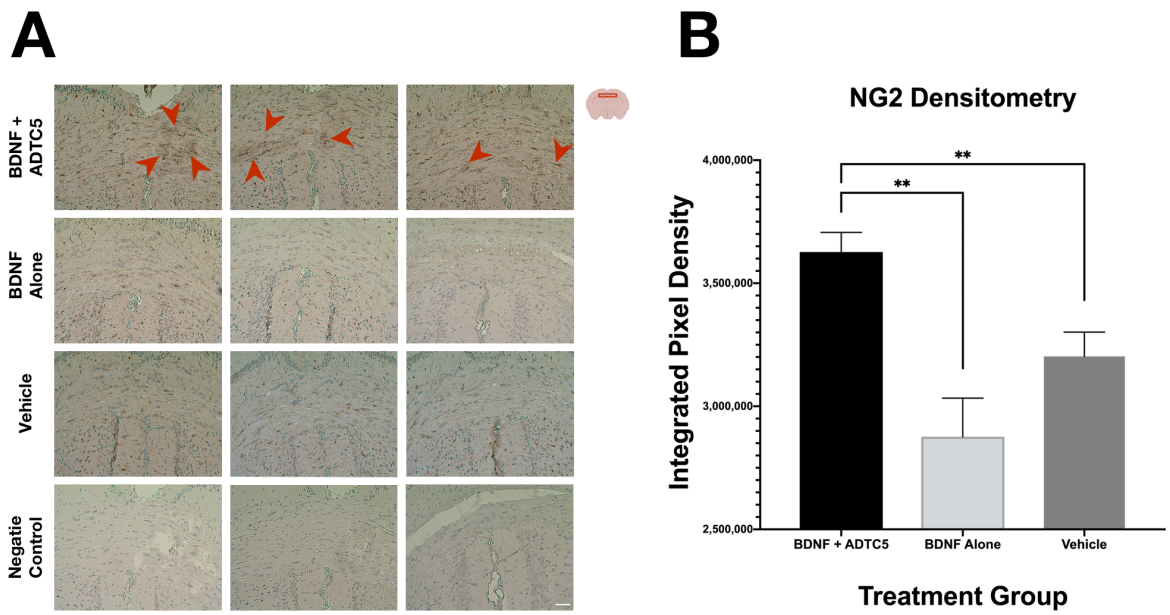

Figure 2.3. The effects of BDNF (5.71 nmol/kg) + ADTC5 (10 µmol/kg), BDNF Alone (5.71 nmol/kg), or vehicle treatments on presence of NG2 receptor in the medial corpus callosum of brains of SJL/elite EAE mice as stained by DAB. **(A)** Color photomicrograph of anti-NG2 staining (brown) taken under identical conditions from the medial corpus callosum for mice treated with BDNF + ADTC5, BDNF alone, vehicle; red arrows point to dense regions of activated NG2-glia. **(B)** Quantitative NG2 density comparison amongst the EAE mice treated with BDNF + ADTC5, BDNF alone, and vehicle; Scale bar = 50 µm; $^{**}p \leq 0.01$*; one-way ANOVA (95% confidence; n = 5).*

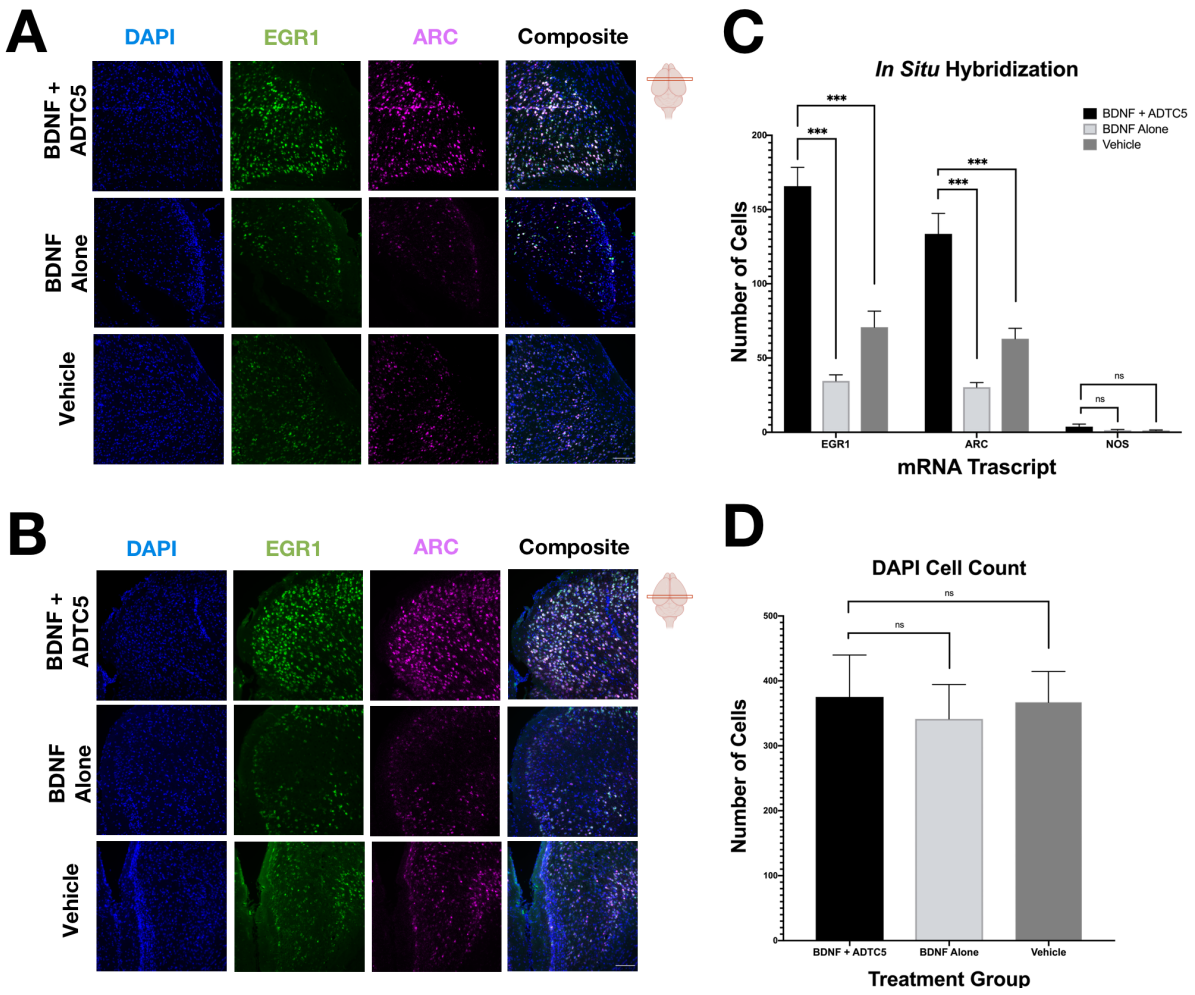

Figure 2.4. The effects of BDNF (5.71 nmol/kg) + ADTC5 (10 µmol/kg), BDNF alone (5.71 nmol/kg), or vehicle treatments on mRNA expression of EGR1 and ARC in the cortex of the brains of SJL/elite EAE mice. **(A, B)** Photomicrograph of DAPI (blue), EGR1 (green), ARC (magenta), and composite images taken of the cortex of the midbrain **(A)** and hindbrain **(B)** of EAE mice treated with BDNF + ADTC5, BDNF alone, or vehicle. **(C)** Quantitative comparison of EGR, ARC, and NOS1 mRNA transcript expression, as determined by cell count, for mice treated with BDNF + ADTC5, BDNF alone, or vehicle. **(D)** Quantitative comparison of DAPI cell count; Scale

bar = 50 μm; ***$p \leq 0.001$; *one-way ANOVA (99% confidence; n = 5). Contrast and brightness of images were adjusted only for display purposes.*

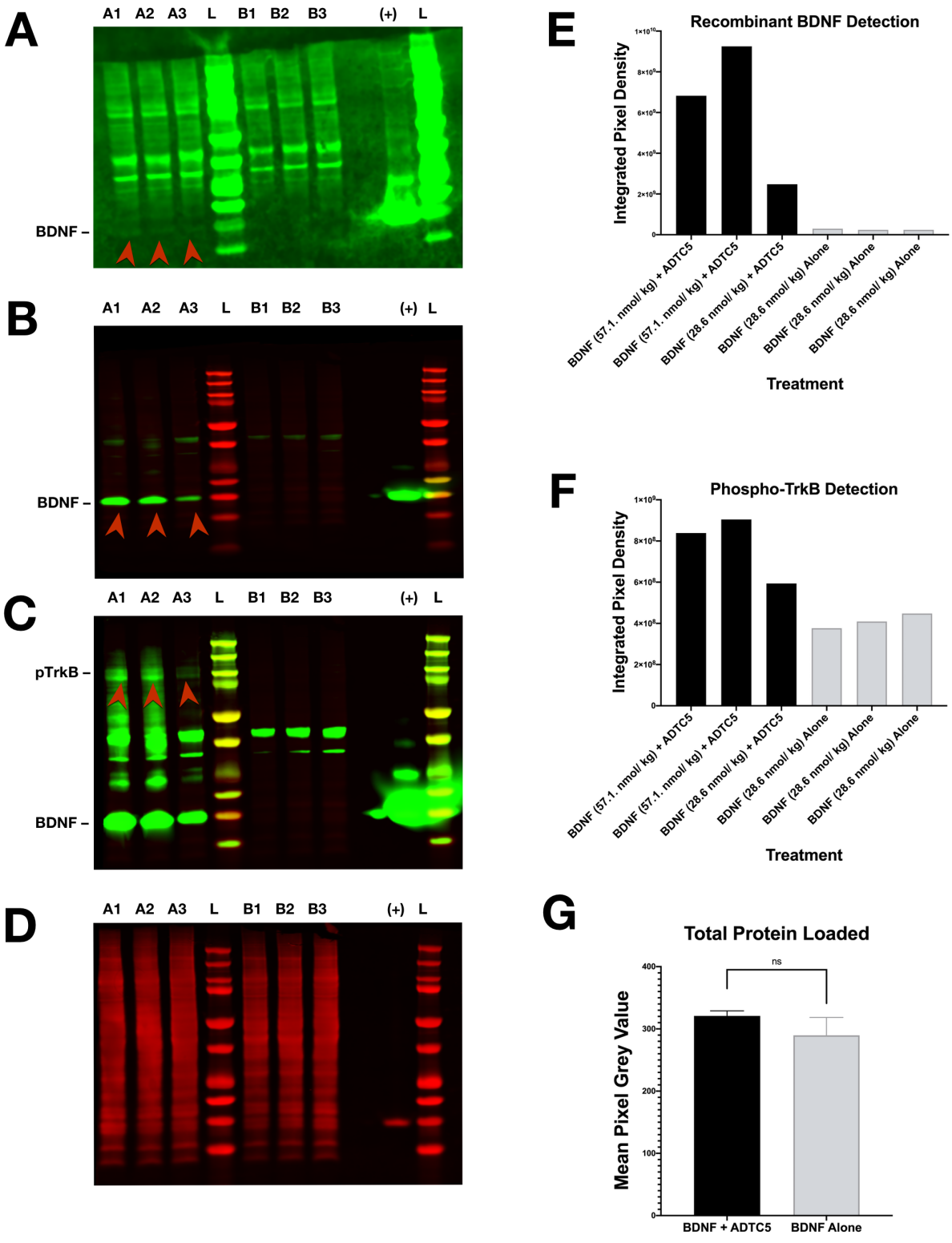
A
A1 A2 A3 L B1 B2 B3 (+) L
BDNF –
B
A1 A2 A3 L B1 B2 B3 (+) L
BDNF –
C
A1 A2 A3 L B1 B2 B3 (+) L
pTrkB –
BDNF –
D
A1 A2 A3 L B1 B2 B3 (+) L
E
Recombinant BDNF Detection
Integrated Pixel Density
BDNF (57.1, nmol/ kg) + ADTC5
BDNF (57.1, nmol/ kg) + ADTC5
BDNF (28.6 nmol/ kg) + ADTC5
BDNF (28.6 nmol/ kg) Alone
BDNF (28.6 nmol/ kg) Alone
BDNF (28.6 nmol/ kg) Alone
Treatment
F
Phospho-TrkB Detection
Integrated Pixel Density
BDNF (57.1, nmol/ kg) + ADTC5
BDNF (57.1, nmol/ kg) + ADTC5
BDNF (28.6 nmol/ kg) + ADTC5
BDNF (28.6 nmol/ kg) Alone
BDNF (28.6 nmol/ kg) Alone
BDNF (28.6 nmol/ kg) Alone
Treatment
G
Total Protein Loaded
ns
Mean Pixel Grey Value
BDNF + ADTC5
BDNF Alone

Figure 2.5. Western blot detection of recombinant BDNF and pTrkB from mice treated with either BDNF + ADTC5 or BDNF alone. **(A)** Western blot probing for recombinant BDNF in the brains of mice that received BDNF (5.71 nmol/kg) + ADTC5 (10 µmol/kg; A1, A2, A3) or BDNF alone (5.71 nmol/kg, B1, B2, B3); 'L' represents molecular weight ladder; '+' represents the positive control of recombinant BDNF; red arrows highlight increased recombinant BDNF detection. **(B)** Western blot probing for recombinant BDNF after dosage increase in healthy mice that received BDNF (57.1 nmol/kg) + ADTC5 (10 µmol/kg; A1, A2), BDNF (28.6 nmol/kg) + ADTC5 (10 µmol/kg; A3), or), BDNF alone (28.6 nmol/kg; B1, B2, B3); red arrows highlight increased recombinant BDNF detection. **(C)** Western Blot probing for pTrkB after dosage increase of healthy mice that received BDNF (57.1 nmol/kg) + ADTC5 (10 µmol/kg; A1, A2), BDNF (28.6 nmol/kg) + ADTC5 (10 µmol/kg; A3), or BDNF alone (28.6 nmol/kg; B1, B2, B3); red arrows highlight increased pTrkB detection. **(D)** Total protein stain (loading control) for samples treated with BDNF 57.1 nmol/kg or 28.6 nmol/kg in B and C. **(E)** Graphical representation of recombinant BDNF detection level in mice that received BDNF (57.1 nmol/kg) + ADTC5 (10 µmol/kg; A1, A2), BDNF (28.6 nmol/kg) + ADTC5 (10 µmol/kg; A3), or BDNF alone (28.6 nmol/kg; B1, B2, B3). **(F)** Graphical representation of pTrkB detection level for mice that received BDNF (57.1 nmol/kg) + ADTC5 (10 µmol/kg; A1, A2), BDNF (28.6 nmol/kg) + ADTC5 (10 µmol/kg; A3), or BDNF alone (28.6 nmol/kg; B1, B2, B3). **(G)** Graphical representation of total protein loaded among all groups. *Contrast and brightness of images were adjusted only for display purposes.*

2.7. References:

1. Laksitorini, M.; Prasasty, V. D.; Kiptoo, P. K.; Siahaan, T. J. Pathways and progress in improving drug delivery through the intestinal mucosa and blood-brain barriers. *Ther Deliv* **2014,** *5*, (10), 1143-63.
2. Steinman, L. Blocking adhesion molecules as therapy for multiple sclerosis: natalizumab. *Nat Rev Drug Discov* **2005,** *4*, (6), 510–8.
3. Duda, P. W.; Schmied, M. C.; Cook, S. L.; Krieger, J. I.; Hafler, D. A. Glatiramer acetate (Copaxone) induces degenerate, Th2-polarized immune responses in patients with multiple sclerosis. *The Journal of clinical investigation* **2000,** *105*, (7), 967-76.
4. Trapp, B. D.; Ransohoff, R.; Rudick, R. Axonal pathology in multiple sclerosis: relationship to neurologic disability. *Curr Opin Neurol* **1999,** *12*, (3), 295-302.
5. Ineichen, B. V.; Plattner, P. S.; Good, N.; Martin, R.; Linnebank, M.; Schwab, M. E. Nogo-A Antibodies for Progressive Multiple Sclerosis. *CNS Drugs* **2017,** *31*, (3), 187-198.
6. Ruggieri, S.; Tortorella, C.; Gasperini, C. Anti lingo 1 (opicinumab) a new monoclonal antibody tested in relapsing remitting multiple sclerosis. *Expert Rev Neurother* **2017,** *17*, (11), 1081-1089.
7. Ciric, B.; Howe, C. L.; Paz Soldan, M.; Warrington, A. E.; Bieber, A. J.; Van Keulen, V.; Rodriguez, M.; Pease, L. R. Human monoclonal IgM antibody promotes CNS myelin repair independent of Fc function. *Brain Pathol* **2003,** *13*, (4), 608-16.
8. Fisher, T. L.; Reilly, C. A.; Winter, L. A.; Pandina, T.; Jonason, A.; Scrivens, M.; Balch, L.; Bussler, H.; Torno, S.; Seils, J.; Mueller, L.; Huang, H.; Klimatcheva, E.; Howell, A.; Kirk,

R.; Evans, E.; Paris, M.; Leonard, J. E.; Smith, E. S.; Zauderer, M. Generation and preclinical characterization of an antibody specific for SEMA4D. *MAbs* **2016,** *8*, (1), 150-62.

9. Crozier, R. A.; Bi, C.; Han, Y. R.; Plummer, M. R. BDNF modulation of NMDA receptors is activity dependent. *J Neurophysiol* **2008,** *100*, (6), 3264-74.
10. Obermeyer, J. M.; Tuladhar, A.; Payne, S. L.; Ho, E.; Morshead, C. M.; Shoichet, M. S. Local Delivery of Brain-Derived Neurotrophic Factor Enables Behavioral Recovery and Tissue Repair in Stroke-Injured Rats. *Tissue Engineering Part A* **2019,** 10.1089/ten.tea.2018.0215, ten.TEA.2018.0215-38.
11. Nagahara, A. H.; Bernot, T.; Moseanko, R.; Brignolo, L.; Blesch, A.; Conner, J. M.; Ramirez, A.; Gasmi, M.; Tuszynski, M. H. Long-term reversal of cholinergic neuronal decline in aged non-human primates by lentiviral NGF gene delivery. *Exp Neurol* **2009,** *215*, (1), 153-9.
12. Kaspar, B. K.; Llado, J.; Sherkat, N.; Rothstein, J. D.; Gage, F. H. Retrograde viral delivery of IGF-1 prolongs survival in a mouse ALS model. *Science* **2003,** *301*, (5634), 839-42.
13. Givalois, L.; Naert, G.; Rage, F.; Ixart, G.; Arancibia, S.; Tapia-Arancibia, L. A single brain-derived neurotrophic factor injection modifies hypothalamo-pituitary-adrenocortical axis activity in adult male rats. *Mol Cell Neurosci* **2004,** *27*, (3), 280-95.
14. Crawford, D. K.; Mangiardi, M.; Song, B.; Patel, R.; Du, S.; Sofroniew, M. V.; Voskuhl, R. R.; Tiwari-Woodruff, S. K. Oestrogen receptor beta ligand: a novel treatment to enhance endogenous functional remyelination. *Brain* **2010,** *133*, (10), 2999-3016.
15. Steelman, A. J.; Thompson, J. P.; Li, J. Demyelination and remyelination in anatomically distinct regions of the corpus callosum following cuprizone intoxication. *Neurosci Res* **2012,** *72*, (1), 32-42.

16. Oldendorf, W. H.; Hyman, S.; Braun, L.; Oldendorf, S. Z. Blood-brain barrier: penetration of morphine, codeine, heroin, and methadone after carotid injection. *Science* **1972,** *178*, (4064), 984-6.

17. Kroll, R. A.; Neuwelt, E. A. Outwitting the blood-brain barrier for therapeutic purposes: Osmotic opening and other means. *Neurosurgery* **1998,** *42*, 1083–99.

18. Ulapane, K. R.; Kopec, B. M.; Moral, M. E. G.; Siahaan, T. J. Peptides and Drug Delivery. *Adv Exp Med Biol* **2017,** *1030*, 167-184.

19. Alaofi, A.; On, N.; Kiptoo, P.; Williams, T. D.; Miller, D. W.; Siahaan, T. J. Comparison of Linear and Cyclic His-Ala-Val Peptides in Modulating the Blood-Brain Barrier Permeability: Impact on Delivery of Molecules to the Brain. *J Pharm Sci* **2016,** *105*, (2), 797-807.

20. Laksitorini, M. D.; Kiptoo, P. K.; On, N. H.; Thliveris, J. A.; Miller, D. W.; Siahaan, T. J. Modulation of intercellular junctions by cyclic-ADT peptides as a method to reversibly increase blood-brain barrier permeability. *J Pharm Sci* **2015,** *104*, (3), 1065-75.

21. On, N. H.; Kiptoo, P.; Siahaan, T. J.; Miller, D. W. Modulation of blood-brain barrier permeability in mice using synthetic E-cadherin peptide. *Mol Pharm* **2014,** *11*, (3), 974-81.

22. Ulapane, K. R.; On, N.; Kiptoo, P.; Williams, T. D.; Miller, D. W.; Siahaan, T. J. Improving Brain Delivery of Biomolecules via BBB Modulation in Mouse and Rat: Detection using MRI, NIRF, and Mass Spectrometry. *Nanotheranostics* **2017,** *1*, (2), 217-231.

23. Ulapane, K. R.; Kopec, B. M.; Siahaan, T. J. In Vivo Brain Delivery and Brain Deposition of Proteins with Various Sizes. *Mol Pharm* **2019,** 10.1021/acs.molpharmaceut.9b00763.

24. Ulapane, K. R.; Kopec, B. M.; Siahaan, T. J. Improving In Vivo Brain Delivery of Monoclonal Antibody Using Novel Cyclic Peptides. *Pharmaceutics* **2019,** *11*, (11).

25. Sajesh, B. V.; On, N. H.; Omar, R.; Alrushaid, S.; Kopec, B. M.; Wang, W.-G.; Sun, H.-D.; Lillico, R.; Lakowski, T. M.; Siahaan, T. J.; Davies, N. M.; Puno, P.-T.; Vanan, M. I.; Miller, D. W. Validation of Cadherin HAV6 Peptide in the Transient Modulation of the Blood-Brain Barrier for the Treatment of Brain Tumors. *Pharmaceutics* **2019,** *11*, 481.

26. Yang, S.; Chen, Y.; Feng, M.; Rodriguez, L.; Wu, J. Q.; Wang, M. Z. Improving eflornithine oral bioavailability and brain uptake by modulating intercellular junctions with an E-cadherin peptide. *J Pharm Sci* **2019,** 10.1016/j.xphs.2019.09.015.

27. Kobayashi, N.; Kiptoo, P.; Kobayashi, H.; Ridwan, R.; Brocke, S.; Siahaan, T. J. Prophylactic and therapeutic suppression of experimental autoimmune encephalomyelitis by a novel bifunctional peptide inhibitor. *Clin Immunol* **2008,** *129*, (1), 69-79.

28. Kobayashi, N.; Kobayashi, H.; Gu, L.; Malefyt, T.; Siahaan, T. J. Antigen-specific suppression of experimental autoimmune encephalomyelitis by a novel bifunctional peptide inhibitor. *J Pharmacol Exp Ther* **2007,** *322*, (2), 879-86.

29. Vasquez, J. J.; Hussien, R.; Aguilar-Rodriguez, B.; Junger, H.; Dobi, D.; Henrich, T. J.; Thanh, C.; Gibson, E.; Hogan, L. E.; McCune, J.; Hunt, P. W.; Stoddart, C. A.; Laszik, Z. G. Elucidating the Burden of HIV in Tissues Using Multiplexed Immunofluorescence and In Situ Hybridization: Methods for the Single-Cell Phenotypic Characterization of Cells Harboring HIV In Situ. *J Histochem Cytochem* **2018,** *66*, (6), 427-446.

30. Gershon, T. R.; Crowther, A. J.; Liu, H.; Miller, C. R.; Deshmukh, M. Cerebellar granule neuron progenitors are the source of Hk2 in the postnatal cerebellum. *Cancer Metab* **2013,** *1*, (1), 15.

31. Smith, P. A.; Schmid, C.; Zurbruegg, S.; Jivkov, M.; Doelemeyer, A.; Theil, D.; Dubost, V.; Beckmann, N. Fingolimod inhibits brain atrophy and promotes brain-derived neurotrophic factor in an animal model of multiple sclerosis. *J Neuroimmunol* **2018,** *318*, 103-113.

32. Vondran, M. W.; Clinton-Luke, P.; Honeywell, J. Z.; Dreyfus, C. F. BDNF+/- mice exhibit deficits in oligodendrocyte lineage cells of the basal forebrain. *Glia* **2010,** *58*, (7), 848-56.

33. Lang, E. M.; Schlegel, N.; Reiners, K.; Hofmann, G. O.; Sendtner, M.; Asan, E. Single-dose application of CNTF and BDNF improves remyelination of regenerating nerve fibers after C7 ventral root avulsion and replantation. *J Neurotrauma* **2008,** *25*, (4), 384-400.

34. VonDran, M. W.; Singh, H.; Honeywell, J. Z.; Dreyfus, C. F. Levels of BDNF impact oligodendrocyte lineage cells following a cuprizone lesion. *J Neurosci* **2011,** *31*, (40), 14182-90.

35. Hu, Y.; Russek, S. J. BDNF and the diseased nervous system: a delicate balance between adaptive and pathological processes of gene regulation. *J Neurochem* **2008,** *105*, (1), 1-17.

36. Alder, J.; Thakker-Varia, S.; Bangasser, D. A.; Kuroiwa, M.; Plummer, M. R.; Shors, T. J.; Black, I. B. Brain-derived neurotrophic factor-induced gene expression reveals novel actions of VGF in hippocampal synaptic plasticity. *J Neurosci* **2003,** *23*, (34), 10800-8.

37. Li, L.; Carter, J.; Gao, X.; Whitehead, J.; Tourtellotte, W. G. The neuroplasticity-associated arc gene is a direct transcriptional target of early growth response (Egr) transcription factors. *Mol Cell Biol* **2005,** *25*, (23), 10286-300.

38. Yin, Y.; Edelman, G. M.; Vanderklish, P. W. The brain-derived neurotrophic factor enhances synthesis of Arc in synaptoneurosomes. *Proc Natl Acad Sci U S A* **2002,** *99*, (4), 2368-73.

39. Novikov, L.; Novikova, L.; Kellerth, J. O. Brain-derived neurotrophic factor promotes survival and blocks nitric oxide synthase expression in adult rat spinal motoneurons after ventral root avulsion. *Neurosci Lett* **1995,** *200*, (1), 45-8.

40. Engelhardt, B.; Liebner, S. Novel insights into the development and maintenance of the blood-brain barrier. *Cell Tissue Res* **2014,** *355*, (3), 687-99.

41. Cosolo, W. C.; Martinello, P.; Louis, W. J.; Christophidis, N. Blood-brain barrier disruption using mannitol: time course and electron microscopy studies. *Am J Physiol* **1989,** *256*, (2 Pt 2), R443-7.

42. Farrell, C. L.; Shivers, R. R. Capillary junctions of the rat are not affected by osmotic opening of the blood-brain barrier. *Acta Neuropathol* **1984,** *63*, (3), 179-89.

43. Yoshii, A.; Constantine-Paton, M. Postsynaptic BDNF-TrkB signaling in synapse maturation, plasticity, and disease. *Dev Neurobiol* **2010,** *70*, (5), 304-22.

44. Numakawa, T.; Suzuki, S.; Kumamaru, E.; Adachi, N.; Richards, M.; Kunugi, H. BDNF function and intracellular signaling in neurons. *Histol Histopathol* **2010,** *25*, (2), 237-58.

45. Reynolds, R.; Dawson, M.; Papadopoulos, D.; Polito, A.; Di Bello, I. C.; Pham-Dinh, D.; Levine, J. The response of NG2-expressing oligodendrocyte progenitors to demyelination in MOG-EAE and MS. *J Neurocytol* **2002,** *31*, (6-7), 523-36.

46. Gold, R.; Hartung, H. P.; Toyka, K. V. Animal models for autoimmune demyelinating disorders of the nervous system. *Mol Med Today* **2000,** *6*, (2), 88-91.

47. Du, Y.; Lercher, L. D.; Zhou, R.; Dreyfus, C. F. Mitogen-activated protein kinase pathway mediates effects of brain-derived neurotrophic factor on differentiation of basal forebrain oligodendrocytes. *J Neurosci Res* **2006,** *84*, (8), 1692-702.

48. Tsiperson, V.; Huang, Y.; Bagayogo, I.; Song, Y.; VonDran, M. W.; DiCicco-Bloom, E.; Dreyfus, C. F. Brain-derived neurotrophic factor deficiency restricts proliferation of oligodendrocyte progenitors following cuprizone-induced demyelination. *ASN Neuro* **2015,** *7*, (1).

49. Habtemariam, S. The brain-derived neurotrophic factor in neuronal plasticity and neuroregeneration: new pharmacological concepts for old and new drugs. *Neural Regen Res* **2018,** *13*, (6), 983-984.

50. Roberts, D. S.; Hu, Y.; Lund, I. V.; Brooks-Kayal, A. R.; Russek, S. J. Brain-derived neurotrophic factor (BDNF)-induced synthesis of early growth response factor 3 (Egr3) controls the levels of type A GABA receptor alpha 4 subunits in hippocampal neurons. *J Biol Chem* **2006,** *281*, (40), 29431-5.

51. Ying, S. W.; Futter, M.; Rosenblum, K.; Webber, M. J.; Hunt, S. P.; Bliss, T. V.; Bramham, C. R. Brain-derived neurotrophic factor induces long-term potentiation in intact adult hippocampus: requirement for ERK activation coupled to CREB and upregulation of Arc synthesis. *J Neurosci* **2002,** *22*, (5), 1532-40.

52. Chen, M. J.; Ivy, A. S.; Russo-Neustadt, A. A. Nitric oxide synthesis is required for exercise-induced increases in hippocampal BDNF and phosphatidylinositol 3' kinase expression. *Brain Res Bull* **2006,** *68*, (4), 257-68.

53. Bonthius, D. J.; Karacay, B.; Dai, D.; Pantazis, N. J. FGF-2, NGF and IGF-1, but not BDNF, utilize a nitric oxide pathway to signal neurotrophic and neuroprotective effects against alcohol toxicity in cerebellar granule cell cultures. *Brain Res Dev Brain Res* **2003,** *140*, (1), 15-28.

54. Wu, D.; Pardridge, W. M. Neuroprotection with noninvasive neurotrophin delivery to the brain. *Proc Natl Acad Sci U S A* **1999,** *96*, (1), 254-9.

55. Zhang, Y.; Pardridge, W. M. Conjugation of brain-derived neurotrophic factor to a blood-brain barrier drug targeting system enables neuroprotection in regional brain ischemia following intravenous injection of the neurotrophin. *Brain Res* **2001,** *889*, (1-2), 49-56.

56. Baseri, B.; Choi, J. J.; Deffieux, T.; Samiotaki, G.; Tung, Y. S.; Olumolade, O.; Small, S. A.; Morrison, B.; Konofagou, E. E. Activation of signaling pathways following localized delivery of systemically administered neurotrophic factors across the blood-brain barrier using focused ultrasound and microbubbles. *Phys Med Biol* **2012,** *57*, (7), N65-81.

57. Kinoshita, M.; McDannold, N.; Jolesz, F. A.; Hynynen, K. Noninvasive localized delivery of Herceptin to the mouse brain by MRI-guided focused ultrasound-induced blood-brain barrier disruption. *Proc Natl Acad Sci U S A* **2006,** *103*, (31), 11719-23.

58. Rodriguez-Frutos, B.; Otero-Ortega, L.; Ramos-Cejudo, J.; Martinez-Sanchez, P.; Barahona-Sanz, I.; Navarro-Hernanz, T.; Gomez-de Frutos Mdel, C.; Diez-Tejedor, E.; Gutierrez-Fernandez, M. Enhanced brain-derived neurotrophic factor delivery by ultrasound and microbubbles promotes white matter repair after stroke. *Biomaterials* **2016,** *100*, (C), 41-52.

59. Baseri, B.; Choi, J. J.; Tung, Y. S.; Konofagou, E. E. Multi-modality safety assessment of blood-brain barrier opening using focused ultrasound and definity microbubbles: a short-term study. *Ultrasound Med Biol* **2010,** *36*, (9), 1445-59.

60. Samiotaki, G.; Vlachos, F.; Tung, Y.-S.; Konofagou, E. E. A quantitative pressure and microbubble-size dependence study of focused ultrasound-induced blood-brain barrier opening reversibility in vivo using MRI. *Magnetic Resonance in Medicine* **2012,** *67*, (3), 769-777.

61. Pal, D.; Audus, K. L.; Siahaan, T. J. Modulation of cellular adhesion in bovine brain microvessel endothelial cells by a decapeptide. *Brain Res* **1997,** *747*, (1), 103-13.

62. Vorbrodt, A. W.; Dobrogowska, D. H. Molecular anatomy of interendothelial junctions in human blood-brain barrier microvessels. *Folia histochemica et cytobiologica / Polish Academy of Sciences, Polish Histochemical and Cytochemical Society* **2004,** *42*, (2), 67-75.

63. Rubin, L. L.; Staddon, J. M. The cell biology of the blood-brain barrier. *Annu Rev Neurosci* **1999,** *22*, 11-28.

Chapter 3: Efficacy Evaluation of Non-Invasive Brain Delivery of BDNF in APP/PS1 Transgenic Mice

3.1. Introduction:

To date, effective treatments for Alzheimer's disease (AD) have remained elusive. Currently, treatment of Alzheimer's disease focuses on managing symptoms by regulating neurotransmitter levels in the CNS and peripheral nervous system. Acetylcholinesterase inhibitors such as donepezil (Aricept®),[1] rivastigmine (Eexelon®),[2] and galantamine (Razadyne®),[3] have been the primary choice of treatment for those with moderate to severe AD. Additionally, N-methyl-d-aspartate (NMDA) receptor regulators, such as memantine (Namenda®)[4] or a combination of acetylcholinesterase inhibition and NMDA regulators (Namzaric®) have been used to treat AD.[5, 6] While these treatments may aid in temporary relief of symptoms such as moderate confusion, sleeplessness, agitation, anxiety, and aggression, their benefits are almost always temporary and ultimately these drugs prove to be highly cost ineffective.[1, 7] Thus, there is an urgent need to find early diagnostic and therapeutic solutions to halt or reverse progress of the disease.

Within the past two decades there have been extensive attempts to develop "disease-modifying drugs" rather than "symptom-suppression drugs." To block the progression of Alzheimer's, developed drugs must interfere with the pathogenic steps responsible for the manifestation of clinical symptoms. Such pathogenic steps include the early build-up of extracellular amyloid-beta plaques, the intercellular build-up of neurofibrillary tangle Tau formations, neuroinflammation, oxidative damage, metal ion deregulation, and cholesterol metabolism.[8] There has been a tremendous effort to develope therapeutics based on preventing the formation of or removing the amyloid-beta (Aβ) plaques in the brain. These potential treatments include enzyme inhibitors, anti-Aβ monoclonal antibodies (mAbs), and immunotherapies. The use of active vaccine therapies,

AN1792 and CAD106, has not been successful due to unforeseen side effects or low efficacy. In the case of AN1792, selected treated patients developed T cell-mediated meningoencephalitis.[9] CAD106 was the only vaccine to advance to phase-3 trials for prevention of Alzheimer's disease; however, the trial results have indicated that such vaccine treatments may be too little too late to provide a significant effect.[10] Active vaccination for treatment of AD was met with additional challenges, including immune response that varies with the age of patients with AD and the propensity for adverse effects. To avoid the complications from active vaccination of AD patients, passive immunization has arisen as an attractive alternative for AD. Thus, administration of mAbs therapeutics ensures consistent and controlled antibody titers in which adverse side effects can be controlled by halting the treatment. The primary drawback of mAb treatments is its high cost due to the repeated doses and expensive cost of antibody production.[10, 11]

Several mAbs have undergone through extensive development and clinical trials for the treatment of AD; however, to date, none have gained FDA approval for the treatment of AD or other CNS diseases regardless of the extensive target validation, *in vitro* success, and excellent PK and safety profiles. Bapineuzumab (AAB-001) was the first antibody drug to reach phase-2 clinical trials for AD since AN1792. Unfortunately, no significant treatment outcomes such as improvement in disability assessment for dementia scores were observed; thus, the trial was discontinued due to the lack of positive results. Since bapineuzumab, at least seven mAbs were evaluated for AD treatment without success.[10, 12, 13] Most recently, after being abandoned, aducanumab has been reevaluated following an additional analysis of clinical trials data. Alternatively, neurotrophic agents such as brain-derived neurotrophic factor (BDNF), nerve growth factor (NGF), and insulin-like growth factor have been investigated for the treatment of

AD.[14, 15] Similar to mAbs, these neurotrophic proteins have met with challenges for their use in the treatments of AD.

One potential hypothesis for the vast failure of mAbs and other proteins as therapeutics for the treatment of AD is their inefficiency in crossing the blood-brain barrier (BBB) with the necessary or sufficient dose to exude their biological activities. Several efforts to improve delivery of mAbs and other proteins into the brain such as osmotic BBB disruption (BBBD),[16-18] "Trojan Horse" delivery method,[19] and ultrasound with microbubbles[20, 21] have shown various levels of success. We also utilized cadherin peptides as BBB modulators (BBBM) to improve brain delivery of molecules across the BBB. Linear and cyclic cadherin peptides as BBBM (i.e., HAV6, ADTC5, HAVN1, HAVN2, and ADTHAV) can improve brain delivery of various sizes of proteins (e.g., 15 kDa lysozyme, 65 kDa albumin, 150 kDa mAb) with different brain deposition levels in C57BL/6 mice.[22-24] Brain delivery of adenanthin, an anticancer drug, with the help of HAV6 peptide as a BBBM has been shown to suppress medulloblastoma brain tumor growth and increase survival in the mouse model compared to placebo animals and animals treated with adenanthin alone.[25] Recently, we treated experimental autoimmune encephalomyelitis (EAE) mice during disease remission with eight injections of BDNF+ADTC5, BDNF alone, ADTC5 alone, and PBS. The results showed that treatment with BDNF+ADTC5 suppressed disease relapse while treatments with BDNF alone, ADTC5 alone, and PBS did not.

In the present study, we evaluated the effects of non-invasive systemic delivery of BDNF into the brain using ADTC5 peptide compared to BDNF alone in APP/PS1 transgenic mice and negative control groups. The AD symptoms of treated APP/PS1 transgenic mice were monitored using cognitive evaluation methods, including Y-maze and novel object recognition assessments. The effects of BDNF brain delivery were also determined by evaluating activated downstream

cellular processes known to be affiliated with neuroregeneration such as NG2, EGR1, and Arc upregulations.

3.2. Materials and Methods:

3.2.1. Animals:

All animal studies were carried out under the approved animal protocol (AUS-74-11) granted by Institutional Animal Care and Use Committee (IACUC) at The University of Kansas. Animal Care Unit (ACU) personnel and veterinarians were involved in the care of the animals used in this study. Female transgenic APP/PS1 (MMRRC stock # 34832-Jax) were obtained from The Jackson Laboratory (Bar Harbor, ME) and housed until at least 6 months of age. Mice received i.v. injections of either BDNF (5.7 nmol/kg) + ADTC5 (10 μmol/kg; $n = 7$), BDNF alone (5.7 nmol/kg; $n = 6$), or vehicle ($n = 6$) every 4 days, for a total of 8 injections. At the end of the study, the mice were euthanized via CO_2 inhalation and perfused with PBS immediately followed by 4% formalin fixative. The brains were extracted and post-fixed overnight in the perfusion-fixation solution.

3.2.2. Cadherin Peptide Synthesis and Purification:

Cadherin Peptide Synthesis and Purification:

ADTC5 peptide was synthesized using a solid-phase peptide synthesizer (Gyros Protein Technologies, Tucson, AZ) as described previously.[23] Briefly, crude peptide was cleaved from the resin with TFA containing scavengers followed by precipitation in cold diethyl ether. The disulfide bond in ADTC5 was formed by stirring the linear peptide precursor in 0.1 M ammonium bicarbonate buffer solution at pH 9.0 in high dilution while bubbling air through the solution. The cyclic ADTC5 was purified using a semi-preparative HPLC X-bridge C18 column (Waters,

Milford, MA) and the product was analyzed by analytical HPLC to be > 95 % pure. The exact mass of cyclic ADTC5 was determined by mass spectrometry.

3.2.3. Y-maze Assessment:

Twenty-four hours following the 8th injection, the mice were subject to Y-maze behavioral assessment. First the mice were habituated to the maze for 8 min with one arm of the maze closed off. Three hours following habituation, the mice were re-introduced to the maze for 5 min with all three arms open. All mice were initially placed in the center of the maze oriented toward the same arm; the maze was thoroughly cleaned with 70% ethanol and Virkon between each trial to remove scent cues. Time in Novel Arm was defined as the percent of total time (5 min) spent in the third arm of the maze (previously closed-off arm). An entry into an arm was defined as the head of the mouse entering.

3.2.4. Novel Object Recognition Assessment:

Twenty-four hours following the Y-maze assessment the mice were subjected to Novel Object Recognition (NOR) assessment. First, mice were individually habituated in an empty open field for 5 min. Twenty-four hours after habituation, 2 identical objects were placed in the open field, 5 cm away from the wall; there were two different sets of identical objects that were randomly selected for each mouse. Mice were individually placed in the field facing away from the objects and were allowed to familiarize themselves with the objects for 10 min. 24 h following familiarization, mice were re-subjected to the open field, but one of the objects was replaced with a novel object; the position of the novel object (right or left side) was randomized for each mouse. The mice were allowed to explore the objects for 10 min and the total amount of time each mouse

spent interacting with each object was measured. For all steps, the open field and object were cleaned with 70% ethanol and Virkon.

3.2.5. Euthanasia, Brain Perfusion, and Extraction:

At the end of the study, mice were euthanized via CO_2 inhalation and perfused with PBS immediately followed by 4% formalin fixative. The brains were extracted and post-fixed overnight in the perfusion-fixation solution then transferred to 70% ethanol PBS solution for paraffin embedding.

3.2.6. Histology and Immunohistochemistry:

Coronal brain sections (10 μm thickness) from were sectioned and mounted onto gelatin-coated slides (Superfrost Plus, Thermo Fisher Scientific, Walmath, MA). For both amyloid beta histology and anti-NG2 immunohistochemistry, sections were deparaffinized using xylene and serially hydrated from 95% ethanol to distilled water. For amyloid beta, slides were stained with Congo Red Solution (Abcam, Cambridge, UK) for 20 min, then dipped in twice in 100% ethanol, cleared with xylene, mounted using synthetic Permount (Fisher Scientific, Hampton, NH) and covered using 2.5 coverslips. Amyloid plaque levels were quantified by counting the number of plaques from the hippocampus at 10X magnification from 5 random sections per group (n = 5).

For anti-NG2 staining, slides were first blocked in a 3% hydrogen peroxide blocking agent then subsequently rinsed using distilled water. Next, heat-induced isotope retrieval (HIER) was performed using a 10 nM sodium citrate, 0.05%, pH 6.0 buffer. In brief, the HIER buffer was brought to a boil and slides were submerged for 15 min and then immediately rinsed with PBS, 0.05% Tween-20 (PBS-T) buffer for 3 min. Slides were then blocked using 10% normal BSA for

6 min and subsequently rinsed with water. The NG2 primary antibody (Abcam) was then applied to the slides in a dilation of 1:1,000 in PBS-T and they were incubated overnight at 4 ºC in a moist chamber. The following steps were performed using the Polink-2 HRP Plus Rabbit DAB Detection System for Immunohistochemistry (Golden Bridge International Labs, Bothell, WA). Briefly, Rabbit Antibody Enhancer (Reagent 1) was applied to the slides and incubated at room temperature for 30 min. The slides were then rinsed with PBS-T and Polymer-HRP for Rabbit (Reagent 2) was applied, after which they were incubated at room temperature for 30 min. The slides were then rinsed with PBS-T and the chromogen was applied; to prepare the chromogen, 2 drops of DAB Chromogen (Reagent 3B) were added to DAB Reagent buffer (Reagent 3A). The slides were incubated with the DAB mixture for 10 min and then rinsed with water. Lastly, the slides were dipped into 100% ethanol twice, dried, mounted using Permount, and coverslipped using 1.5 coverslips. Anto-NG2-stained slides were imaged using a Leica DM750 Compound Bright Field Upright Microscope and imaged at 40x magnification under identical exposure times. Anti-NG2 levels were quantified via densitometry analysis at 40x magnification from 5 random sections per group (n = 5).

3.2.7. Fluorescent *in Situ* Hybridization:

Coronal brain sections (10 μm thickness) were sectioned and washed three times in PBS before mounting on gelatin-coated glass slides (Superfrost Plus, Thermo Fisher Scientific). Tissues were allowed to dry at RT and were then stored at –20 ºC until use. Fluorescence *in situ* hybridization (FISH) was performed using RNAscope® Technology 2.0, Advanced Cell Diagnostics (ACD), Hayward, CA) Multiplex Reagent Kit V2.[26-28] In short, mounted tissue sections were deparaffinized using xylene and serially dehydrated in 50%, 70%, 95%, and 100% ethanol for

5 min each. Between all pretreatment steps, tissue sections were briefly washed with nanopure water. Pretreatment solution 1 (hydrogen peroxide reagent) was applied for 10 min at RT, and then the tissue sections were boiled in pretreatment solution 2 (target retrieval reagent) for 15 min. Mounted slices were pretreated with solution 3 (protease reagent) for 30 min at 40 ºC in the HybEz™ hybridization system (ACD). Following tissue pretreatment, the following transcript probes were applied to all sections: Mm-Mapk1-C1 (Cat. # 458161), Mm-Arc-C2 (Cat. # 316911-C2), and Mm-Egr1-C3 (Cat. # 423371-C3), which correspond to mitogen-activated protein kinase 1 (Mapk1, activity-related cytoskeleton-associated protein (Arc), and early growth response 1 (Egr1), respectively. Probes were hybridized to sections for 2 h at 40 ºC and subsequently washed for 2 min at room temperature. Following hybridization, hybridize AMP 1 was applied to each slide, which was then incubated for 30 min at 40 ºC. The same process was repeated for hybridize AMP 2 and 3. For HRP-C1 signal development (Mapk1), HRP-C1 was applied to the slides, and they were incubated for 15 min at 40 ºC and then washed. For C1, Opal® 650 (Akoya Biosciences, Menlo Park, CA) was applied and incubated for 30 min at 40 ºC and then washed. Following the wash, HRP blocker was applied to each slide, which was incubated for 15 min at 40 ºC and then washed. This process was repeated for C2 (Arc)**,** and C3 (Egr1) using Opal® 620 and 520, respectively. The resulting transcript-fluorophore labeling is as follows: Mapk-650, Arc-620, EGR1-520. All sections were counterstained by incubating DAPI for 30 sec at RT following by rinsing. Slides were then covered using ProLong Gold Antifade Mounting Media and 1.5 coverslips. Slides were allowed to dry in the dark overnight at 4 ºC. All sections were imaged within 2 weeks.

Fluorescent images were taken using an Olympus Inverted Epifluorescence Microscope XI81 (Olympus Life Solutions, Waltham, MA) running SlideBook Version 6.0 (3i, Ringsby, CT)

equipped with a digital CMOS camera (2000x2000), automatic XYZ stage position, ZDC autofocus, and a xenon lamp excitation source. Images were taken under identical exposure times (100 msec) using a 40x objective and appropriate filter sets for each fluorophore (*i.e.,* DAPI–DAPI, FITC–Opal® 520, Texas red–Opal® 620, and Cy 5.5–Opal® 650). To determine the degree of mRNA transcript expression, 4 images of the CA1 region of the hippocampus regions were randomly selected from mouse samples of each group, and the total fluorescence signal intensity for each channel was quantified. For display purposes, images were pseudo-colored and brightness-adjusted using ImageJ; green was assigned to Opal® 520 (EGR1), red to Opal® 620 (ARC), cyan to Opal® 650, and grey to DAPI.

3.2.8. Statistics and Data Analysis:

All statistics and data analyses were performed using GraphPad Prism (San Diego, CA). Analysis of variance (ANOVA) and Student's T-test were performed when appropriate, both operating at 95% confidence intervals with a *p*-value of less than 0.05 used as the criterion for statistical significance unless otherwise stated.

3.3. Results:

3.3.1. Effect of BDNF on Cognitive Performance in Y-maze and NOR Assessment:

The ability of ADTC5 to deliver BDNF into the brains of mice after I.V. injection was assessed by determining the effects of BDNF on improving cognitive function in APP/PS1 Alzheimer's disease animal model as determined by Y-maze and NOR assessments. The efficacy of BDNF (5.71 nmol/kg) + ADTC5 (10 μmol/kg; $n = 7$) was compared to that of BDNF alone (5.71 nmol/kg; $n = 6$), and vehicle ($n = 6$). Once mice reached 6 months of age, i.v. injections were administered

every 4 days for a total of 8 injections. Twenty-four hours following the final injection, mice were subjected to Y-maze and NOR assessments.

For the Y-maze, mice that received BDNF + ADTC5 performed significantly better than mice that received BDNF alone or vehicle (**Figure 3.1**). The mice that received BDNF + ADTC5 spent a greater percentage of time ($F_{(2,15)} = 3.99$; $p < 0.05$) and had a higher number of entries ($F_{(2,15)} = 5.63$; $p < 0.05$) into the third arm of the maze than did the groups that received BDNF alone or vehicle (**Figure 3.1**).

For the NOR assessment, the mice that received BDNF + ADTC5 performed significantly better than mice that received BDNF alone or vehicle. The mice that received BDNF + ADTC5 spent a greater percentage of time with the novel object ($F_{(2,16)} = 6.55$; $p < 0.01$) than did the mice that received BDNF alone or vehicle **(Figure 3.2)**. Lastly, there was no significant difference in total time spent with either of the two objects (*i.e.,* all groups spent similar amounts of time interacting with either object; $F_{(2,16)} = 0.682$; $p = 0.52$; **Figure 3.2**).

3.3.2. Effect of BDNF Delivery on Amyloid Beta Plaques in Hippocampus:

The means by which BDNF delivery to the brain improved cognitive performance in mice was investigated by comparing the amount of amyloid-beta plaques in mice that received BDNF + ADTC5, BDNF alone, or vehicle. Our results indicated that all groups expressed high variability levels of plaques in the hippocampus regardless of the treatment and there was no significant difference in the number amyloid beta plaques across groups ($F_{(2,12)} = 0.096$; $p = 0.91$, $n = 5$; **Figure 3.3**).

3.3.3. Effect of BDNF Delivery on NG2-Glia:

We have previously demonstrated that BDNF delivery to EAE mice via ADTC5 induced oligodendrocyte maturation via significant increased levels of NG2 receptors. Furthermore, others have shown that $BDNF^{+/+}$ mice demonstrate distinct upregulation of NG2 glia following the development of cuprizone-induced lesions compared to $BDNF^{+/-}$ and $BDNF^{-/-}$ mice.[29, 30] We probed whether BDNF delivery via ADTC5 would induce oligodendrocyte maturation in the APP/PS1 mouse model by staining for anti-NG2 in the cortex. A higher degree of NG2 staining as indicated by a darker/lower pixel value was found in mice that received BDNF + ADTC5 compared to the mice received either BDNF alone or vehicle (**Figure 3.4**); $F_{(2,12)} = 11.16$; $p < .01$, $n = 5$.

3.3.4. Effect of BDNF on EGR1, ARC, and MAPK1 mRNA Transcript Expression:

BDNF is known to stimulate to stimulate downstream transcription factors such as, tropomyosin receptor kinase B (TrkB), mitogen-associated protein kinase 1 (MAPK1) cyclic AMP response element binding protein (CREB), early growth response-1 (EGR1), and activity-related cytoskeleton associated protein (ARC).[31-33] We have previously demonstrated that delivering BDNF via ADTC5 to EAE mice results in an increase in EGR-1 and ARC mRNA transcript expression. Additionally, others have shown that EGR1 directly targets ARC expression.[34, 35] We quantified levels of EGR1, ARC, and MAPK1 mRNA transcripts via fluorescence *in situ* hybridization (FISH). **Figure 3.5** shows brain sections from the CA1 region of the hippocampus. Mice that received BDNF + ADTC5 show significant increases in EGR1 ($F_{(2,9)} = 23.48$; $p < 0.001$, $n = 5$) and ARC ($F_{(2,9)} = 7.33$; $p < 0.05$, $n = 5$) transcript levels compared to mice that received BDNF alone or vehicle; very high levels of MAPK1 expression were found

in all groups; however, no significant differences were observed ($F_{(2,9)} = 0.08$; $p = 0.92$, $n = 5$; **Figure 3.5**).

3.4. Discussion

In this study, we delivered BDNF using ADTC5 into the brains of transgenic APP/PS1 mice, which is an animal model for AD. BDNF was chosen because it is endogenous in nature, thus posing low potential for adverse side effects in transgenic APP/PS1 mice. Because BDNF alone cannot penetrate the BBB, the hope was that BDNF with the help of ADTC5 could enter the brain and exert its activity to induce neuro-regeneration. The results from this study showed that we have demonstrated that multiple systemic injections of BDNF+ADTC5 can significantly improve cognitive performance and activate downstream cellular processes known to be associated with BDNF exposure when compared to injections of BDNF alone or vehicle. This suggests that ADTC5 enhanced the brain delivery of BDNF. The mice treated with BDNF+ADTC5 demonstrated a statistically significant performance in Y-Maze and NOR behavioral assessments compared to mice that received BDNF alone or vehicle. Furthermore, mice that received BDNF + ADTC5 showed a significant increase in NG2 glia, EGR1, and ARC mRNA transcripts compared to mice that received BDNF alone or vehicle (**Figures 3.4 & 3.5**).

In the EAE animal model, a model for multiple sclerosis, multiple injections of BDNF+ADTC5 were able to ameliorate EAE symptoms, induce remyelination, promote NG2 glia maturation, and upregulate ARC and EGR1 compared to mice that received BDNF alone, or vehicle. In the same study, BDNF delivered with ADTC5 could be detected in the brain homogenates using Western blot analysis. In contrast, when BDNF was delivered alone, there was virtually no detectable signal of recombinant BDNF in the Western blots of the brain homogenates.

In the same study, administration of BDNF+ADTC5 stimulated the phosphorylation of TrkB in the brain as a marker of BDNF brain delivery while administration of BDNF alone did not trigger TrkB phosphorylation, indicating that BDNF alone could not penetrate the BBB. Additionally, ADTC5 alone did not produce the activity to improve EAE scores, suggesting that it has no inherent neuro-regenerative properties. Here, we show in a different animal model that ADTC5 can be used to deliver BDNF to improve disease symptoms.

Another cadherin peptide, HAV6, was used as BBB modulator to improve the brain delivery of adenanthin (ade), an anticancer drug, to treat medulloblastoma brain tumor.[23] Although adenanthin is a hydrophobic and soluble molecule, it cannot cross the BBB because it is a substrate for the efflux pump, P-glycoprotein (Pgp). In healthy mice, the brain delivery of adhenathin was significantly enhanced by its co-administration with HAV6.[23] In a medulloblastoma animal model, multiple treatments with a combination of adenanthin and HAV suppressed the brain tumor growth and increased animal survival compared to those treated with adenanthin alone or placebo.[23] In some case, additional treatment with the adenanthin + HAV6 eliminated the brain tumor completely. In addition, multiple treatments with HAV6 did not induce microglia activation and astrogliosis, which normally occur due to neuroinflammation. This study suggests the potential viability of modulating the BBB with cadherin peptides to deliver therapeutics for brain tumors.

Recently, ADTC5 has been shown to improve brain delivery of 15 kDa lysozyme, 65 kDa albumin, and 150 kDa IgG mAb in C57BL/6 mice.[21,22] However, ADTC5 could not deliver 220 kDa fibronectin into the brain, suggesting that there is a size limit of molecules that can be delivered into the brain. It is interesting to discover that ADTC5 created time- and size-dependent of opening of pores in the intercellular junctions of the BBB. The time-dependent opening of the BBB was evaluated using a pretreatment experiment to determine the reversibility of the pore

openings. In this case, ADTC5 was administered first and, after a certain number of minutes, different sizes of molecules were delivered. The result showed that ADTC5 allowed the BBB permeation of a small molecules such as gadopentetic acid (Gd-DTPA) in a time window of 2 h; however, no molecules could pass through the BBB after 4-h delay. In contrast, ADTC5 allowed only 65 kDa albumin to enter the brain after 10-min delay, but no albumin could enter the brain after 40-min delay. Finally, the maximum delay time allowed for IgG mAb to penetrate the BBB was less than 10 min. These results suggest that the large pore openings created by ADTC5 collapse to smaller pores in a time-dependent manner. Taken together, ther results show that ADTC5 has the robust activity to modulate the BBB for improved entrance of small and large molecules.

In this study, the Y-maze and NOR behavior assessments were used to evaluate cognitive performance because these methods have been well established and validated. In preclinical studies, they have been widely used to assess cognitive impairment in transgenic animals that is similar to cognitive tests performed in humans; thus, the results have translational values in evaluating potential therapeutics for AD.[36-41] The advantage of these assessment methods is that the animals do not have to be subjected to stressful conditions like food or water deprivation as well as physical stress. Stressful conditions such as those in the Morris water maze could alter the cognitive performance. In our studies, animals that received multiple treatments of BDNF + ADTC5 had significant behavior improvements in Y-maze and NOR tests compared to the animal groups that received BDNF alone or vehicle. Others have found that exercise induces the upregulation of BDNF, which leads to the enhancement of brain plasticity; in addition, upregulation in BDNF has been associated with improved performance in behavioral tests in AD animal models.[42-45] Additionally, Bechara *et al.* (2014) demonstrated that a single

intracerebroventricular (i.c.v.) injection of BDNF can mimic exercise-induced brain plasticity and result in an improvement in an object displacement task.[46] Our results are congruent with those of others that indicate that BDNF can be delivered in therapeutically relevant doses using ADTC5 to improve cognitive performance.

To obtain a deeper understanding of how BDNF improves cognitive performance, amyloid-beta plaques were stained using Congo red and all groups exhibited high levels of plaques (**Figure 3.3**). There were no significant differences in the number of amyloid beta plaques among all three groups. Our results reflect that of Nagahara *et al*. (2013) who showed that BDNF delivery using a Lenti-BDNF vector demonstrated improved hippocampal-dependent learning but showed no reduction in amyloid beta plaques.[47] They also demonstrated that BDNF treatment ameliorated cell loss and improved synaptophysin immunoreactivity in the hippocampus. Similarly, using fluorescence *in situ* hybridization, we showed an increase in mRNA transcripts (EGR1 and ARC; **Figure 3.5**) associated with synaptic plasticity in the hippocampi of mice treated with BDNF + ADTC5 without a reduction in amyloid-beta plaque load (**Figure 3**). Therefore, it is likely BDNF is ameliorating APP/PS1 symptoms by modulating hippocampal plasticity and not by reducing amyloid-beta plaque loads.

NG2 glia are thought to play an integral role in several processes including modulation of synaptic response, remyelination, and integration of neurons into synaptic networks.[48] Some researchers have found that the presence of high amyloid beta-plaque loads and exacerbated APP/PS1 symptoms could cause increased levels of NG2 glia as a response to increased neuroinflimation.[49, 50] Our results indicated a significant increase in NG2 glia in the brains of mice that received BDNF + ADTC5 compared to those that received BDNF alone or vehicle (**Figure 3.4**). A similar result was observed when we treated EAE mice with BDNF + ADTC5, BDNF

alone, and vehicle; a significant upregulation of NG2 glia in the corpus callosum was found in BDNF + ADTC5-treated mice compared to those treated with BDNF alone and vehicle. Similarly, Nakajima *et al.* (2010) showed that targeted retrograde gene delivery of BDNF suppressed apoptosis of neurons and oligodendroglia and resulted in a significant promotion of NG2 expression after spinal cord injury in rats.[51] Furthermore, McTigue *et al.* (1998) demonstrated that transplanting fibroblasts producing BDNF into contused adult rat spinal cords resulted in a significant increase in expansion of oligodendrocyte lineage cells.[52] These combined findings provide strong evidence that BDNF delivery can ameliorate CNS damage via promotion of NG2 oligodendrocytes to provide a good motivation to utilize BDNF for treatment of neurodegenerative diseases.

3.5. Conclusion:

This study has shown the potential utility of cadherin peptides such as ADTC5 as blood-brain barrier modulators (BBBM) to increase the delivery of BDNF into the brain to improve cognitive behavior and neuroregeneration in transgenic APP/PS1 mice as an animal model for AD. ADTC5 was shown to be effective in delivering BDNF into the brains of the EAE animal model and improved the disease symptoms as well as inducing activation remyelination and neuro-regeneration markers in the brain. In the future, cadherin peptides such as BBBM can be used to deliver many other proteins, for example, mAbs, enzymes, neurotrophic factors, and hormones for treating brain diseases.

3.6. Figures and Figure Legends:

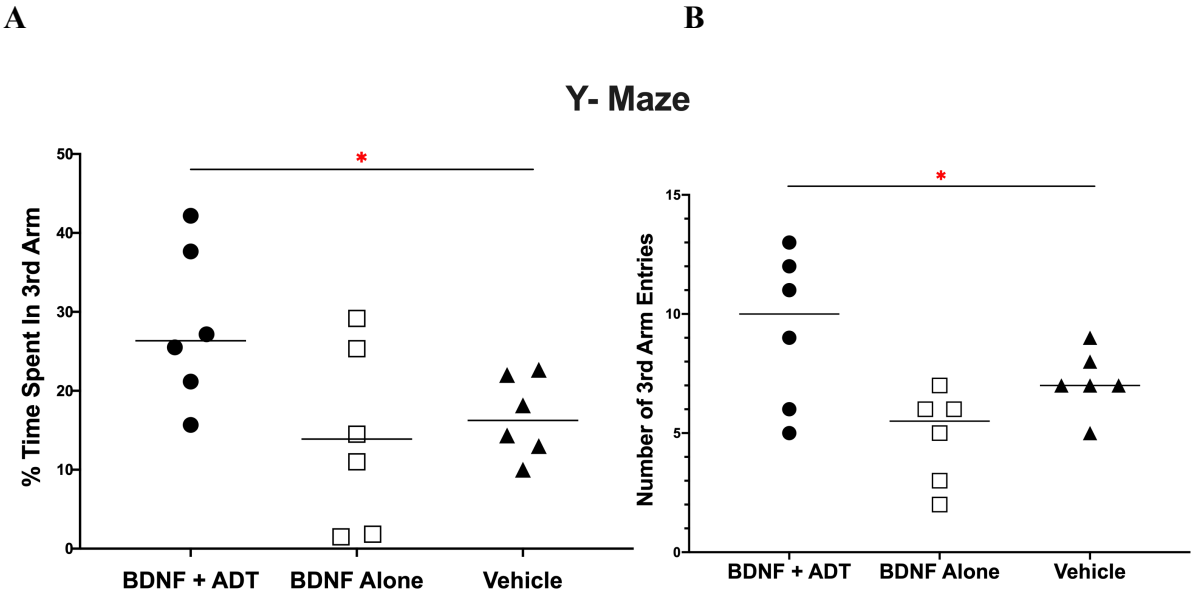

Figure 3.1. The effect of treatments of APP/PS1 mice, an animal model for Alzheimer's disease with BDNF (5.71 nmol/kg) + ADTC5 (10 µmol/kg), BDNF alone (5.71 nmol/kg), or vehicle on Y-Maze cognitive assessment. **(A)** The percent of total time spent in the maze that mice spent in the third arm/novel arm. **(B)** The total number of entries mice made into the third arm of the maze. *$p < 0.05$; one way ANOVA (95% confidence, n =5).

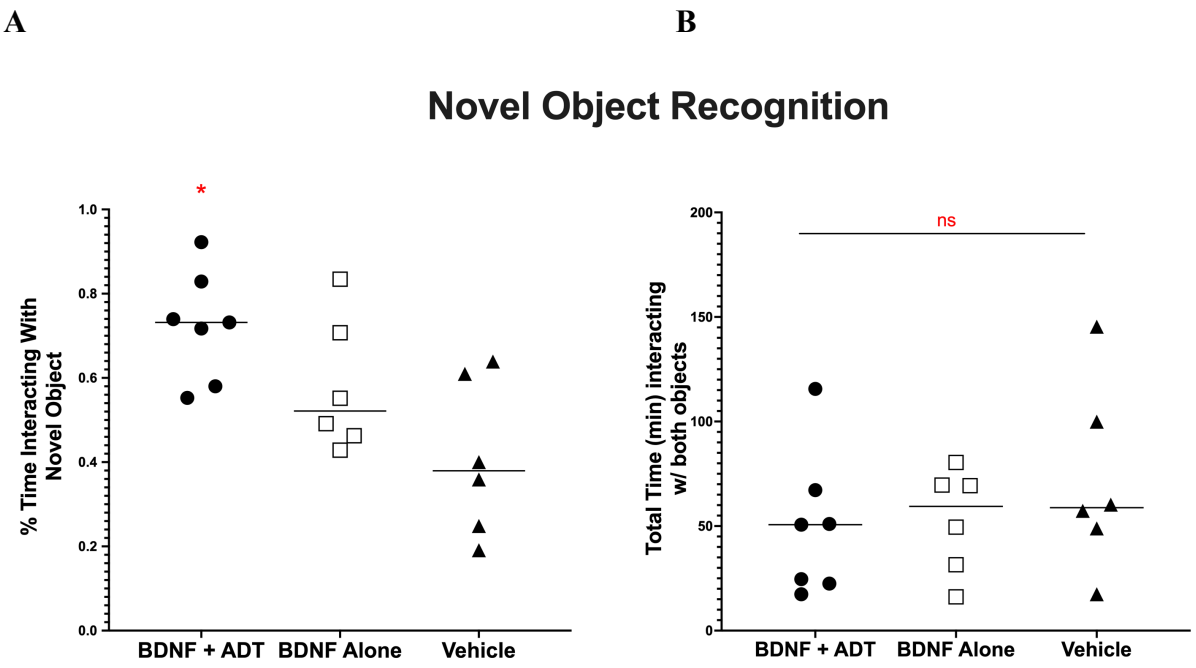

Figure 3.2. The effect of treatment of APP/PS1 mice with BDNF (5.71 nmol/kg) + ADTC5 (10 µmol/kg), BDNF alone (5.71 nmol/kg), or vehicle on novel object recognition (NOR) cognitive assessment. **(A)** The percent of total time spent in the open that mice spent exploring/interacting with the novel object. **(B)** The total amount of time mice spent exploring either object. *$p < .05$; one way ANOVA (95% confidence, n =5).

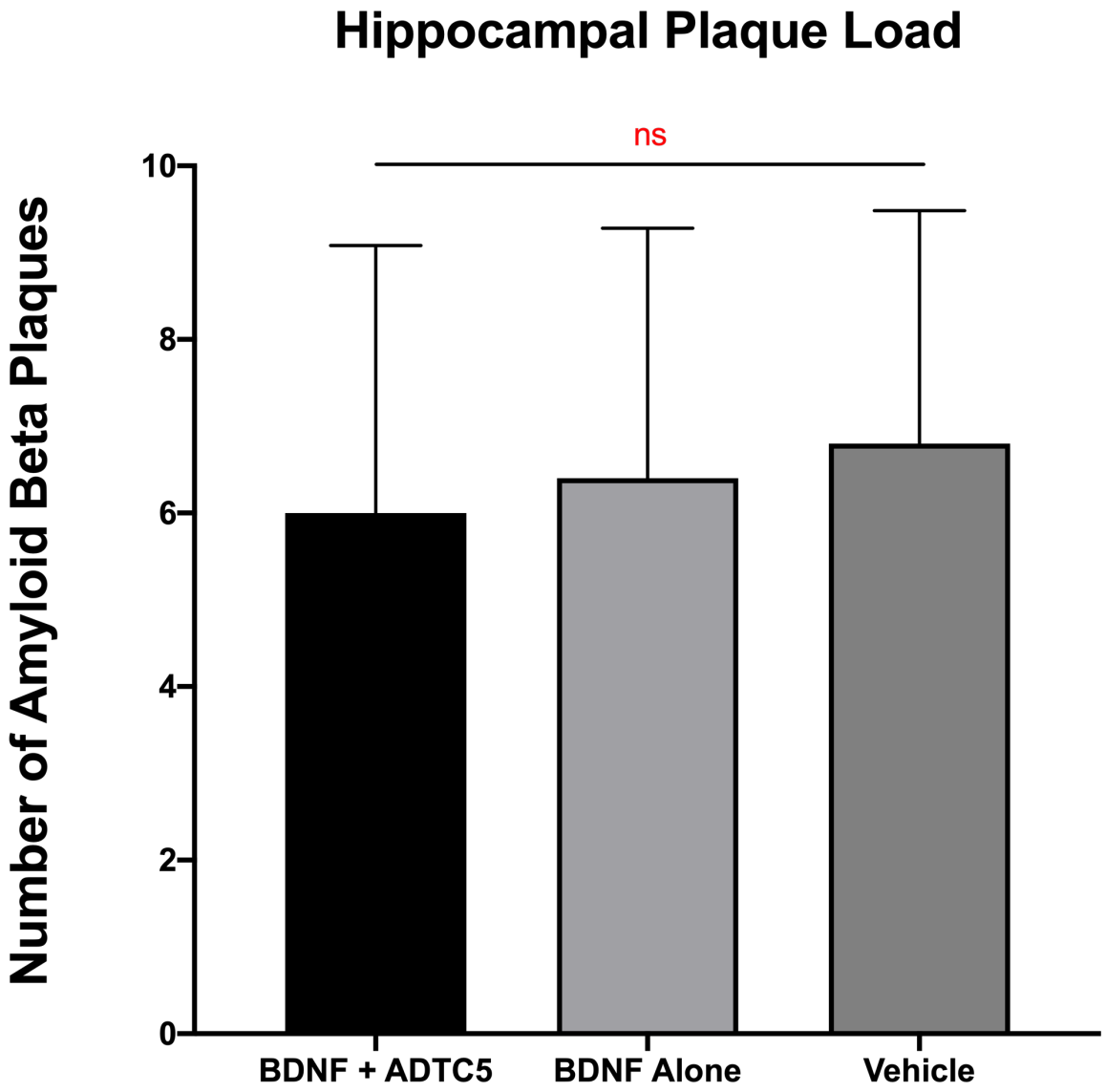

Figure 3.3. The effect of treatment of APP/PS1 mice with BDNF (5.71 nmol/kg) + ADTC5 (10 µmol/kg), BDNF alone (5.71 nmol/kg), or vehicle on hippocampal amyloid plaque load, as determined via Congo red staining.

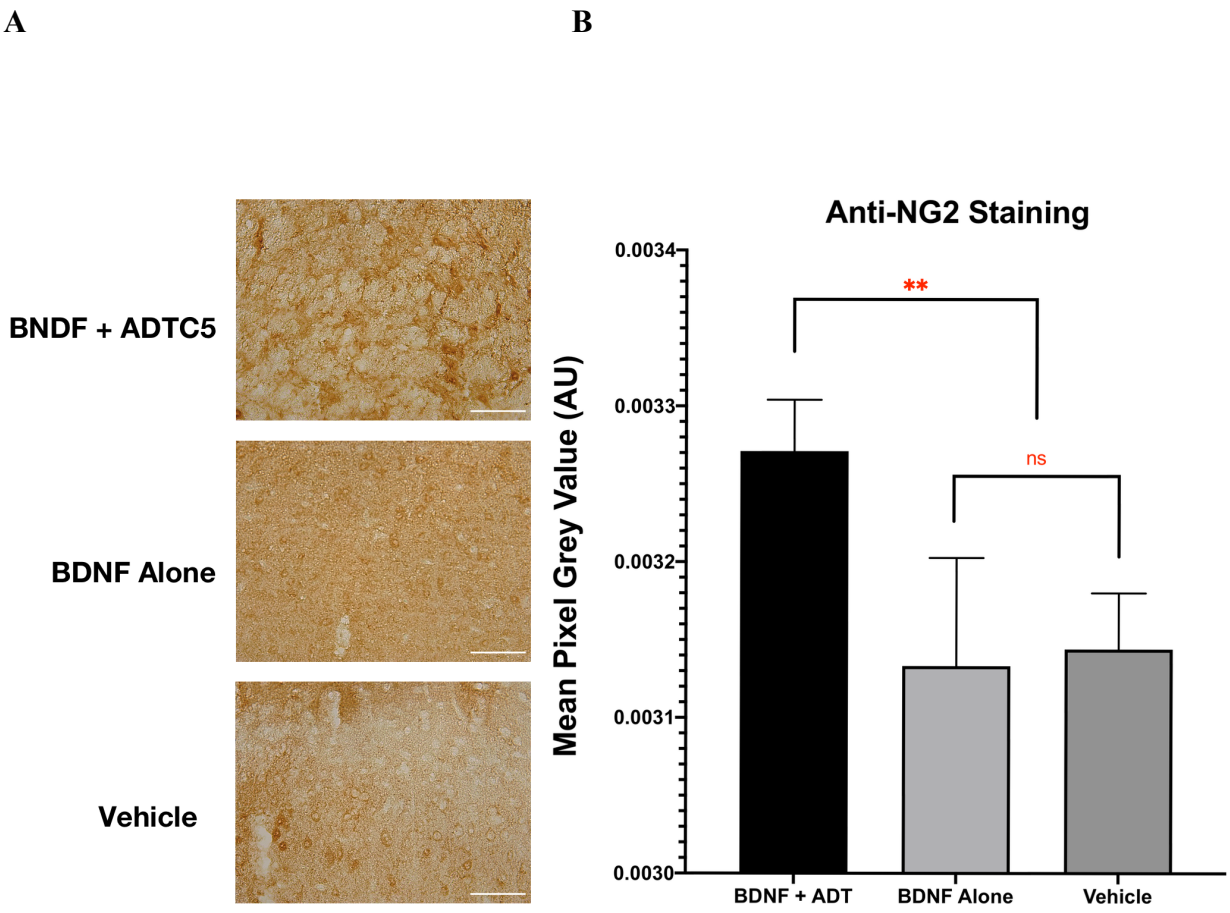

Figure 3.4. The effect of treatment of APP/PS1 mice with BDNF (5.71 nmol/kg) + ADTC5 (10 µmol/kg), BDNF alone (5.71 nmol/kg), or vehicle on the presence of NG2 receptors in the cortex as stained by DAB. **(A)** Color photomicrograph of anti-NG2 staining (brown) taken under identical conditions from the cortex of mice treated with BDNF + ADTC5, BDNF alone, and vehicle; red arrows point to dense regions of activated NG2-glia. **(B)** Quantitative NG2 density comparison among the APP/PS1 mice treated with BDNF + ADTC5, BDNF alone, and vehicle; Scale bar = 100 µm; $^{**}p \leq 0.01$*; one-way ANOVA (95% confidence; n = 5).*

A

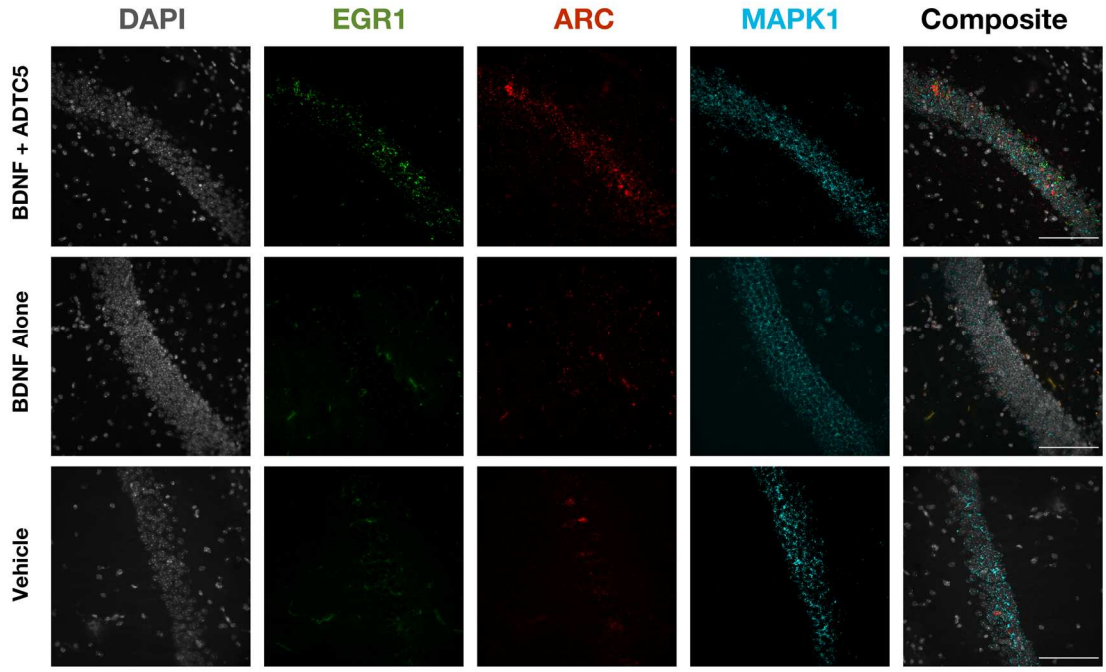
DAPI
EGR1
ARC
MAPK1
Composite
BDNF + ADTC5
BDNF Alone
Vehicle

B

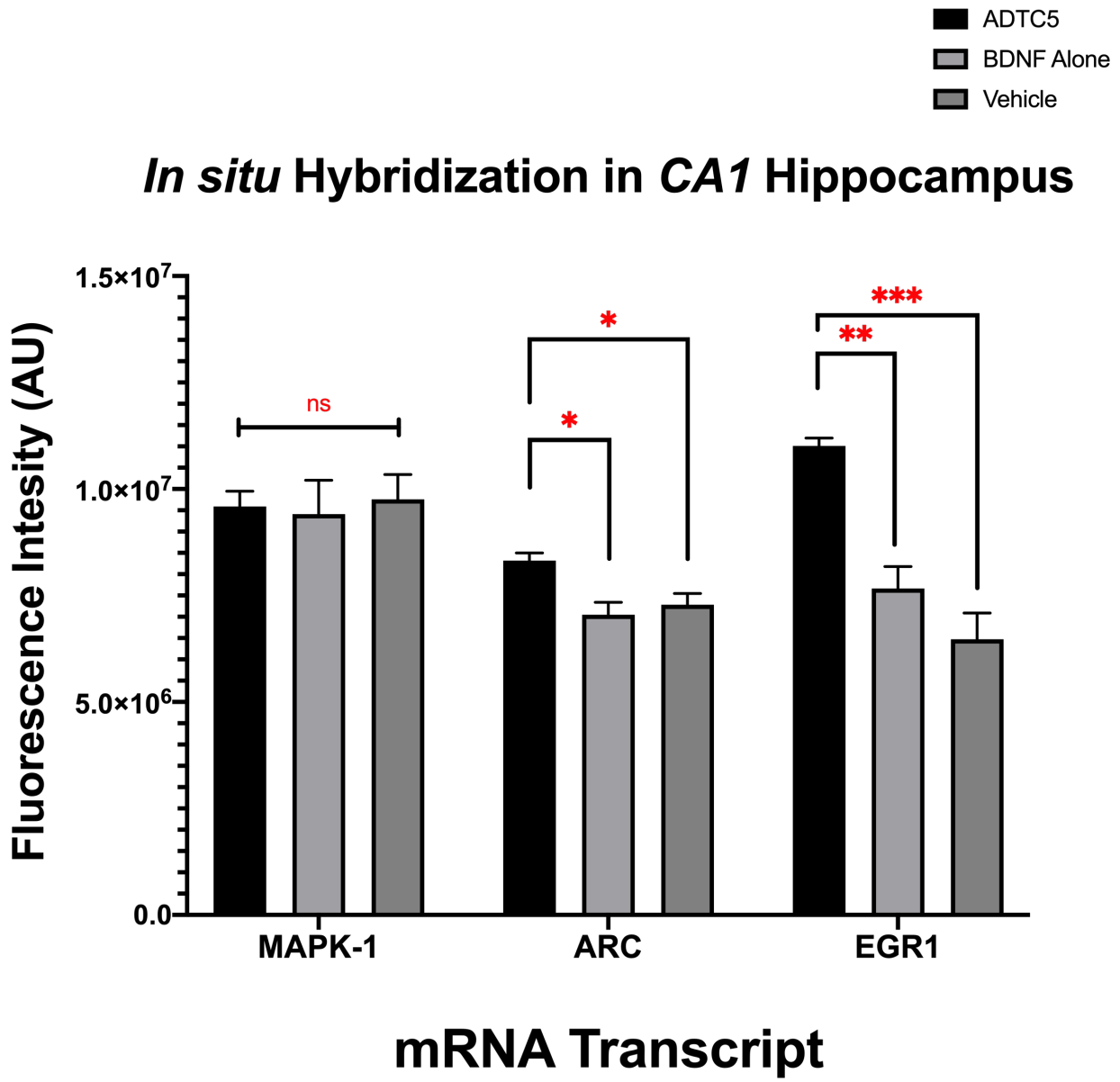

Figure 3.5. The effects of BDNF (5.71 nmol/kg) + ADTC5 (10 µmol/kg), BDNF alone (5.71 nmol/kg), or vehicle treatments on mRNA expression of MAPK1, EGR1, ARC in the CA1 region of the hippocampus of the brains of APP/PS1 mice. **(A)** Photomicrograph of DAPI (grey), EGR1

(green), ARC (red), MAPK (cyan) and composite images taken of the hippocampus of APP/PS1 mice treated with BDNF + ADTC5, BDNF alone, or vehicle. **(B)** Quantitative comparison of MAPK1 EGR, and ARC, and mRNA transcript expression, as determined by fluorescence intensity, for mice treated with BDNF + ADTC5, BDNF alone, or vehicle. Scale bar = 100 μm; *p* ≤ .-5; ***p* ≤ 0.001; *one-way ANOVA (99% confidence; n =* 4*). Contrast and brightness of images were adjusted only for display purposes.*

3.7. References:

1. Courtney, C.; Farrell, D.; Gray, R.; Hills, R.; Lynch, L.; Sellwood, E.; Edwards, S.; Hardyman, W.; Raftery, J.; Crome, P.; Lendon, C.; Shaw, H.; Bentham, P.; Group, A. D. C. Long-term donepezil treatment in 565 patients with Alzheimer's disease (AD2000): randomised double-blind trial. *Lancet* **2004,** *363*, (9427), 2105-15.
2. Rosler, M.; Anand, R.; Cicin-Sain, A.; Gauthier, S.; Agid, Y.; Dal-Bianco, P.; Stahelin, H. B.; Hartman, R.; Gharabawi, M. Efficacy and safety of rivastigmine in patients with Alzheimer's disease: international randomised controlled trial. *BMJ* **1999,** *318*, (7184), 633-8.
3. Loy, C.; Schneider, L., *Galantamine for Alzheimer's disease*. John Wiley & Sons, Ltd: 1996; Vol. 16.
4. Reisberg, B.; Doody, R.; Stoffler, A.; Schmitt, F.; Ferris, S.; Mobius, H. J.; Memantine Study, G. Memantine in moderate-to-severe Alzheimer's disease. *N Engl J Med* **2003,** *348*, (14), 1333-41.
5. Prasher, V. P. Review of donepezil, rivastigmine, galantamine and memantine for the treatment of dementia in Alzheimer's disease in adults with Down syndrome: implications for the intellectual disability population. *Int J Geriatr Psychiatry* **2004,** *19*, (6), 509-15.
6. Scarpini, E.; Scheltens, P.; Feldman, H. Treatment of Alzheimer's disease: current status and new perspectives. *Lancet Neurol* **2003,** *2*, (9), 539-47.
7. Loveman, E.; Green, C.; Kirby, J.; Takeda, A.; Picot, J.; Payne, E.; Clegg, A. The clinical and cost-effectiveness of donepezil, rivastigmine, galantamine and memantine for Alzheimer's disease. *Health Technol Assess* **2006,** *10*, (1), iii-iv, ix-xi, 1-160.

8. Yiannopoulou, K. G.; Papageorgiou, S. G. Current and future treatments for Alzheimer's disease. *Ther Adv Neurol Disord* **2013,** *6*, (1), 19-33.

9. Gilman, S.; Koller, M.; Black, R. S.; Jenkins, L.; Griffith, S. G.; Fox, N. C.; Eisner, L.; Kirby, L.; Rovira, M. B.; Forette, F.; Orgogozo, J. M.; Team, A. N. S. Clinical effects of Abeta immunization (AN1792) in patients with AD in an interrupted trial. *Neurology* **2005,** *64*, (9), 1553-62.

10. van Dyck, C. H. Anti-Amyloid-beta Monoclonal Antibodies for Alzheimer's Disease: Pitfalls and Promise. *Biol Psychiatry* **2018,** *83*, (4), 311-319.

11. Lemere, C. A. Immunotherapy for Alzheimer's disease: hoops and hurdles. *Mol Neurodegener* **2013,** *8*, 36.

12. Salloway, S.; Sperling, R.; Fox, N. C.; Blennow, K.; Klunk, W.; Raskind, M.; Sabbagh, M.; Honig, L. S.; Porsteinsson, A. P.; Ferris, S.; Reichert, M.; Ketter, N.; Nejadnik, B.; Guenzler, V.; Miloslavsky, M.; Wang, D.; Lu, Y.; Lull, J.; Tudor, I. C.; Liu, E.; Grundman, M.; Yuen, E.; Black, R.; Brashear, H. R.; Bapineuzumab; Clinical Trial, I. Two phase 3 trials of bapineuzumab in mild-to-moderate Alzheimer's disease. *N Engl J Med* **2014,** *370*, (4), 322-33.

13. Cummings, J. L.; Cohen, S.; van Dyck, C. H.; Brody, M.; Curtis, C.; Cho, W.; Ward, M.; Friesenhahn, M.; Rabe, C.; Brunstein, F.; Quartino, A.; Honigberg, L. A.; Fuji, R. N.; Clayton, D.; Mortensen, D.; Ho, C.; Paul, R. ABBY: A phase 2 randomized trial of crenezumab in mild to moderate Alzheimer disease. *Neurology* **2018,** *90*, (21), e1889-e1897.

14. Nagahara, A. H.; Tuszynski, M. H. Potential therapeutic uses of BDNF in neurological and psychiatric disorders. *Nat Rev Drug Discov* **2011,** *10*, (3), 209-19.

15. Tuszynski, M. H.; Thal, L.; Pay, M.; Salmon, D. P.; U, H. S.; Bakay, R.; Patel, P.; Blesch, A.; Vahlsing, H. L.; Ho, G.; Tong, G.; Potkin, S. G.; Fallon, J.; Hansen, L.; Mufson, E. J.; Kordower, J. H.; Gall, C.; Conner, J. A phase 1 clinical trial of nerve growth factor gene therapy for Alzheimer disease. *Nat Med* **2005,** *11*, (5), 551-5.

16. Chakraborty, S.; Filippi, C. G.; Wong, T.; Ray, A.; Fralin, S.; Tsiouris, A. J.; Praminick, B.; Demopoulos, A.; McCrea, H. J.; Bodhinayake, I.; Ortiz, R.; Langer, D. J.; Boockvar, J. A. Superselective intraarterial cerebral infusion of cetuximab after osmotic blood/brain barrier disruption for recurrent malignant glioma: phase I study. *J Neurooncol* **2016,** *128*, (3), 405-15.

17. Riina, H. A.; Fraser, J. F.; Fralin, S.; Knopman, J.; Scheff, R. J.; Boockvar, J. A. Superselective intraarterial cerebral infusion of bevacizumab: a revival of interventional neuro-oncology for malignant glioma. *J Exp Ther Oncol* **2009,** *8*, (2), 145-50.

18. Williams, P. C.; Henner, W. D.; Roman-Goldstein, S.; Dahlborg, S. A.; Brummett, R. E.; Tableman, M.; Dana, B. W.; Neuwelt, E. A. Toxicity and efficacy of carboplatin and etoposide in conjunction with disruption of the blood-brain tumor barrier in the treatment of intracranial neoplasms. *Neurosurgery* **1995,** *37*, (1), 17-27; discussion 27-8.

19. Pardridge, W. M. Delivery of Biologics Across the Blood-Brain Barrier with Molecular Trojan Horse Technology. *BioDrugs* **2017,** *31*, (6), 503-519.

20. Downs, M. E.; Buch, A.; Sierra, C.; Karakatsani, M. E.; Teichert, T.; Chen, S.; Konofagou, E. E.; Ferrera, V. P. Long-Term Safety of Repeated Blood-Brain Barrier Opening via Focused Ultrasound with Microbubbles in Non-Human Primates Performing a Cognitive Task. *PLoS One* **2015,** *10*, (5), e0125911.

21. Baseri, B.; Choi, J. J.; Deffieux, T.; Samiotaki, G.; Tung, Y. S.; Olumolade, O.; Small, S. A.; Morrison, B.; Konofagou, E. E. Activation of signaling pathways following localized delivery of systemically administered neurotrophic factors across the blood-brain barrier using focused ultrasound and microbubbles. *Phys Med Biol* **2012,** *57*, (7), N65-81.

22. Ulapane, K. R.; Kopec, B. M.; Siahaan, T. J. Improving In Vivo Brain Delivery of Monoclonal Antibody Using Novel Cyclic Peptides. *Pharmaceutics* **2019,** *11*, (11).

23. Ulapane, K. R.; Kopec, B. M.; Siahaan, T. J. In Vivo Brain Delivery and Brain Deposition of Proteins with Various Sizes. *Mol Pharm* **2019,** 10.1021/acs.molpharmaceut.9b00763.

24. Ulapane, K. R.; On, N.; Kiptoo, P.; Williams, T. D.; Miller, D. W.; Siahaan, T. J. Improving Brain Delivery of Biomolecules via BBB Modulation in Mouse and Rat: Detection using MRI, NIRF, and Mass Spectrometry. *Nanotheranostics* **2017,** *1*, (2), 217-231.

25. Sajesh, B. V.; On, N. H.; Omar, R.; Alrushaid, S.; Kopec, B. M.; Wang, W.-G.; Sun, H.-D.; Lillico, R.; Lakowski, T. M.; Siahaan, T. J.; Davies, N. M.; Puno, P.-T.; Vanan, M. I.; Miller, D. W. Validation of Cadherin HAV6 Peptide in the Transient Modulation of the Blood-Brain Barrier for the Treatment of Brain Tumors. *Pharmaceutics* **2019,** *11*, 481.

26. Vasquez, J. J.; Hussien, R.; Aguilar-Rodriguez, B.; Junger, H.; Dobi, D.; Henrich, T. J.; Thanh, C.; Gibson, E.; Hogan, L. E.; McCune, J.; Hunt, P. W.; Stoddart, C. A.; Laszik, Z. G. Elucidating the Burden of HIV in Tissues Using Multiplexed Immunofluorescence and In Situ Hybridization: Methods for the Single-Cell Phenotypic Characterization of Cells Harboring HIV In Situ. *J Histochem Cytochem* **2018,** *66*, (6), 427-446.

27. Gershon, T. R.; Crowther, A. J.; Liu, H.; Miller, C. R.; Deshmukh, M. Cerebellar granule neuron progenitors are the source of Hk2 in the postnatal cerebellum. *Cancer Metab* **2013,** *1*, (1), 15.

28. Smith, P. A.; Schmid, C.; Zurbruegg, S.; Jivkov, M.; Doelemeyer, A.; Theil, D.; Dubost, V.; Beckmann, N. Fingolimod inhibits brain atrophy and promotes brain-derived neurotrophic factor in an animal model of multiple sclerosis. *J Neuroimmunol* **2018,** *318*, 103-113.

29. Vondran, M. W.; Clinton-Luke, P.; Honeywell, J. Z.; Dreyfus, C. F. BDNF+/- mice exhibit deficits in oligodendrocyte lineage cells of the basal forebrain. *Glia* **2010,** *58*, (7), 848-56.

30. VonDran, M. W.; Singh, H.; Honeywell, J. Z.; Dreyfus, C. F. Levels of BDNF impact oligodendrocyte lineage cells following a cuprizone lesion. *J Neurosci* **2011,** *31*, (40), 14182-90.

31. Li, N.; Liu, G. T. The novel squamosamide derivative FLZ enhances BDNF/TrkB/CREB signaling and inhibits neuronal apoptosis in APP/PS1 mice. *Acta Pharmacol Sin* **2010,** *31*, (3), 265-72.

32. Hu, Y.; Russek, S. J. BDNF and the diseased nervous system: a delicate balance between adaptive and pathological processes of gene regulation. *J Neurochem* **2008,** *105*, (1), 1-17.

33. Alder, J.; Thakker-Varia, S.; Bangasser, D. A.; Kuroiwa, M.; Plummer, M. R.; Shors, T. J.; Black, I. B. Brain-derived neurotrophic factor-induced gene expression reveals novel actions of VGF in hippocampal synaptic plasticity. *J Neurosci* **2003,** *23*, (34), 10800-8.

34. Li, L.; Carter, J.; Gao, X.; Whitehead, J.; Tourtellotte, W. G. The neuroplasticity-associated arc gene is a direct transcriptional target of early growth response (Egr) transcription factors. *Mol Cell Biol* **2005,** *25*, (23), 10286-300.

35. Edelmann, E.; Lessmann, V.; Brigadski, T. Pre- and postsynaptic twists in BDNF secretion and action in synaptic plasticity. *Neuropharmacology* **2014,** *76 Pt C*, 610-27.

36. Saito, T.; Matsuba, Y.; Mihira, N.; Takano, J.; Nilsson, P.; Itohara, S.; Iwata, N.; Saido, T. C. Single App knock-in mouse models of Alzheimer's disease. *Nat Neurosci* **2014,** *17*, (5), 661-3.

37. Conrad, C. D. A critical review of chronic stress effects on spatial learning and memory. *Prog Neuropsychopharmacol Biol Psychiatry* **2010,** *34*, (5), 742-55.

38. Ohno, M.; Cole, S. L.; Yasvoina, M.; Zhao, J.; Citron, M.; Berry, R.; Disterhoft, J. F.; Vassar, R. BACE1 gene deletion prevents neuron loss and memory deficits in 5XFAD APP/PS1 transgenic mice. *Neurobiol Dis* **2007,** *26*, (1), 134-45.

39. Kim, H. Y.; Kim, H. V.; Yoon, J. H.; Kang, B. R.; Cho, S. M.; Lee, S.; Kim, J. Y.; Kim, J. W.; Cho, Y.; Woo, J.; Kim, Y. Taurine in drinking water recovers learning and memory in the adult APP/PS1 mouse model of Alzheimer's disease. *Sci Rep* **2014,** *4*, 7467.

40. McClean, P. L.; Holscher, C. Liraglutide can reverse memory impairment, synaptic loss and reduce plaque load in aged APP/PS1 mice, a model of Alzheimer's disease. *Neuropharmacology* **2014,** *76 Pt A*, 57-67.

41. McLean, S.; Ganong, A. H.; Seeger, T. F.; Bryce, D. K.; Pratt, K. G.; Reynolds, L. S.; Siok, C. J.; Lowe, J. A., 3rd; Heym, J. Activity and distribution of binding sites in brain of a nonpeptide substance P (NK1) receptor antagonist. *Science* **1991,** *251*, (4992), 437-9.

42. Bo, H.; Kang, W.; Jiang, N.; Wang, X.; Zhang, Y.; Ji, L. L. Exercise-induced neuroprotection of hippocampus in APP/PS1 transgenic mice via upregulation of mitochondrial 8-oxoguanine DNA glycosylase. *Oxid Med Cell Longev* **2014,** *2014*, 834502.

43. Kim, S. E.; Ko, I. G.; Shin, M. S.; Kim, C. J.; Jin, B. K.; Hong, H. P.; Jee, Y. S. Treadmill exercise and wheel exercise enhance expressions of neutrophic factors in the hippocampus of lipopolysaccharide-injected rats. *Neurosci Lett* **2013,** *538*, 54-9.

44. Wrann, C. D.; White, J. P.; Salogiannnis, J.; Laznik-Bogoslavski, D.; Wu, J.; Ma, D.; Lin, J. D.; Greenberg, M. E.; Spiegelman, B. M. Exercise induces hippocampal BDNF through a PGC-1alpha/FNDC5 pathway. *Cell Metab* **2013,** *18*, (5), 649-59.

45. Bechara, R. G.; Kelly, A. M. Exercise improves object recognition memory and induces BDNF expression and cell proliferation in cognitively enriched rats. *Behav Brain Res* **2013,** *245*, 96-100.

46. Bechara, R. G.; Lyne, R.; Kelly, A. M. BDNF-stimulated intracellular signalling mechanisms underlie exercise-induced improvement in spatial memory in the male Wistar rat. *Behav Brain Res* **2014,** *275*, 297-306.

47. Nagahara, A. H.; Mateling, M.; Kovacs, I.; Wang, L.; Eggert, S.; Rockenstein, E.; Koo, E. H.; Masliah, E.; Tuszynski, M. H. Early BDNF treatment ameliorates cell loss in the entorhinal cortex of APP transgenic mice. *J Neurosci* **2013,** *33*, (39), 15596-602.

48. Dimou, L.; Gallo, V. NG2-glia and their functions in the central nervous system. *Glia* **2015,** *63*, (8), 1429-51.

49. Nielsen, H. M.; Ek, D.; Avdic, U.; Orbjorn, C.; Hansson, O.; Netherlands Brain, B.; Veerhuis, R.; Rozemuller, A. J.; Brun, A.; Minthon, L.; Wennstrom, M. NG2 cells, a new trail for Alzheimer's disease mechanisms? *Acta Neuropathol Commun* **2013,** *1*, 7.

50. Dong, Y. X.; Zhang, H. Y.; Li, H. Y.; Liu, P. H.; Sui, Y.; Sun, X. H. Association between Alzheimer's disease pathogenesis and early demyelination and oligodendrocyte dysfunction. *Neural Regen Res* **2018,** *13*, (5), 908-914.

51. Nakajima, H.; Uchida, K.; Yayama, T.; Kobayashi, S.; Guerrero, A. R.; Furukawa, S.; Baba, H. Targeted retrograde gene delivery of brain-derived neurotrophic factor suppresses

apoptosis of neurons and oligodendroglia after spinal cord injury in rats. *Spine (Phila Pa 1976)* **2010,** *35*, (5), 497-504.

52. McTigue, D. M.; Horner, P. J.; Stokes, B. T.; Gage, F. H. Neurotrophin-3 and brain-derived neurotrophic factor induce oligodendrocyte proliferation and myelination of regenerating axons in the contused adult rat spinal cord. *J Neurosci* **1998,** *18*, (14), 5354-65.

Chapter 4: Time-Dependent Brain Delivery of Monoclonal Antibody and Its Clearance from the Brain

4.1. Introduction:

Monoclonal antibodies (mAbs) have been successfully used to treat patients with various diseases; however, they have not been successfully utilized to treat brain diseases. Several mAbs in clinical trials for treatment of central nervous system (CNS) diseases did not receive approval from the FDA due to their lack of efficacy.[1] Because mAbs are designed with known targets and mechanisms, they are very attractive for development as therapeutic agents. In addition, they have excellent specificity, good half-lives, and low toxicity. There is a continued push to develop new mAbs for treating brain diseases, although most mAbs cannot efficiently cross the BBB. In addition, their brain diffusion and clearance properties have not been well studied. Therefore, there is an urgent need to study various methods to improve delivery of mAbs into the brain as well as their clearance from the brain.

Many developed mAbs for brain diseases have good activity in *in vitro* and *in vivo* animal models during preclinical studies; they also frequently show ideal pharmacokinetic profiles in early clinical trials. Regardless of these promising early results, all have failed after phase-2 or -3 clinical trials. As an example, seven different developed mAbs for Alzheimer's disease that target different epitopes of amyloid-beta failed to received FDA approval.[2] More recently, the clinical trial of anti-Tau mAb (8E12) was halted during phase-2 clinical trial after the data showed insufficient benefits to patients.[3] Because of insufficient efficacy in multiple sclerosis (MS) patients, clinical trials of four mAbs, anti-Nogo-A, anti-LINGO-1, sHIgM22, and VX15/2503 for inducing remyelination, were halted.[4-7] The inability of mAbs to cross the BBB could be one of

the potential reasons for their low efficacy. In addition, clearance from the brain could be an important factor that influences the biological activity of mAbs in the brain.

Several methods have been investigated to improve brain delivery of mAbs as therapeutics. Brain delivery of 2.5 mg/kg bevacizumab using the osmotic BBB disruption (BBBD) method has been investigated in two pediatric patients with refractory radiation necrosis. After treatment, the patients could regain muscle strength.[8] Although BBBD has demonstrated effectiveness in general, some patients have developed complications such as anaphylaxis, seizures, and cerebral edema.[9] A combination of focused ultrasound (FUS) and microbubbles for brain delivery of drugs and the repeated use of this method has been shown to be safe in non-human primates; however, the use of FUS has not been evaluated in humans.[10]

Our group has recently demonstrated that cadherin peptides can be used as BBB modulators (BBBM). They have been shown to significantly enhance *in vivo* delivery of small to large molecules, including lysozyme, brain-derived neurotrophic factor (BDNF), and albumin, IgG mAb into the brain in mice.[11-16] Although many studies have focused on the delivery of mAbs into the brain, the data on mAb brain clearance after delivery are still limited. In this study, we examined the time-dependent IgG mAb delivery and its clearance from the brain. A combination of IgG mAb and ADTC5 or IgG mAb alone also was administered via i.v. in C57BL/6 mice, and the circulation time in the blood after administration was varied between 0.25 and 72 h. Then, the mAb depositions in the brain, liver, kidney, lung, spleen, and heart were quantified using near IR fluorescence (NIRF) imaging. Finally, the duration of the BBB opening created by ADTC5 peptide to allow IgG mAb penetration into the brain was evaluated by pretreatment with ADTC5 followed by administration of mAb delayed for 0, 20, or 40 min.

4.2. Materials and Methods:

4.2.1. Chemicals and Reagents:

The solvents and reagents for peptide synthesis and purification were purchased from Sigma Aldrich Chemical Company (St. Louis, MO) and Fisher Scientific, Inc. (Hampton, NH). The Fmoc amino acids used for the automated peptide synthesizer were purchased from Gyros Protein Technologies, Inc. (Tucson, AZ). The IRdye800CW Donkey anti-Goat IgG was acquired from LI-COR, Inc. (Lincoln, NE).

4.2.2. Peptide Synthesis and Purification:

The synthesis linear peptide precursor to cyclic ADTC5 peptide was accomplished using an automated Tribute solid-phase peptide synthesizer (Gyros Protein Technologies, Inc.). The peptide was cleaved from the resin using a trifluoro acetic acid (TFA) solution containing scavengers such as phenol, tri-isopropyl silane (TIPS), and water. TFA solution was added to cold diethyl ether to precipitate the peptide as a crude product. After filtration, the crude peptide was purified using semi-preparative HPLC with a C18 column Waters XBridge C18 (19 mm × 250 mm, 5 μm particle size; Waters Corporation, Milford, MA). The purified linear peptide precursor was dissolved in high dilution with bicarbonate buffer solution at pH 9.0, and the solution was bubbled with air to oxidize the two thiol groups to make a cyclic peptide with disulfide bond. The procedure produced a cyclic peptide monomer as a major product with low amounts of dimers and oligomers. Similar to the linear precursor, the cyclic monomer was purified using semi-preparative HPLC. The purity of each isolated fraction was determined by analytical HPLC using a C18 column (Luna C18: 4.6

mm × 250 mm, 5 μm particle size, 100 Å; Phenomenex, Inc., Torrance, CA) followed by peptide identification using time-of-flight mass spectrometry.

4.2.3. Animals:

C57BL/6 mice were used in this study, and each experiment utilized 3 mice per group (n = 3) using a random selection of male and female with similar body weights for each group. The animal studies were done according to an animal protocol approved by the Institutional Animal Care and Use Committee (IACUC) at The University of Kansas. The animals were housed and cared for by personnel of the Animal Care Unit under the supervision of attending veterinarians.

4.2.4. Preparation of Stock Solutions and Calibration Curves:

The stock solution of IRDye800CW-IgG mAb was prepared and stored at –80 °C prior to serial dilution using phosphate-buffered saline (PBS) to generate standard solutions with various concentrations. After standard solutions of IgG mAb were prepared, 10 μL of each standard solution was added into 200 μL of blank brain homogenates. Then, each spiked brain homogenate (n = 3) was scanned using a Licor Odyssey CLx imaging system (Licor, Lincoln, NE) to acquire the NIRF signal intensity from the IgG mAb. The result produces a linear correlation between NIRF signals and IgG mAb concentrations from 0.5 to 50 ng/mL. To quantify the amount of IgG mAb in the brain, the brain was homogenized in 2.0 mL PBS by mechanical disruption, and three 200 μL samples (n = 3) from a brain homogenate were added into different wells. Each well was scanned for NIRF signal using the Odyssey CLx scanner. Finally, the detected NIRF signal intensity was interpolated into the calibration curve to determine the amount of IgG mAb in pmol per gram brain.

4.2.5. Time-Dependent Brain Delivery IRdye800CW-IgG mAb using ADTC5 in C57BL/6 Mice:

The effects of time-dependent brain delivery of IgG mAb using ADTC5 were assessed in C57BL/6 mice with 3 mice/group (n = 3). The depositions of IgG mAb in the brains and other organs were quantitatively determined using NIRF imaging using an Odyssey CLx scanner. For each study, the animal was injected i.v. via tail vein with 21.6 nmol/kg IRdyeR800CW-IgG mAb with or without 13 μmol/kg ADTC5. The first study was accomplished for evaluating the effects of circulation time on IgG mAb depositions in the brain and other organs (liver, kidney, spleen, lung, and heart). Six groups of mice were administered a single dose of IgG mAb + ADTC5 while another six groups were administered with IgG mAb alone. A pair of IgG mAb + ADTC5 and IgG alone groups were sacrificed after various circulation times at 0.25, 1, 2, 24, 48, and 72 h. After sacrifice, each mouse was subjected to a *trans*-cardiac perfusion process using PBS with 0.5% Tween-20 to remove excess IgG mAb in brain capillaries to prevent false positive detection. The brain and other organs were then harvested and rinsed with PBS. Protein depositions in the brain and other organs were quantified by NIRF imaging using an Odyssey CLx NIRF scanner.

The second study was carried out to determine the duration of BBB modulation induced by ADTC5 that allows permeation of IgG mAb across the BBB. In this case, the IgG mAb was administered via i.v. injection 20 or 40 min after administration of ADTC5. Then, 15 min after injection of IgG mAb, the mice were sacrificed followed by *trans*-cardiac perfusion process. The brain was isolated for quantification of IgG mAb deposition.

4.2.6. Capillary Depletion Method:

To ensure that the brain perfusion method was effective in removing the delivered mAb from the microvessel endothelial cells, capillary depletion experiments were performed to compare the

brain deposition of the protein in brain homogenates with and without microvessel endothelial cells using the previous method.[11, 14]

4.2.7. Data Processing and Statistical Analysis:

All data were processed using Graphpad Prism (San Diego, CA), and PKsolver. The data from the circulation time-based brain delivery of IgG mAb with or without ADTC5 were compared using ANOVA with Holm-Sidak post-hoc tests for multiple comparisons or t-Tests. Statistical significance was determined by correcting for multiple comparisons using the Holm-Sidak method. A p-value of < 0.05 was the criterion for statistical significance. Outliers were removed using Grubbs test (95% confidence intervals). All numbers are presented as mean ± SD.

4.3. Results:

4.3.1. Time-dependent Brain Deposition of IgG mAb:

To quantitatively determine the brain deposition of IgG mAb, a calibration curve was generated with excellent linearity of $R^2 \geq 0.99$. The amounts of delivered IgG mAb were determined by interpolating the NIRF signal intensity onto the calibration curve. A capillary depletion experiment was carried out to ensure that there was no remaining IgG mAb in the brain capillaries. The result showed that there was less than 2% difference between capillary depleted and non-depleted brain homogenates, suggesting that the brain perfusion method was efficient in removing the remaining IgG mAb from the brain capillaries.

The effects of ADTC5 and various circulation times on IgG mAb brain depositions were assessed. At 0.25-h circulation time, the brain amount(s) of IgG mAb was significantly higher when delivered along with ADTC5 compared to that of IgG mAb alone (**Table 4.1, Figure 4.1**).

The qualitative NIRF images of the brains after time-dependent treatments with IgG + mAb and IgG alone were clearly distinguishable (**Figure 4.1A**). The quantitative comparisons of time-dependent brain depositions of IgG mAb after administrations over a 72-h time period are shown in **Figure 4.1B**. In the IgG mAb + ADTC5 group after 0.25 h circulation time, the amount of IgG mAb in the brain was the highest, while the amount in the brain decreased rapidly when the circulation times were lengthened from 0.25 h to 2 h (**Figure 4.1C; Table 4.1**). From 2 to 48 h time points, the decrease in brain deposition was less dramatic than at the 0.25–2.0 h time points (**Figure 4.1B**). There were significant differences in mAb brain depositions between the IgG mAb + ADTC5 and IgG mAb groups at 0.25 or 1.0 h circulation times. However, these differences were less pronounced or not significant between 2 and 48 h circulation times.

The time-dependent amounts of IgG mAb in the brains were used to estimate the half-lives ($t_{1/2}$) of IgG mAb after delivery with and without ADTC5 (**Figure 4.1B**). There are two different phases found in the brain depositions of IgG mAb when delivered with ADTC5; thus, the estimated $t_{1/2alpha}$ and $t_{1/2beta}$ of IgG mAb when delivered with ADTC5 were 0.34 ± 0.22 h and 65.50 ± 12.09 h, respectively. In contrast, the half-life for IgG mAb when delivered alone was 58.60 ± 10.62 h.

4.3.2. Depositions of IgG mAb in Other Organs:

The effects of ADTC5 on depositions of IgG mAb in other organs such as liver, spleen, kidney, lung, and heart were compared to control, and quantifications were done using NIRF intensities on different organs (**Figure 4.2**). Qualitatively in the NIRF images, the majority of the IgG mAb was found in the liver compared to other organs such as spleen, kidney, lungs, and heart of animals treated with IgG mAb + ADTC5 (**Figure 4.2A**) and IgG mAb alone (**Figure 4.2B**). Quantitative determinations showed that the depositions in the liver have the highest peak at the 1-h time point,

and decrease dramatically after the 2-h time point and continually decline for over 72 h. In addition, there were no significant differences in the liver depositions of IgG mAb between groups treated with mAb + ADTC5 and mAb alone over the 72-h time points (**Figure 4.2C & D**). These results indicate that ADTC5 did not influence the deposition of IgG mAb in the liver.

The effects of ADTC5 on IgG mAb depositions in spleen, kidney, lungs, and heart were also compared in the presence or absence of ADTC5 (**Figure 4.2E**). The deposition of IgG mAb was higher in all four organs at the 2-h time point, and the amounts of IgG mAb in these four organs dropped at the 24-, 48-, and 72-h time points. There were no statistical differences found in the spleen, kidney, lung, and heart of mice treated with ADTC5 + IgG mAb or IgG mAb alone.

The comparisons of time-dependent brain and liver depositions are shown in **Figure 4.3**. It was interesting to find that the IgG mAb brain deposition peaked at 0.25-h circulation time while the deposition in the liver peaked at the 2-h circulation time. This suggests that clearance by the liver may influence the time-dependent IgG mAb deposition in the brain. These comparisons showed that ADTC5 had a big impact on the delivery of IgG mAb into the brain but not into the liver.

4.3.3. Duration of BBB modulation for IgG mAb Brain Delivery:

The duration of pore openings in the BBB intercellular junctions created by ADTC5 was evaluated using a 20- or 40-min delay between the administrations of ADTC5 and IgG mAb. As a negative control, IgG mAb was administered alone via i.v. (**Figure 4.4**). The delivered molecules were allowed to circulate for 15 min; then, the animals were sacrificed, followed by quantification of IgG mAb in the brain. In the groups without delay in administration, there was a significant amount of IgG mAb in the brains of the mAb +ADTC5 group compared to mAb control alone

(**Figure 4.4**). Compared to IgG mAb alone group (4.01 ± 1.08 pmol/g brain), there were no significant differences between mice that received IgG mAb after a 20-min (4.02 ± 2.72 pmol/g brain) or 40-min (2.62 ± 0.40 pmol/g) delay. The result suggests that the BBB pore opening was closed to the mAb in 20 min or less.

4.4. Discussion:

There is a considerable degree of interest and effort by the pharmaceutical industry to utilize mAbs for the treatment of brain diseases because they are normally designed for ah known target molecule with a specific function(s) or mechanism of action. Thus, mAbs normally have high specificity, low side effects, and an extended half-life. Many mAbs have been evaluated in clinics, but many of those have not been successful in showing the expected efficacies and benefits to patients with brain diseases. The physicochemical properties of mAbs are not favorable for passive diffusion through the transcellular pathway because they cannot readily partition into the cell membranes of the BBB endothelial cells. Similarly, the presence of the tight junctions inhibits them from passively diffusing through the paracellular pathways of the BBB. Alternatively, mAbs can cross the BBB via pinocytosis or receptor-mediated endocytosis. Although these processes have been exploited to deliver mAbs, success in improving mAb brain delivery has been limited due to the possible low efficiency in transporting the mAb from the blood into the brain.

In this study, the brain delivery of mAb has been accomplished using ADTC5, which inhibits cadherin-cadherin interactions at the adherens junctions to increase the porosity of the BBB paracellular pathways. ADTC5 significantly increased brain depositions of IgG mAb after i.v. administration compared to IgG mAb alone. It is interesting to find that the IgG mAb brain deposition was the highest when the circulation time was 0.25 h and, as the circulation time was

increased, the brain deposition also decreased. After 2 h circulation time, the differences in IgG mAb brain depositions were no longer significant between IgG mAb + ADTC5 and IgG mAb alone. After 72 hours, there was essentially no detectable difference between delivery of IgG peptide and IgG control. These results indicate that IgG mAb was rapidly cleared from the brain.

Our previous studies using magnetic resonance imaging (MRI) showed that BBB modulation using ADTC5 was rapid (within a matter of minutes); when a combination of 65 kDa galbumin + ADTC5 was administered via i.v., a significant brain deposition of galbumin was observed within 3 min compared to when control galbumin was administered alone.[14] To evaluate the transient and reversible modulation of the BBB by ADTC5, pretreatment studies were carried out. In this study, the animals were first treated with ADTC5 and, after a certain delay period, galbumin was administered, followed by brain scanning using MRI. When the delay was 10 min, a significant amount of galbumin was observed in the brain.[14] However, when the delay was increased to 40 min, the amount of galbumin observed in the brain was similar to that seen in control.[14] These results indicated that the BBB modulation was transient and reversible and the BBB pore opening for molecules the size of 65 kDa galbumin was between 10 to 40 min. In the current study, we also determined the duration of BBB opening for 150 kDa IgG mAb. The result showed that 20- or 40-min delay after treatment with ADTC5 did not allow the IgG to enter the brain (**Figure 4.4**). This indicates that large paracellular pores created by ADTC5 to allow IgG mAb to enter the brain collapsed in less than 20 min. A previous study has shown that ADTC5 cannot enhance the delivery of 220 kDa fibronectin, indicating that there is a molecular weight limit for the pore opening by ADTC5.[15] In summary, the effect of ADTC5 in opening the BBB was fast and the duration of opening was 20 min or less. Thus, there is a time- and molecular size-dependent opening in the BBB paracellular pathway created by ADTC5.

ADTC5 and HAV6 peptides have been compared when delivering various sized proteins such as 15 kDa lysozyme, 65 kDa albumin, 150 kDa mAb, and 220 kDa fibronectin at a dose of 21.6 nmol/kg. ADTC5 enhanced the brain delivery of lysozyme, albumin, and mAb but not fibronectin in C57BL/6 mice.[15] In contrast, HAV6 peptide delivered lysozyme but not albumin and IgG mAb into the mouse brains of mice. In a separate study, HAV6 delivered galbumin to the brain when it was administered at 600 nmol/kg, which was 27 times the dose of albumin (21.6 nmol/kg).[14] It was interesting to find that new cyclic peptides (HAVN1 and HAVN2) derived from HAV6 with N- to C-terminal cyclization can improve the brain delivery of IgG mAb compared to control.[16] Linear and cyclic ADTHAV peptides with combination sequences from HAV6 and ADTC5 were shown to be very effective in delivering IgG mAb into the brain.[16] These results suggest that there is a size-dependent delivery by cadherin peptides as BBB modulators. It was also found that the dose of delivered protein can influence its deposition in the brain. It is proposed that the difference in the modulatory activities of cadherin peptides were due to their binding mechanisms to cadherins in the intercellular junctions of the BBB.

There are many unknown aspects of the way that mAbs enter the brain from the systemic circulation as well as their clearance from the brain. A few studies have focused on the kinetics and mechanisms of clearance from the brain; thus, this information will be useful for optimizing the brain delivery and deposition of mAbs during treatments of brain diseases. It is unclear whether the mAb would have a different half-life in the CNS compared to in plasma. Two independent studies have demonstrated that the clearance of insulin administered to rat cerebral spinal fluid (CSF) to be either 13 or 21 mL/day/kg,[17] whereas the clearance of IgM and IgG3 mAbs in rats was reported to be 42 and 101 mL/day/kg, respectively.[18] A separate study was done to compare the clearance rates of IgG mAb and insulin by co-administering both proteins into the lateral ventricle;

following this, samples from CSF were collected at various time-points. The results showed that clearances of IgG mAb and insulin were 103 ml/day/kg and 129 ml/day/kg for IgG, respectively; the reported CSF half-lives for IgG mAb and insulin were 36.0 min and 43.2 min, respectively.[19]

Our study showed that the half-life for IRdyeR800CW-IgG mAb (21.6 nmol/kg) delivered at a dose using ADTC5 was 0.34 ± 0.22 h (20 min) when determined between 0.25 to 2 h time points, and the second half-life was 65.50 ± 12.09 h when determined between 2–72 h time points. Chang *et al.* determined the half-life of trastuzumab (Herceptin®) in the brain to be 105 h when administered at a dose of 10 mg/kg (66 nmol/kg).[6] Using microdialysis, the mAb half-lives were 115 and 180 h, respectively, when the samples were collected from the lateral ventricle and cisterna magna. There is considerable variability in the reports of half-lives of protein clearance from the brain; one of the reasons is that some studies relied on determining the protein concentrations in the CSF without determining the time-dependence of protein depositions in brain tissue. The differences in method of delivery presumably contribute to the variability of depositions at different regions of the brain. The mAb physicochemical properties and the availability of a mAb binding target will also influence its clearance from the brain. The administered dose and method of administration as well as location of mAb detection may contribute to the observed PK profiles. In our study, BBB modulation to deliver the mAb could contribute to the equilibrium process between the blood and the brain. The time-dependent rapid decrease in the brain deposition in the first 2 h could be due to mAb clearance through the CSF. It has been proposed that clearance of mAb from the brain could involve the participation of neonatal Fc receptors (FcRn) at the BBB.

The clearance of many non-endogenous molecules from brain tissue to CSF after delivery across the BBB has been shown to be rapid and presumably via receptor and/or or equilibrium-based flow of large molecules out of the brain tissue into CSF. The total estimated volume of CSF

in the human brain is approximately 140 mL, and it is estimated that in humans the entire CSF volume is produced and excreted into the blood every 4 to 5 hours.[20] Noguchi *et al.* reported that a bulk flow clearance of mAb is 29.0 mL/day/kg.[19] Thus, CSF is rapidly turned over, and molecules that are transferred into the CSF are transported to the blood rather quickly. However, the bulk flow and diffusion of molecules from brain tissue to CSF has not been widely studied. Blasberg *et al*. demonstrated that chemotherapy drugs administered intrathecally penetrate the brain parenchyma very slowly, and for each mm the distance from the CSF is increased, the penetration decreases logarithmically.[21] Additionally, Krewson *et al.* (1995) demonstrated that when nerve growth factor (NGF) was administered directly to the brain interstitial tissue, it was generally transported only 2–3 mm in any direction from the site of implantation, with trace amounts found throughout the rest of the brain.[22]

During administration of IgG mAb with and without ADTC5, the majority of the IgG mAb was deposited in the liver, with low amounts deposited in the kidney, heart, lung, and spleen. There was no effect of ADTC5 peptide on IgG mAb depositions the liver, kidney, spleen, lung, and heart **(Figure 4.2**). In a comparison of time-dependent IgG mAb depositions in the brain and liver, the highest deposition of IgG mAb was at the 0.25-h time point when the deposition in the liver was still low (**Figure 4.3**). When the deposition of IgG mAb in the brain dropped at the 2-h time point, the deposition in the liver was at the maximum level. A similar trend was found in kidney, spleen, lung, and heart. These results suggest that there is a possible correlation between the clearance of IgG mAb from the brain and increased deposition in the liver.

Cadherin peptides have been used to deliver therapeutic agents into the brains of animal models of brain diseases. HAV6 peptide delivers significant amounts of an anticancer drug, adenanthin, to the brains of mice with medulloblastoma brain tumors (D425 tumor cells).[23] Treatments with a

combination of HAV6 and adenanthin decreased tumor load and increased survival rate in medulloblastoma mice compared to those treated with adenanthin alone or untreated mice.[23] In a separate study, ADTC5 was used to deliver brain-derived neurotrophic factor (BDNF) to prevent disease relapse in the experimental autoimmune encephalomyelitis (EAE) animal model compared to BDNF alone, ADTC5 alone, and PBS. Pathology evaluations of the brains indicated that a combination of BDNF and ADTC5 significantly promotes remyelination, upregulates NG2 cells, and activates downstream cellular processes in SJL mice compared with those treated with BDNF alone or untreated mice. Most recently, we have demonstrated that BDNF delivery in conjunction with ADTC5 can improve cognitive performance in APP/PS1 mice, a model for Alzheimer's disease. The recent success in delivering therapeutically relevant molecules implies that molecules of various sizes can be broadly delivered across the BBB in therapeutically relevant doses in part due to the vast degree of vasculature in the brain (over 400 miles of capillary tissue). When this is compared to the approximate surface area of the choroid plexus (0.021 m^2) where CSF is produced, it is clear how there can be an advantage for delivering molecules across the BBB rather than via absorption from CSF. Although the mechanisms by which ADTC5 and other cadherin peptides modulate the BBB is relatively well understood, how the delivered protein molecules, especially IgG mAbs, are shuttled out of the brain or whether BBB modulation plays a role is yet to be determined. Future studies probing whether ADTC5 has residual effects on clearance of molecules from the brain may provide insight on how to optimize the transport of mAb and other proteins into, within, and out of the brain.

The binding mechanisms of cadherin peptides (i.e., HAV6 and ADTC5 peptides) to the extracellular 1 (EC1) domain of E-cadherin have been determined using heteronuclear ^{1}H, ^{15}N-heteronuclear single quantum coherence (^{1}H, ^{15}N-HSQC) NMR spectroscopy and molecular

docking experiments.[24] The results indicated that HAV6 and ADTC5 peptides have different binding sides on the EC1 domain of E-cadherin. Utilizing the X-ray crystal structure of C-cadherin, homophilic interactions of cadherins can be divided into *cis* and *trans* interactions. The *cis* interaction occurs when an EC1 domain from one cadherin protein binds to an EC2 domain of another cadherin from the same cell membranes. The *trans* interaction is when an EC1 domain of one cadherin from a membrane of one cell binds to an EC1 domain of another cadherin from the opposing cell. It is hypothesized that HAV6 binds at the EC1 domain surface to inhibit the *cis* interaction between EC1 and EC2 domains of two neighbor cadherins from the same cell membranes. In contrast, it is hypothesized that ADTC5 peptide binds to a hydrophobic pocket of the EC1 domain to block the *trans*-EC1-EC1 interactions of cadherins from cell membranes of the opposite cells in a manner that blocks the *trans* interaction. Thus, it is proposed that the pore sizes that were created by ADTC5 were larger than those created by HAV6 due to inhibition of *trans* interactions compared to the inhibition of *cis*-interactions. Studies to test the proposed hypotheses will be carried out in the future.

4.5. Conclusion:

In this study, we found that ADTC5 enhanced delivery of IgG mAb into the brain and that the circulation time influenced the brain deposition. When the circulation time was increased, the brain deposition of IgG mAb was decreased, indicating a time-dependent clearance of IgG mAb from the brain. The deposition of IgG mAb in the brain dropped quickly when circulation time was increased within a 2-h period. The window of BBB opening caused by ADTC5 was less than 20 min. During the circulation of the IgG mAb, the majority of IgG mAb was deposited in the liver with limited amounts in the kidney, spleen, lung, and heart. There was no effect of ADTC5 on the

depositions of mAb in the liver, kidney, lung, spleen, or heart. In the future, there is a need to study the mechanisms of clearance of IgG mAb from the brain.

4.6. Tables, Figures, and Figure Legends:

Table 4.1. Circulation time-dependent IgG mAb brain depositions upon delivery with and without ADTC5			
Circulation Time	ADTC5 pmol/g (mean ± SD)	Control pmol/g (mean ± SD)	*p* value
0.25 h	13.32 ± 1.93	4.01 ± 1.08	0.0001****
1 h	8.23 ± 1.81	2.96 ± 0.34	0.0001****
2 h	5.73 ± 1.62	4.21 ± 2.12	0.25
24 h	4.40 ± 1.07	2.42 ± 0.45	0.09
48 h	3.49 ± 0.35	2.16 ± 0.04	0.33
72 h	1.69 ± 0.36	1.43 ± 0.22	0.94

A

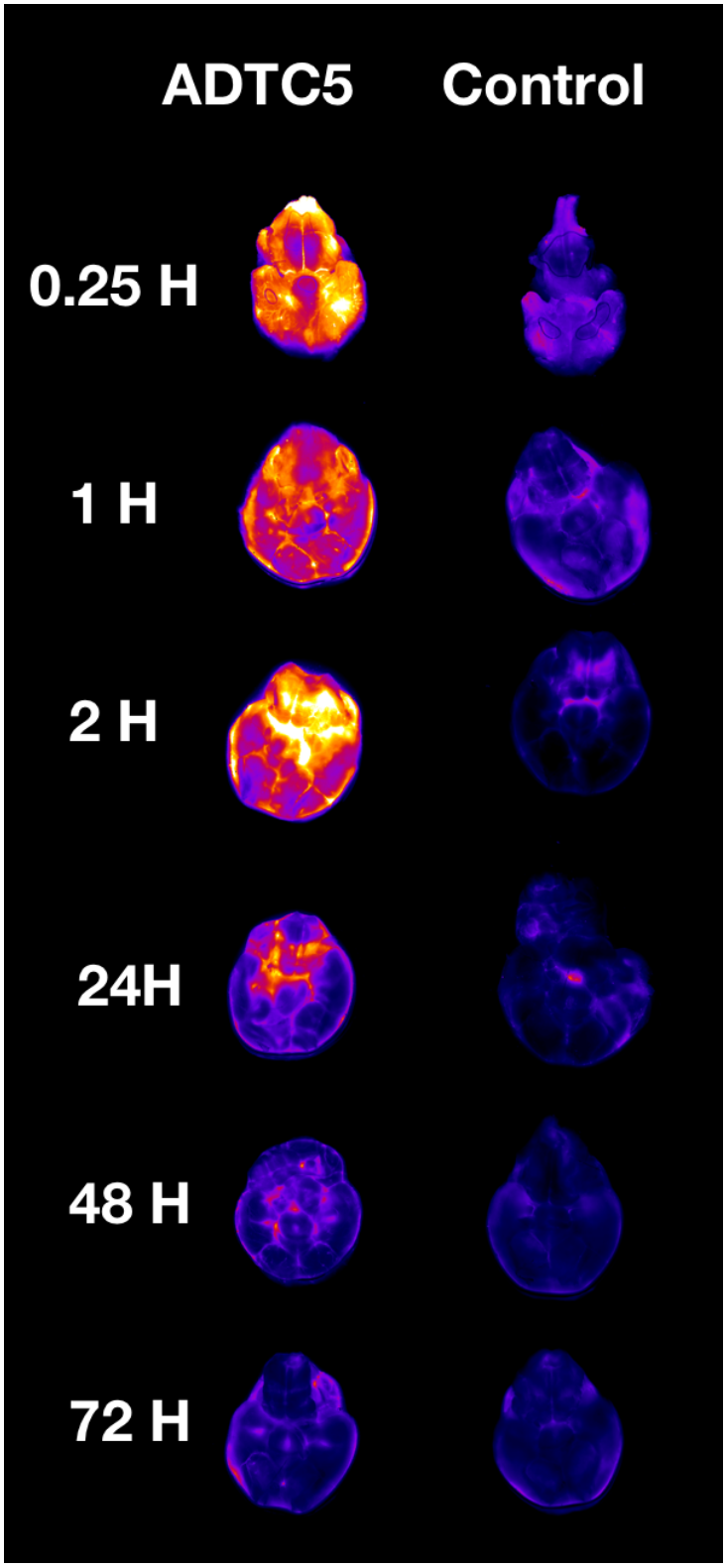

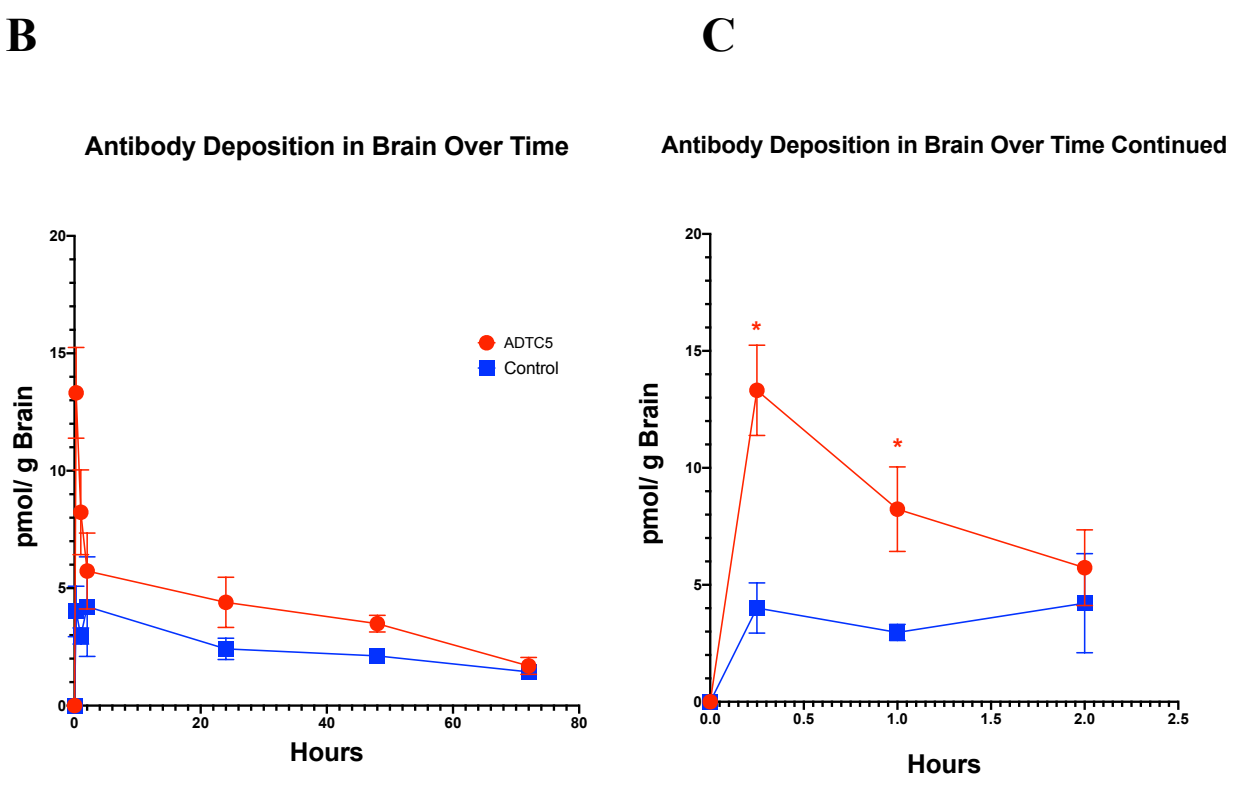

Figure 4.1. The effects of ADTC5 on the deposition of IRdye800CW-IgG mAb in the brain from 0.25 to 72-h circulation time period. Brain depositions were determined qualitatively and quantitatively in pmol/g brain using NIRF imaging after delivery of IgG mAb alone (21.6 nmol/kg) or with ADTC5 (13 µmol/kg). **(A)** The NIRF images of intact brains after delivery of IgG mAb with ADTC5 (*left*) and IgG alone as control (*right*). The yellow-red colors represent the brain depositions of IgG mAb with a dark blue color as a background of brain tissues. **(B)** The quantitative amounts of IRdye800CW-IgG mAb in the brain over a 72-h time period. **(C)** The expansion of brain depositions of IRdye800CW-IgG mAb over the first 2-h time period. The asterisk (*) designates a significant difference between mice dosed with or without ADTC5. Data are shown as mean ± SD with the number of animals, $n = 3$, for each time point of each group.

A

B

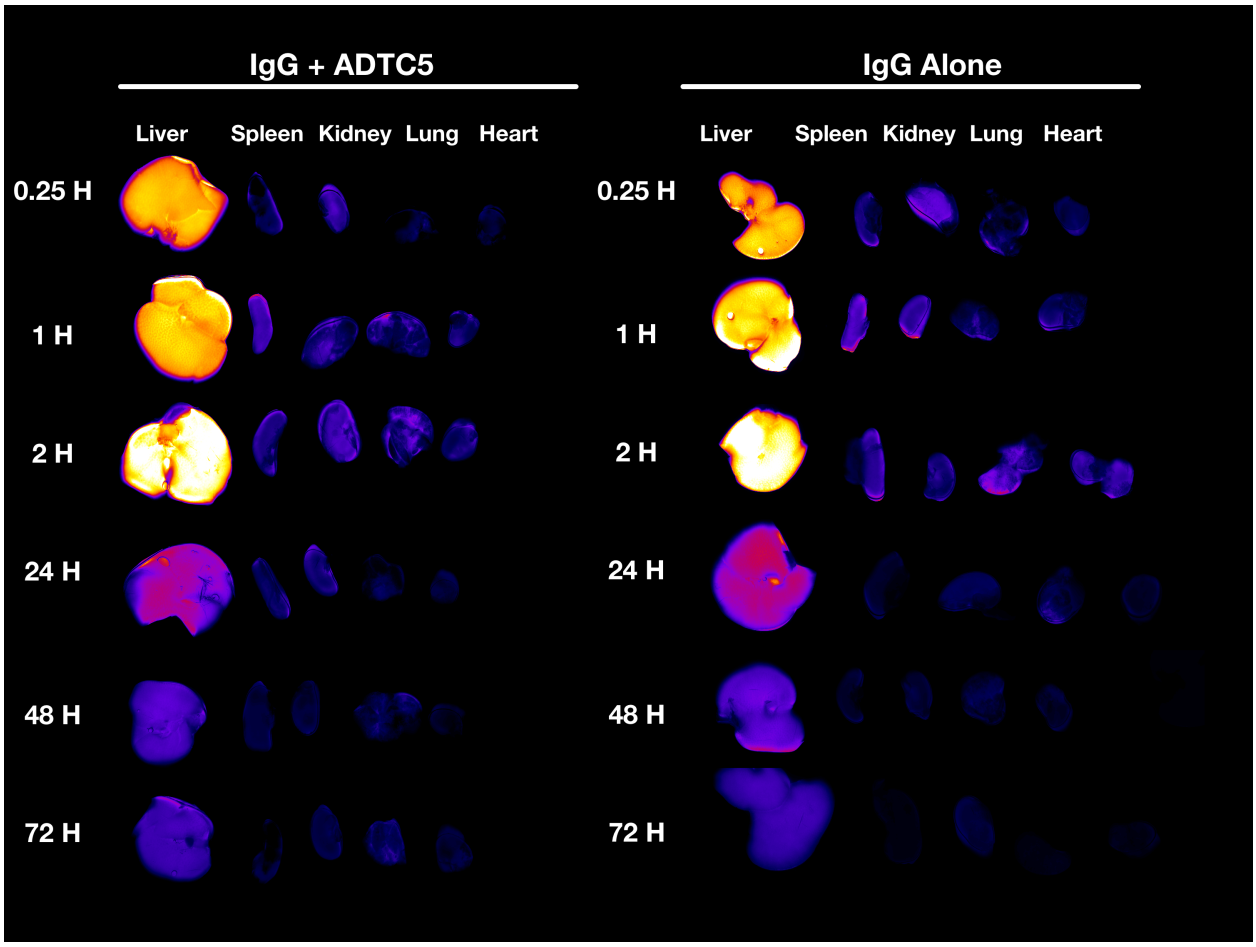
IgG + ADTC5
IgG Alone
Liver
Spleen
Kidney
Lung
Heart
0.25 H
1 H
2 H
24 H
48 H
72 H

C

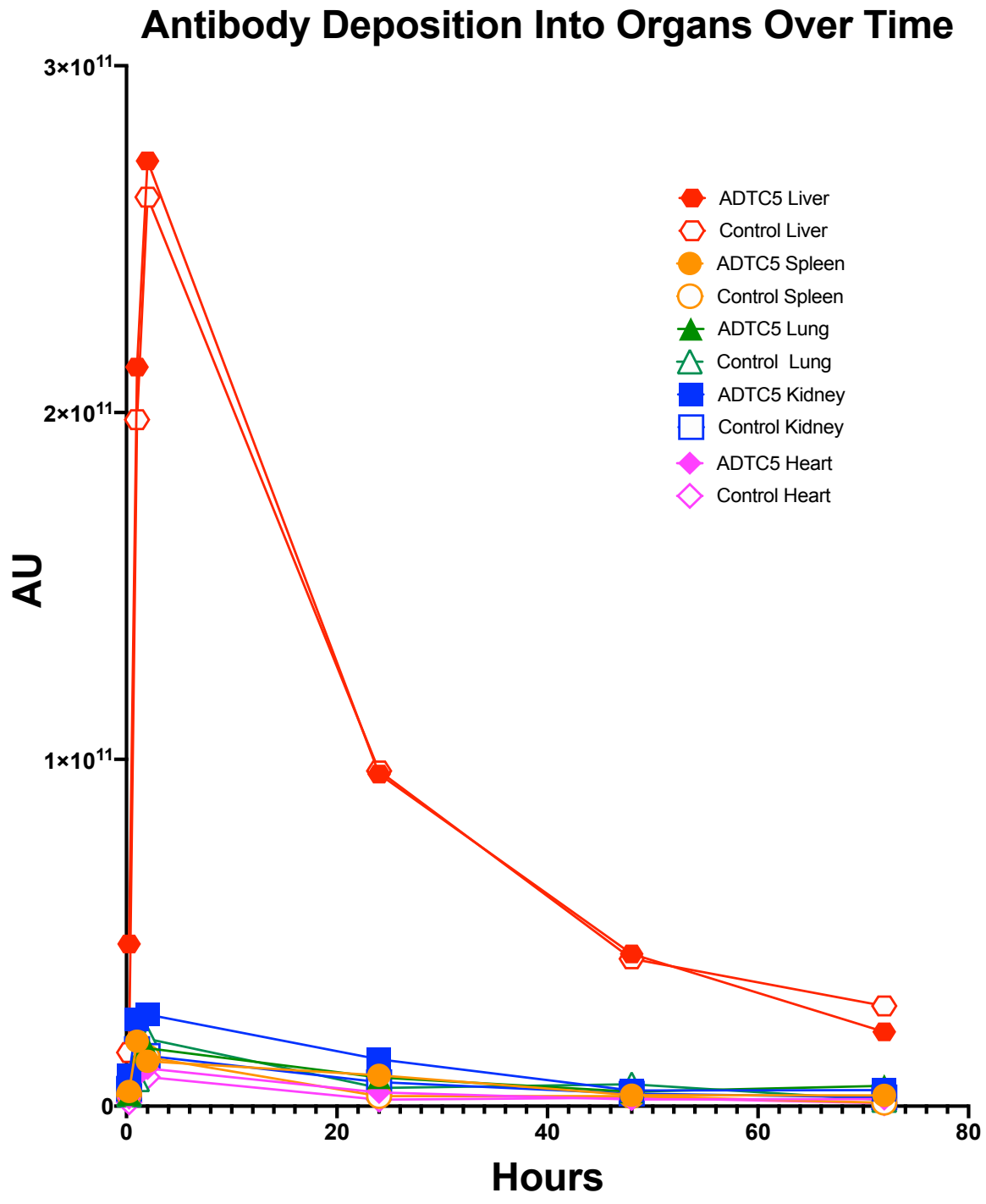
Antibody Deposition Into Organs Over Time
3×10^11
2×10^11
1×10^11
0
AU
0
20
40
60
80
Hours
ADTC5 Liver
Control Liver
ADTC5 Spleen
Control Spleen
ADTC5 Lung
Control Lung
ADTC5 Kidney
Control Kidney
ADTC5 Heart
Control Heart

D

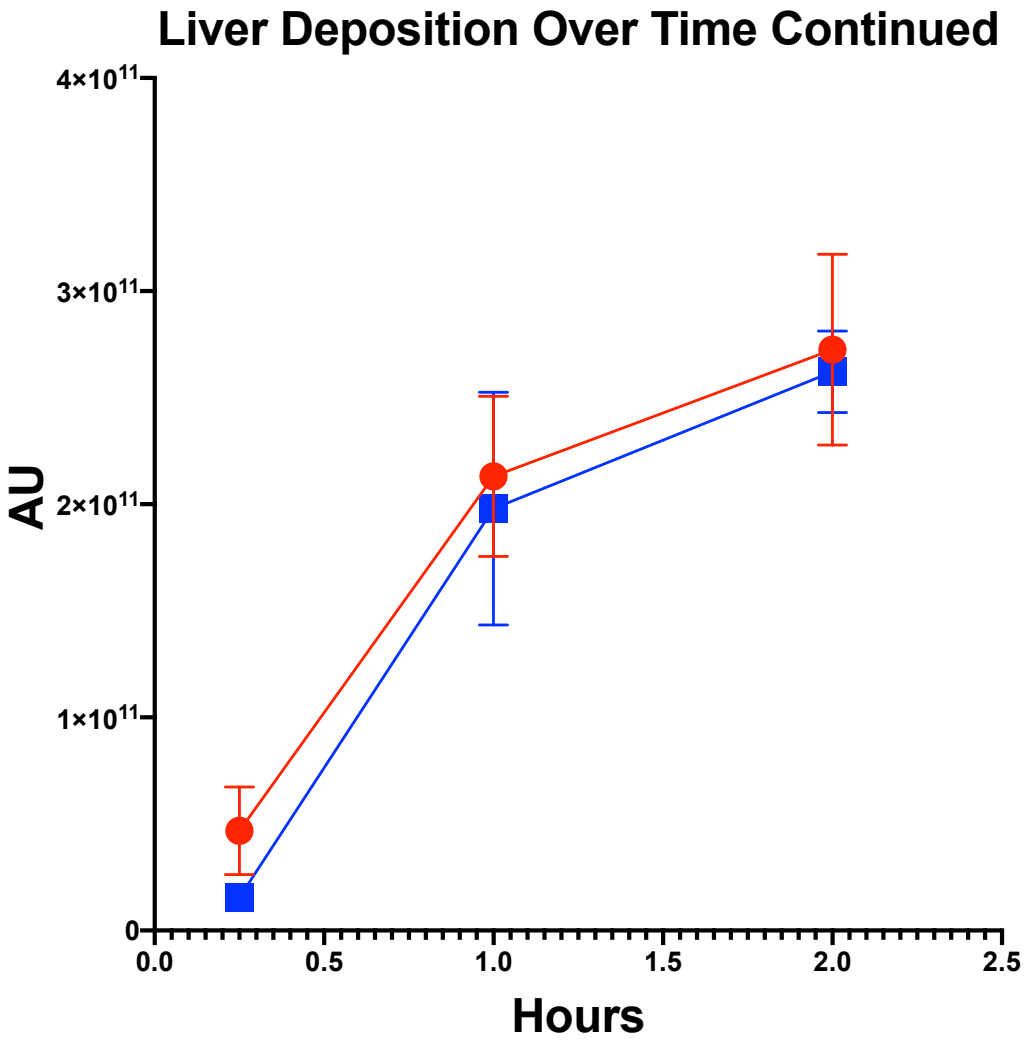
Liver Deposition Over Time Continued
4×10^11
3×10^11
2×10^11
1×10^11
0
AU
0.0
0.5
1.0
1.5
2.0
2.5
Hours

E

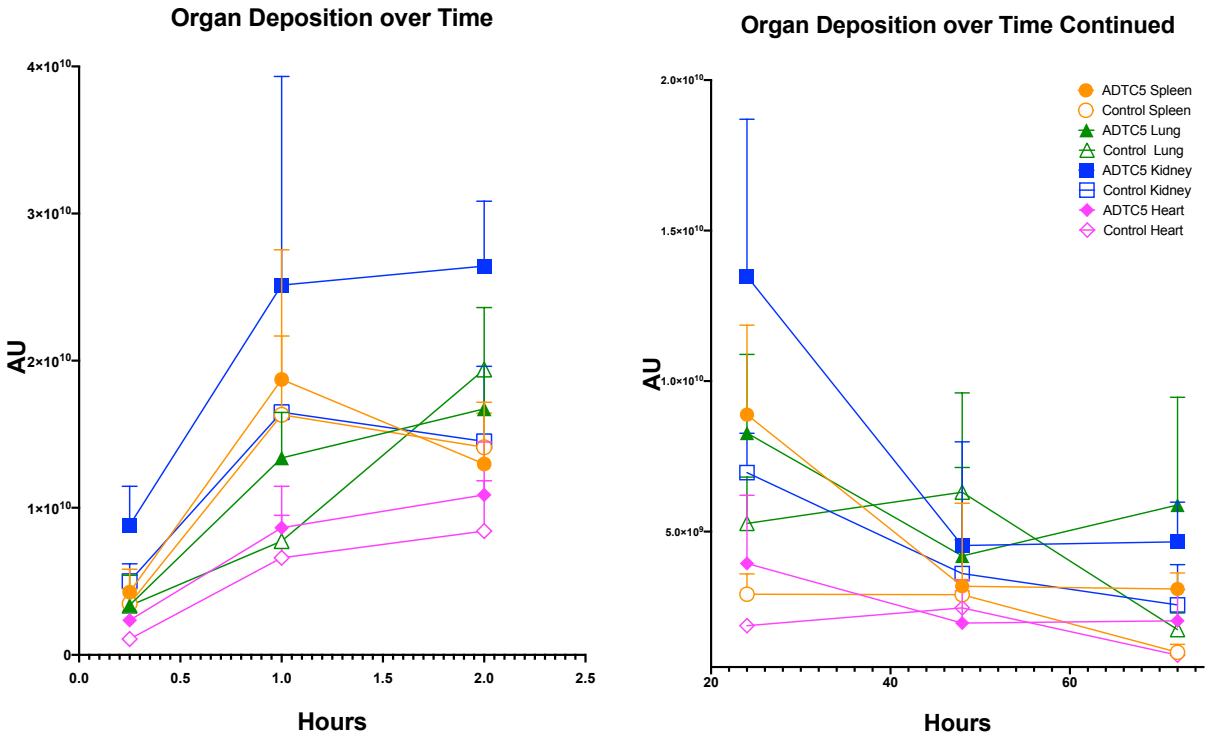

Figure 4.2. The depositions of IRdye800CW-IgG mAb in liver, spleen, kidney, lung, and heart after i.v. administrations with or without ADTC5 between circulation times of 0.25 and 72 h. **(A & B)** The qualitative NIRF images show IgG mAb depositions in liver, spleen, kidney, lung, and heart tissues after administrations of **(A)** IgG mAb + ADTC5 and **(B)** IgG mAb alone. The yellow-red colors indicate depositions of IgG mAb and the dark blue color is the background of organ tissues. **(C)** Comparisons of quantitative NIRF signals from IgG mAb in the liver, spleen, kidney, lung, and heart tissues. The majority of depositions were found in the liver. There were no significant differences in the liver depositions of IgG mAb when delivered with and without ADTC5. **(D)** The expansion of liver depositions between 0.25–2.0 h show that there was no effect

of ADTC5 on IgG mAb deposition in liver. **(E)** Comparisons of IgG mAb depositions in spleen, kidney, lungs, and heart when delivered with ADTC5 between 0.25 and 2 h (*left*) and between 24 and 72 h (*right*). There were no significant differences in IgG mAb depositions in spleen, kidney, lung, and heart between ADTC-treated and control mice over 72 h. Organ deposition was quantitatively determined by NIRF signal intensities for all organs. Data are shown as mean ± SD with the number of animals, $n = 3$, for each time point of each group.

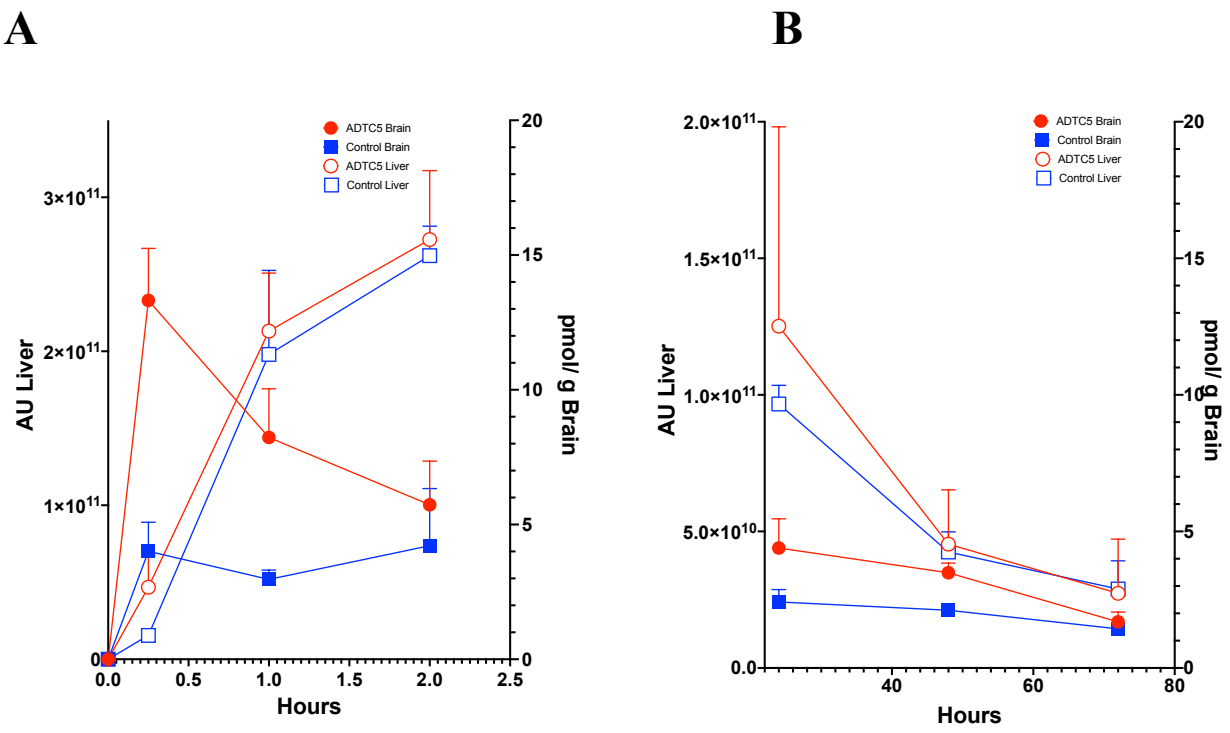

Figure 4.3. Comparisons between brain and liver depositions when IRdye800CW-IgG mAb was administered with and without ADTC5. **(A)** ADTC5 enhanced the brain depositions of IgG mAb compared to control but did not have any effect on the deposition of IgG mAb in the liver in the 0.25–2.0 h time period. The peak of IgG mAb in the liver was at 2 h circulation time. **(B)** There were no significant enhancements of IgG mAb by ADTC5 in the brain and liver when monitored between 24 – 48 h time period. Data are shown as mean ± SD with the number of animals, n = 3, for each time point of each group.

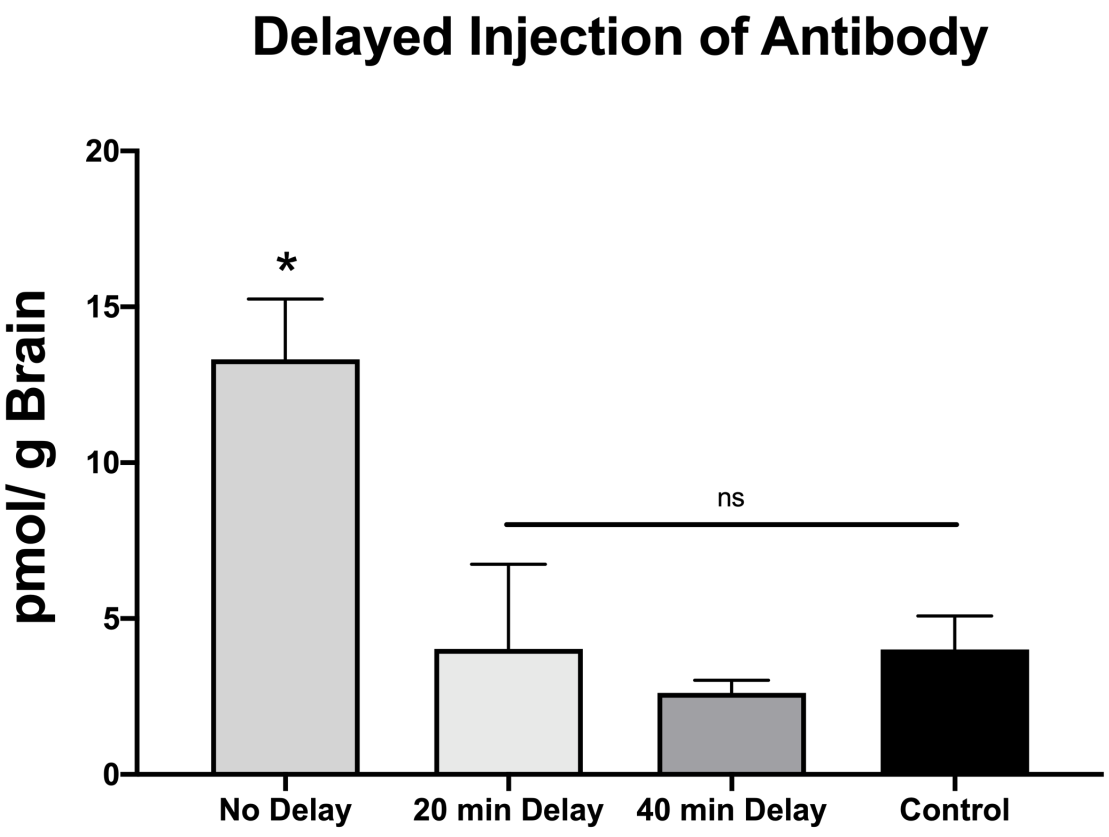

Figure 4.4. The effects of 0, 20, and 40 min delay between the delivery of ADTC5 (13 μmol/kg) and IRdye800CW-IgG mAb (21.6 nmol/kg) to evaluate the time-dependent paracellular pore opening for allowing IgG mAb to enter the brain. The IgG mAb was allowed to circulate for 15 min prior to animal sacrifice for quantification of its deposition in the brain using NIRF imagin. A significant enhancement of brain deposition of IgG mAb was observed when IgG mAb and ADTC5 were delivered together compared to when IgG mAb was delivered alone. A delay of 20 or 40 min in delivering IgG mAb after administration of ADTC5 resulted in no significant differences in IgG mAb depositions compared to control IgG mAb alone. This indicates that the BBB pore opening was closed at 20 min or less for 150 kDa IgG mAb. The asterisk (*) designates a significant difference between mice dosed with IgG mAb + ADTC5 and those receiving IgG mAb alone. Data are shown as mean ± SD with the number of animals, with n = 3 for each time point of each group.

4.7. References:

1. Chang, H. Y.; Morrow, K.; Bonacquisti, E.; Zhang, W.; Shah, D. K. Antibody pharmacokinetics in rat brain determined using microdialysis. *MAbs* **2018,** *10*, (6), 843-853.
2. van Dyck, C. H. Anti-Amyloid-beta Monoclonal Antibodies for Alzheimer's Disease: Pitfalls and Promise. *Biol Psychiatry* **2018,** *83*, (4), 311-319.
3. Florian, H.; Arnold, S. E.; Bateman, R.; Braunstein, J. B.; Budur, K.; Kerwin, D. R.; Soares, H.; Wang, D.; Holtzman, D. M. BBV-8E12, A HUMANIZED ANTI-TAU MONOCLONAL ANTIBODY, FOR TREATING EARLY ALZHEIMER'S DISEASE: UPDATED DESIGN AND BASELINE CHARACTERISTICS OF A PHASE 2 STUDY. *Alzheimer's & Dementia* **2019,** *15* (7), 251–252.
4. Ineichen, B. V.; Plattner, P. S.; Good, N.; Martin, R.; Linnebank, M.; Schwab, M. E. Nogo-A Antibodies for Progressive Multiple Sclerosis. *CNS Drugs* **2017,** *31*, (3), 187-198.
5. Ruggieri, S.; Tortorella, C.; Gasperini, C. Anti lingo 1 (opicinumab) a new monoclonal antibody tested in relapsing remitting multiple sclerosis. *Expert Rev Neurother* **2017,** *17*, (11), 1081-1089.
6. Ciric, B.; Howe, C. L.; Paz Soldan, M.; Warrington, A. E.; Bieber, A. J.; Van Keulen, V.; Rodriguez, M.; Pease, L. R. Human monoclonal IgM antibody promotes CNS myelin repair independent of Fc function. *Brain Pathol* **2003,** *13*, (4), 608-16.
7. Fisher, T. L.; Reilly, C. A.; Winter, L. A.; Pandina, T.; Jonason, A.; Scrivens, M.; Balch, L.; Bussler, H.; Torno, S.; Seils, J.; Mueller, L.; Huang, H.; Klimatcheva, E.; Howell, A.; Kirk, R.; Evans, E.; Paris, M.; Leonard, J. E.; Smith, E. S.; Zauderer, M. Generation and preclinical characterization of an antibody specific for SEMA4D. *MAbs* **2016,** *8*, (1), 150-62.

8. Dashti, S. R.; Spalding, A.; Kadner, R. J.; Yao, T.; Kumar, A.; Sun, D. A.; LaRocca, R. Targeted intraarterial anti-VEGF therapy for medically refractory radiation necrosis in the brain. *J Neurosurg Pediatr* **2015,** *15*, (1), 20-5.

9. Chakraborty, S.; Filippi, C. G.; Wong, T.; Ray, A.; Fralin, S.; Tsiouris, A. J.; Praminick, B.; Demopoulos, A.; McCrea, H. J.; Bodhinayake, I.; Ortiz, R.; Langer, D. J.; Boockvar, J. A. Superselective intraarterial cerebral infusion of cetuximab after osmotic blood/brain barrier disruption for recurrent malignant glioma: phase I study. *J Neurooncol* **2016,** *128*, (3), 405-15.

10. Downs, M. E.; Buch, A.; Sierra, C.; Karakatsani, M. E.; Teichert, T.; Chen, S.; Konofagou, E. E.; Ferrera, V. P. Long-Term Safety of Repeated Blood-Brain Barrier Opening via Focused Ultrasound with Microbubbles in Non-Human Primates Performing a Cognitive Task. *PLoS One* **2015,** *10*, (5), e0125911.

11. Kiptoo, P.; Sinaga, E.; Calcagno, A. M.; Zhao, H.; Kobayashi, N.; Tambunan, U. S.; Siahaan, T. J. Enhancement of drug absorption through the blood-brain barrier and inhibition of intercellular tight junction resealing by E-cadherin peptides. *Mol Pharm* **2011,** *8*, (1), 239-49.

12. On, N. H.; Kiptoo, P.; Siahaan, T. J.; Miller, D. W. Modulation of blood-brain barrier permeability in mice using synthetic E-cadherin peptide. *Mol Pharm* **2014,** *11*, (3), 974-81.

13. Laksitorini, M. D.; Kiptoo, P. K.; On, N. H.; Thliveris, J. A.; Miller, D. W.; Siahaan, T. J. Modulation of intercellular junctions by cyclic-ADT peptides as a method to reversibly increase blood-brain barrier permeability. *J Pharm Sci* **2015,** *104*, (3), 1065-75.

14. Ulapane, K. R.; On, N.; Kiptoo, P.; Williams, T. D.; Miller, D. W.; Siahaan, T. J. Improving Brain Delivery of Biomolecules via BBB Modulation in Mouse and Rat: Detection using MRI, NIRF, and Mass Spectrometry. *Nanotheranostics* **2017,** *1*, (2), 217-231.

15. Ulapane, K. R.; Kopec, B. M.; Siahaan, T. J. In Vivo Brain Delivery and Brain Deposition of Proteins with Various Sizes. *Mol Pharm* **2019,** 10.1021/acs.molpharmaceut.9b00763.

16. Ulapane, K. R.; Kopec, B. M.; Siahaan, T. J. Improving In Vivo Brain Delivery of Monoclonal Antibody Using Novel Cyclic Peptides. *Pharmaceutics* **2019,** *11*, (11).

17. Fujiyoshi, M.; Tachikawa, M.; Ohtsuki, S.; Ito, S.; Uchida, Y.; Akanuma, S.; Kamiie, J.; Hashimoto, T.; Hosoya, K.; Iwatsubo, T.; Terasaki, T. Amyloid-beta peptide(1-40) elimination from cerebrospinal fluid involves low-density lipoprotein receptor-related protein 1 at the blood-cerebrospinal fluid barrier. *J Neurochem* **2011,** *118*, (3), 407-15.

18. Bergman, I.; Burckart, G. J.; Pohl, C. R.; Venkataramanan, R.; Barmada, M. A.; Griffin, J. A.; Cheung, N. K. Pharmacokinetics of IgG and IgM anti-ganglioside antibodies in rats and monkeys after intrathecal administration. *J Pharmacol Exp Ther* **1998,** *284*, (1), 111-5.

19. Noguchi, Y.; Kato, M.; Ozeki, K.; Ishigai, M. Pharmacokinetics of an intracerebroventricularly administered antibody in rats. *MAbs* **2017,** *9*, (7), 1210-1215.

20. Pardridge, W. M. Drug transport in brain via the cerebrospinal fluid. *Fluids Barriers CNS* **2011,** *8*, (1), 7.

21. Blasberg, R. G.; Patlak, C.; Fenstermacher, J. D. Intrathecal chemotherapy: brain tissue profiles after ventriculocisternal perfusion. *J Pharmacol Exp Ther* **1975,** *195*, (1), 73-83.

22. Krewson, C. E.; Klarman, M. L.; Saltzman, W. M. Distribution of nerve growth factor following direct delivery to brain interstitium. *Brain Res* **1995,** *680*, (1-2), 196-206.

23. Sajesh, B. V.; On, N. H.; Omar, R.; Alrushaid, S.; Kopec, B. M.; Wang, W. G.; Sun, H. D.; Lillico, R.; Lakowski, T. M.; Siahaan, T. J.; Davies, N. M.; Puno, P. T.; Vanan, M. I.; Miller, D. W. Validation of Cadherin HAV6 Peptide in the Transient Modulation of the Blood-Brain Barrier for the Treatment of Brain Tumors. *Pharmaceutics* **2019,** *11*, (9).

24. Alaofi, A.; Farokhi, E.; Prasasty, V. D.; Anbanandam, A.; Kuczera, K.; Siahaan, T. J. Probing the interaction between cHAVc3 peptide and the EC1 domain of E-cadherin using NMR and molecular dynamics simulations. *J Biomol Struct Dyn* **2017,** *35*, (1), 92-104.

Chapter 5: Summary and Future Directions

5.1. Summary:

The goal of this project was to enhance the delivery of the neurodegenerative protein, brain derived neurotrophic factor BDNF, and to further understand the dynamics of antibody delivery to the brain. The aims were to (i) deliver BDNF across the blood–brain barrier (BBB) via the use of ADTC5 peptide in EAE mice and evaluate if BDNF can be delivered in a therapeutically relevant dose, (ii) expand BDNF delivery to a separate animal model to evaluate BDNF use as a potential therapeutic for Alzheimer's disease, (iii) to evaluate the pharmacokinetics of an IgG monoclonal antibody (mAb) in the brain to further understand how they can be used as a therapeutic for brain disease. The BBB limits the penetration of protein therapeutics into the brain, making it difficult to deliver diagnostics and therapeutics into the brain. How the integrity of the BBB changes with brain disease has been previously evaluated and has been thought to be highly disrupted in Alzheimer's and multiple sclerosis (MS); however, we demonstrated the BBB of EAE and APP/PS1 mice is intact enough so that BDNF cannot penetrate the brain on its own.[1-4]

In the second chapter of this dissertation, we demonstrated that ADTC5 could be used to enhance the delivery of BDNF to EAE mice and that repeated administration of BDNF + ADTC5 could be used to treat the disease and prevent disease relapse. The mice that received BDNF + ADTC5 improved significantly in clinical body score compared to mice that received BDNF alone, ADTC5 alone, or vehicle. Furthermore, mice that received BDNF + ADTC5 showed increased myelin levels in the lateral corpus callosum, increased NG2 glia in the medial corpus callosum, and upregulated mRNA transcripts for early growth response-1 (EGR1) and activity-related cytoskeleton associated protein (ARC). To confirm directly that BDNF was entering the brain, BDNF was administered with or without ADTC5 to healthy mice and then detected using western

blot; there were clear BDNF bands in the brain homogenates of mice that received BDNF + ADTC5, whereas the bands representing mice that received BDNF alone showed virtually no detectable signal.

In the third chapter, we demonstrated that the ADTC5 + BDNF delivery combination could be used to ameliorate the disease in a transgenic Alzheimer's mouse model (APP/PS1). To initially assess BDNF's efficacy in the APP/PS1 model, we administered repeated doses of BDNF + ADTC5, BDNF alone, or vehicle and subjected mice to behavioral/cognitive assessments. We showed that mice that received BDNF + ADTC5 performed significantly better in both the Y-maze and novel object recognition (NOR) assessments compared to mice that received BDNF alone or vehicle. Similar to the EAE mouse model, we also showed an increase in NG2 glia in the cortex and upregulation of EGR1 and ARC mRNA transcripts in the cortex. We also probed for amyloid-beta plaques using a Congo red stain and saw high plaque loads in all mice groups, indicating BDNF is improving cognitive function likely by improving synaptic plasticity via NG2 glia and not by reducing plaque load.

In the fourth chapter, we wanted to further understand the pharmacokinetics of IgG mAbs when delivered to the brain via ADTC5. We recently demonstrated in separate experiments that ADTC5 along with other cyclic and linear peptides could significantly enhance brain deposition in mice of a near infrared fluorescent (NIRF) antibody, IRDye800CW-IgG mAb.[5,6] We discovered an increased in circulation time of IRDye800CW-IgG + ADTC5 resulted in a decreased deposition into the brain, indicating that there is a rapid time-dependent clearance from the brain with a majority of the clearance occurring in the liver. We also discovered that across a 72-hour circulation time period, ADTC5 does not significantly enhance antibody deposition in peripheral organs. The last point of interest was determining how long the BBB remains open for an antibody

to penetrate. Previously, it has been shown that for 65 kDa galbumin, the BBB remains open between 10 to 40 minutes.[7] However, for an antibody, we discovered the BBB only remains open for in less than 20 min, indicating the effect of ADTC5 is short lasting for delivering mAb. A more specific time point will be evaluated in the future using MRI.

5.2. Future Directions:

5.2.1. Brain Delivery of Various mAbs and Fab Fragments:

We chose to deliver the donkey–anti-goat IRDye800CW-IgG because it had no specific target in mouse and thus served as a freely circulating mAb, making it ideal for studying deposition into the brain and peripheral organs with or without ADTC5. There are several mAbs on the market that demonstrate excellent selectivity and efficacy for the treatment of various disease; however, none of these mAbs can readily enter the brain.[8] Others have demonstrated the use of hypertonic mannitol to improve the delivery of bevacizumab and cetuximab for the treatment of cancers; however, there are known complications with using hypertonic mannitol, making repeated administration risky.[9] It has been previously demonstrated via MRI that ADTC5 does not significantly alter cerebral blood flow[10] and that cadherin peptides can be used enhance the delivery of anticancer drug, adenathin for the treatment of medulloblastoma in mice.[11] Given the ability for ADTC5 to enhance antibody deposition into the brain, there is good reason to believe ADTC5 can improve the delivery of functional mAbs such bevacizumab or ranibizumab to treat a mouse model for brain tumors. Additionally, ADTC5 can likely be used to improve the delivery of an anti-Aβ mAb to reduce plaque load in APP/PS1. An important aspect would be to see if mice cognitively improve with the reduction of amyloid-β mAb and if there is associated cellular signals

indicating an improvement in brain health. The significance of amyloid-β versus Tau plaques is highly debated amongst industry, medical, and academic professionals.[12]

5.2.2. Mechanisms of mAb Efflux Out of the Brain:

We demonstrated that the presence of a delivered antibody to the brain is relatively short lived. It is known that the CSF half-life in mice and humans is very rapid, with a complete turnover happening every 4 to 5 hours.[13,14] There has been extensive studies of antibody receptors on the systemic side of the BBB with hopes to exploit them to deliver antibodies to the brain.[15] However, the means by which antibodies are expelled out of the brain has only been evaluated on by a few different groups[16,17] Antibodies are thought to be shuffled out of the CNS via neonatal Fc receptors (FcRn); however, the kinetics and saturation limits of these receptors toward various mAbs are unknown. Additionally, it is not known whether ADTC5 can affect antibody efflux from the brain or rather just the influx. One way to probe at this would be to deliver an fluorescently labeled antibody via ICV, and to administer ADTC5 systemically to see if there is a modulated efflux from the brain. Additionally, the antibody can also be administered ICV with or without ADTC5 to observe the effect of ADTC5 on mAb clearance from the brain. Taken together, it is important to understand the dynamics of antibodies in the brain in order to improve dosing regiments, antibody design, and BBB modulation parameters in order to optimize mAb pharmacokinetic profiles for treatments of brain diseases.

5.3. References:

1. Bennett, J.; Basivireddy, J.; Kollar, A.; Biron, K. E.; Reickmann, P.; Jefferies, W. A.; McQuaid, S. Blood–brain barrier disruption and enhanced vascular permeability in the multiple sclerosis model EAE. *Journal of Neuroimmunology* **2010**, *229* (1-2), 180–191 DOI: 10.1016/j.jneuroim.2010.08.011.
2. Do, T. M.; Alata, W.; Dodacki, A.; Traversy, M.-T.; Chacun, H.; Pradier, L.; Scherrmann, J.-M.; Farinotti, R.; Calon, F.; Bourasset, F. Altered cerebral vascular volumes and solute transport at the blood-brain barriers of two transgenic mouse models of Alzheimer's disease. *NP* **2014**, *81* (c), 311–317 DOI: 10.1016/j.neuropharm.2014.02.010.
3. Fabis, M. J.; Scott, G. S.; Kean, R. B.; Koprowski, H.; Hooper, D. C. Loss of blood-brain barrier integrity in the spinal cord is common to experimental allergic encephalomyelitis in knockout mouse models. *Proc Natl Acad Sci USA* **2007**, *104* (13), 5656–5661 DOI: 10.1073/pnas.0701252104.
4. Minogue, A. M.; Jones, R. S.; Kelly, R. J.; McDonald, C. L.; Connor, T. J.; Lynch, M. A. Age-associated dysregulation of microglial activation is coupled with enhanced blood-brain barrier permeability and pathology in APP/PS1 mice. *Neurobiology of Aging* **2014**, *35* (6), 1442–1452 DOI: 10.1016/j.neurobiolaging.2013.12.026.
5. Ulapane; Kopec; Siahaan. Improving In Vivo Brain Delivery of Monoclonal Antibody Using Novel Cyclic Peptides. *Pharmaceutics* **2019**, *11* (11), 568–15 DOI: 10.3390/pharmaceutics11110568.
6. Ulapane, K. R.; Kopec, B. M.; ORCID: 0000-0001-7250-0627, T. J. S. In Vivo Brain Delivery and Brain Deposition of Proteins with Various Sizes. *Mol. Pharmaceutics* **2019**, 1–12 DOI: 10.1021/acs.molpharmaceut.9b00763.

7. Ulapane, K. R.; On, N.; Kiptoo, P.; Williams, T. D.; Miller, D. W.; Siahaan, T. J. Improving Brain Delivery of Biomolecules via BBB Modulation in Mouse and Rat: Detection using MRI, NIRF, and Mass Spectrometry. *Nanotheranostics* **2017**, *1* (2), 217–231 DOI: 10.7150/ntno.19158.

8. Mehta, D.; Jackson, R.; Paul, G.; Shi, J.; Sabbagh, M. Why do trials for Alzheimer's disease drugs keep failing? A discontinued drug perspective for 2010-2015. *Expert Opinion on Investigational Drugs* **2017**, *26* (6), 735–739 DOI: 10.1080/13543784.2017.1323868.

9. Chakraborty, S.; Filippi, C. G.; Wong, T.; Ray, A.; Fralin, S.; Tsiouris, A. J.; Praminick, B.; Demopoulos, A.; McCrea, H. J.; Bodhinayake, I.; et al. Superselective intraarterial cerebral infusion of cetuximab after osmotic blood/brain barrier disruption for recurrent malignant glioma: phase I study. *Journal of Neuro-Oncology* **2016**, *128* (3), 405–415 DOI: 10.1007/s11060-016-2099-8.

10. Modulation of blood-brain barrier permeability in mice using synthetic E-cadherin peptide. *Mol. Pharm.* **2014**, *11* (3), 974–981 DOI: 10.1021/mp400624v.

11. Sajesh, B. V.; On, N. H.; Omar, R.; Alrushaid, S.; Kopec, B. M.; Wang, W.-G.; Sun, H.-D.; Lillico, R.; Lakowski, T. M.; Siahaan, T. J.; et al. Validation of Cadherin HAV6 Peptide in the Transient Modulation of the Blood-Brain Barrier for the Treatment of Brain Tumors. *Pharmaceutics* **2019**, *11* (9), 481 DOI: 10.3390/pharmaceutics11090481.

12. Bloom, G. S. Amyloid-β and Tau. *JAMA Neurol* **2014**, *71* (4), 505–4 DOI: 10.1001/jamaneurol.2013.5847.

(13) Noguchi, Y.; Kato, M.; Ozeki, K.; Ishigai, M. Pharmacokinetics of an intracerebroventricularly administered antibody in rats. **2017**, 1–6 DOI: 10.1080/19420862.2017.1345834.

14. Pardridge, W. M. The blood-brain barrier: bottleneck in brain drug development. *NeuroRx* **2005**, *2* (1), 3–14 DOI: 10.1602/neurorx.2.1.3.

15. Pardridge, W. M. Blood–brain barrier delivery. *Drug Discovery Today* **2007**, *12* (1-2), 54–61 DOI: 10.1016/j.drudis.2006.10.013.

16. Cooper, P. R.; Ciambrone, G. J.; Kliwinski, C. M.; Maze, E.; Johnson, L.; Li, Q.; Feng, Y.; Hornby, P. J. Efflux of monoclonal antibodies from rat brain by neonatal Fc receptor, FcRn. *Brain Research* **2013**, *1534* (C), 13–21 DOI: 10.1016/j.brainres.2013.08.035.

17. Zhang, Y.; Pardridge, W. M. Mediated efflux of IgG molecules from brain to blood across the blood-brain barrier. *Journal of Neuroimmunology* **2001**, *114* (1-2), 168–172.